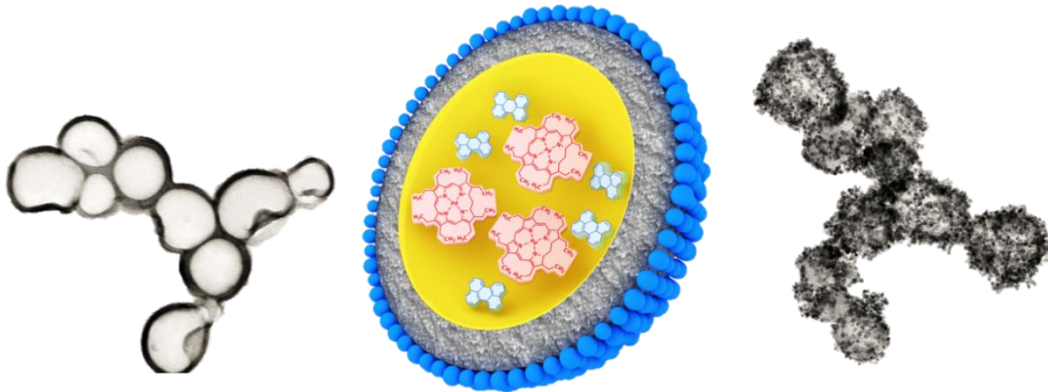




# Luminescence Properties in Polymer and Polymer/Inorganic Nanocapsules



## Dissertation

zur Erlangung des Grades

„Doktor der Naturwissenschaften“

im Promotionsfach Chemie

am Fachbereich Chemie, Pharmazie und Geowissenschaften

der Johannes Gutenberg-Universität Mainz

vorgelegt von

**Kartheek Katta**

geboren in Kallur, Indien



MAX-PLANCK-GESELLSCHAFT

Mainz, im April 2016



Die vorliegende Arbeit wurde am  
Max-Planck-Institut für Polymerforschung in Mainz  
unter Anleitung von

Prof. Dr. Katharina Landfester

in der Zeit von Mai 2013 bis April 2016 angefertigt.







## Table of Contents

1. Motivation .....	11
2. Theoretical background.....	14
2.1. Luminescence .....	14
2.1.1. Basic principles and mechanism of triple–triplet annihilation upconversion (TTA-UC) process.....	16
2.2. Colloidal systems.....	21
2.2.1. Stability of colloids .....	22
2.2.2. Emulsions.....	26
2.2.3. Emulsion polymerization .....	28
2.2.4. Stability of emulsions .....	30
2.2.5. Emulsion stabilization via solid particles: Pickering emulsions.....	32
2.2.6. Capsule formation .....	34
3. Characterization techniques .....	38
3.1 Transmission electron microscopy (TEM) .....	38
3.2 Scanning electron microscopy (SEM).....	38
3.3 Dynamic light scattering (DLS) .....	38
4. Results and discussion.....	40
4.1. Influence of molecular oxygen on the fluorescence and TTA-UC process.....	40
4.1.1. Photooxidation of perylene .....	40
4.1.2. Different approaches to improve the luminescence efficiency (fluorescence and TTA-UC process).....	43
4.2. Synthesis of nanocapsules using different polymer materials as shell .....	43
4.2.1. Synthesis of poly(methyl methacrylate) and poly(L-lactic acid) nanocapsules via solvent evaporation polymerization method .....	45
4.2.2. Free-radical miniemulsion polymerization method .....	47
4.2.3. Conclusions.....	50

4.3. Synthesis of nanocapsules containing TTA-UC dyes under protective conditions.....	50
4.3.1. Study of TTA-UC properties in nanocapsules synthesized under different conditions.....	52
4.3.3. Conclusions.....	56
4.4. Improving the efficiency of encapsulated fluorophores with ceria/polymer hierarchical nanocapsules <sup>123</sup> .....	57
4.4.1. Encapsulation of terrylene diimide (TDI) in hybrid nanocapsules: State of the art	58
4.4.2. Protecting the nanocapsules from oxygen: Crystallization of cerium(IV) oxide on the nanocapsule surface .....	62
4.4.3. Fluorescent properties of the nanocapsules .....	64
4.4.3. Conclusions.....	68
4.5. Inorganic protection of polymer nanocapsules: Screening of different materials on polystyrene capsules .....	69
4.5.1. Overview of different strategies for deposition of inorganic materials .....	69
4.5.2. Protection of polymer nanocapsules with silicate clay formed ex situ .....	73
4.5.3. In situ crystallization of hydroxyapatite and cerium oxide on the surface of polymer nanocapsules .....	76
4.5.4. Fluorescence properties of polymer and polymer/inorganic nanocapsules .....	78
4.5.3. Conclusions.....	80
4.6. Pickering miniemulsion method.....	80
4.6.1. Deposition of silicate clay on polystyrene nanocapsules.....	80
4.6.2. Fluorescent properties .....	83
5. General conclusions .....	85
6. Zusammenfassung der Ergebnisse .....	87
7. Experimental section .....	90
7.1. Materials .....	90
7.2. Experiment details for Section 4.2 .....	92
7.2.1. Synthesis of poly(methyl methacrylate) nanocapsules .....	92



---

7.2.2. Synthesis of poly(L -lactide) nanocapsules .....	92
7.2.3. Preparation of stock solutions .....	92
7.2.4. Synthesis of nanocapsules via miniemulsion polymerization .....	93
7.2.5. Preparation of stock solutions .....	93
7.3. Experiment details for Section 4.3 .....	93
7.3.1. Synthesis of carboxyl-functionalized polystyrene nanocapsules.....	93
7.3.2. Preparation of stock solutions .....	94
7.4. Experiment details for Section 4.4 .....	94
7.4.1 Synthesis of carboxylated polystyrene nanocapsules .....	94
7.4.2. Synthesis of the TDI dye and preparation of its stock Solution .....	94
7.4.3. Synthesis of the CeO <sub>2</sub> /polymer hybrid nanocapsules .....	94
7.5. Experiment details for Section 4.5 .....	95
7.5.1. Synthesis of polystyrene nanocapsules via miniemulsion polymerization method	95
7.5.2. Deposition of clay on the surface of amino-functionalized nanocapsules via layer- by-layer deposition method.....	95
7.5.3. In situ crystallization of hydroxyapatite and ceria on the surface of carboxylate- functionalized nanocapsules .....	95
7.5.4. Preparation of stock solutions .....	96
7.6. Experiment details for Section 4.6 .....	96
7.6.1. Synthesis of polystyrene nanocapsules via polymerization method.....	96
7.6.2. Synthesis of polystyrene nanocapsules via Pickering miniemulsion method.....	96
7.6.3. Preparation of stock solutions .....	96
7.7. Analytical Tools .....	97
7.7.1. Scanning electron microscopy (SEM) .....	97
7.7.2. Transmission electron microscopy (TEM) .....	97
7.7.3. Dynamic light scattering (DLS).....	97
7.7.4. Particle charge detector (PCD) .....	97
7.7.5. Energy dispersive X-ray spectroscopy (EDX).....	98

## Table of contents

---

7.7.6. Thermogravimetric analysis (TGA).....	98
7.7.7. X-Ray powder diffraction .....	98
7.7.8. Field desorption mass spectra measurements .....	98
7.7.9. Photoluminescence measurements.....	98
8. Abbreviations and symbols .....	100
9. References .....	103
10. Acknowledgements .....	112

# 1. Motivation

Nanoconfined materials have originated a considerable growth of research in the area of life science, with applications including bioimaging and drug delivery.<sup>1-4</sup> Biodegradable polymeric nanoparticles have the capability of encapsulating hydrophobic or hydrophilic materials which are useful for several *in vivo* therapeutic applications.<sup>5-9</sup> Polymeric hybrid nanoconfined materials have the ability to alter different properties by varying the size, composition, porosity, stability, surface functionality, and colloidal stability. These materials have unique features with a large functional surface which is able to bind, absorb and carry other compounds, such as drugs or fluorescent dyes.<sup>10-14</sup> A challenging task still remains to select perfect nanoparticle compositions and their surface modifications with enhanced selectivity and reproducibility to achieve the fluorescent features required for bioimaging.

Fluorescence imaging is a useful non-invasive technique for the detection of biomolecules without radiopharmaceuticals, and exhibits distinct advantages with high spatial and temporal resolution, which is of advantage in biological and biomedical applications.<sup>2, 15-16</sup> The visualization of fluorescent dyes or proteins as labels for molecular processes or structures is known as fluorescence imaging. Photostability, quantum yield, and fluorescent lifetime are the most important parameters of a fluorophore and they need to be taken into account in detection of biomolecules.<sup>17</sup> The interaction between fluorophore molecules and dissolved oxygen results in reducing the stability of the fluorophore, which decreases to a large extent the capability for *in vivo* practical applications.<sup>18-19</sup> Hence, to improve the efficiency of bioimaging and medical diagnosis, the photodegradation process of a fluorophore has to be inhibited. Moreover, many researchers have chosen specific methods to prevent the fluorophore from interacting with dissolved oxygen by altering the chemical structure of the dye molecules.<sup>3, 20-21</sup> To date, the most common approach to prevent the photooxidation of fluorophores is to encapsulate them in specific nanoparticles or biodegradable polymers.<sup>22-24</sup>

The general objective of this thesis is to avoid photodegradation which is caused by the presence of triplet states even in highly fluorescent dyes. Different methods for the encapsulation of hydrophobic fluorescent materials into micro- and nanocapsules have been represented in literature. However, most of the work neglects the fact that capsules are prepared under ambient conditions, which results in trapping of the molecular oxygen within the particle system during the synthetic procedure. In general, nanocapsules are synthesized

using different methods, such as macroemulsion<sup>25</sup> or micro- and miniemulsion polymerization methods.<sup>26-27</sup> Particularly, miniemulsion polymerization is a versatile technique to synthesize a wide range of hybrid structures with different morphologies. The main advantage of miniemulsion polymerization is the stability of the emulsion droplets and that the polymerization step can also be carried out even in unconventional conditions, such as in the absence of water in nonaqueous miniemulsions and at high temperature conditions.<sup>28-29</sup> The miniemulsion process is used to produce nanocapsules and useful to encapsulate hydrophobic fluorescent dyes.<sup>28-31</sup>

Fluorescence is a one-photon Stokes process in which the emitted photon has lower energy than that of the excitation photon.<sup>32</sup> Autofluorescence is one of the major problems seen in fluorescence microscopy of living objects, caused by emissive properties of the surrounding environment, often observed when ultraviolet to green light sources are used to produce fluorescence. The upconversion (UC) process allows the generation of higher energy photons by using lower energy ones for excitation.<sup>33</sup> Bioimaging of biomolecules using upconversion emission luminescence process is one of the solutions to solve the autofluorescence problem. In comparison to visible light, the near-infrared (NIR) light undergoes less diffuse scattering, causes less photodamage, and can penetrate deeper into tissues, being therefore preferred for life science applications. Upconversion fluorescent nanoparticles with NIR excitation are well suited for bioimaging in comparison to fluorescent materials. The use of such upconversion nanoparticles have several advantages, such NIR light allows a deep penetration into tissues, causing less photodamage on living organisms and high detection sensitivity.<sup>34-36</sup>

Upconversion has been demonstrated in different systems, for example in rare earth ion-doped inorganic glasses<sup>37</sup> showing cooperative energy transfer,<sup>38</sup> two-photon absorption,<sup>33, 39</sup> and triplet–triplet annihilation upconversion (TTA-UC).<sup>38, 40</sup> TTA-UC was first observed in 1962 by Parker at low temperature (70–200 K)<sup>41</sup> and was defined as p-type delayed fluorescence. Its advantages over other UC processes have been recently demonstrated when non-coherent excitation (e.g., sunlight) was used.<sup>42</sup> The main advantage of TTA-UC process is the relative high quantum yield, which can be achieved even at low excitation intensity (tens of  $\text{mW cm}^{-2}$ ).<sup>43-44</sup> Other fundamental advantages of the bimolecular supported TTA-UC process is its inherent independence on a coherence of an excitation light<sup>45-46</sup> and, because of the usage of organic molecules having broad absorption spectra, extremely low requirements on a spectral power density (tens of  $\mu\text{W nm}^{-1}$ ).<sup>42</sup> In spite of the discussed advantages, the direct application of the TTA-UC process in biomedical applications has a significant limitation: the

TTA-UC process is achieved by two organic molecules (a sensitizer and an emitter molecule) dissolved in organic solvents (e.g., toluene, hexadecane, tetrahydrofuran) that are not bio-compatible, limiting therefore any application in bioimaging.<sup>47</sup> However, the TTA-UC process was successfully transferred in water environments by the synthesis of dendrimer complexes,<sup>48</sup> encapsulating UC dyes in micelles of non-ionic surfactants,<sup>49-50</sup> semicrystalline cellulose nanocontainers<sup>51</sup> and in polymeric nanocapsules synthesized either by free-radical miniemulsion polymerization or by the solvent evaporation method in miniemulsion.<sup>52-53</sup> Due to the presence of molecular oxygen within the nanocapsules and in emulsion systems, absorbed by the sensitizer, a remarkable amount of singlet oxygen can be created. In its turn, the singlet oxygen is known as a very aggressive species and can lead to remarkable oxidative damage of the used emitter or sensitizer molecules.<sup>54-56</sup>

The specific objectives of this thesis are to protect the fluorescent and upconversion organic dye molecules from the molecular oxygen and reduce the influence of singlet oxygen. To achieve this target, we use different strategies to obtain sustainable and reproducible luminescence efficiency in polymeric nanocapsules. The thesis focuses on the encapsulation of hydrophobic luminescent dyes into nanocapsules via miniemulsion polymerization, and it is explained how to avoid the influence of molecular oxygen. The first strategy to control the entry of molecular oxygen into nanocapsules was to change the shell material by taking into account the crystallinity nature. For this purpose, nanocapsules were prepared using different polymeric materials such as polystyrene (PS), poly(methyl methacrylate) (PMMA), poly(acrylonitrile) (PAN) and poly(L-lactide) (PLLA) (see Section 4.2). The second strategy was to prepare TTA-UC based nanocapsules under protective conditions by avoiding the influence of sunlight during the synthetic procedure (see Section 4.3). The third strategy was to armor the nanocapsules by depositing cerium(IV) oxide on the surface via an *in situ* crystallization procedure (see Section 4.4). Further inorganic materials were also deposited on the surface of nanocapsules by various techniques (see Section 4.5). Finally, silicate clay solid particles were placed on the surface of the nanocapsules during the synthesis by Pickering miniemulsion (see Section 4.6).

## 2. Theoretical background

Luminescent materials have been attracting a considerable interest because spreading of photons in any medium leads to conversion of their energy, which can be used for various physical and biological applications. The basic principles involved in the luminescent process and in different kinds of emission processes from various electronically excited states are described in Section 2.1. The corresponding difference between the maxima of the absorption and emission spectrum is the so-called Stokes shift. Usually, the energy of the emitted photon is lower than the energy of the absorbed photon and is known as down-shifting. The increase of the energy of the emitted photon is called upconversion (UC), which is in contrast to other luminescent emission processes. The spectrum of upconversion emitted photons will be shifted into a region of higher light frequencies and this shift is known as Anti-Stokes shift. The upconversion process can occur in different systems and we focus on the triplet-triplet annihilation upconversion process (TTA-UC). The basic principles and the mechanism involved in the TTA-UC process are explained in Section 2.1.1. The influence of molecular oxygen on the TTA-UC quenching process is explained in Section 2.1.1.2.

The fluorescent and upconversion materials can be incorporated into different colloidal systems depending on their applications. An overview of colloidal systems with different materials and states of matter is explained in Section 2.2. The stability of colloids is an important aspect to be considered and is addressed in Section 2.2.1. The basic principles of miniemulsion and the types of emulsions are illustrated in Section 2.2.2. The different strategies to obtain the stabilization of emulsions are discussed in 2.2.3 and furthermore, the stabilization of emulsions by solid particles is explained in Section 2.2.4 which is so-called Pickering stabilization. The basic principles for the formation of nanocapsules are described in Section 2.2.5. The different types methods used to produce nanocapsules are explained in the last part of this chapter.

### 2.1. Luminescence

The spontaneous emission of electromagnetic radiation from electronically excited states (or vibrational excited states if revolved) not in thermal equilibrium with its environment is defined as luminescence. Depending on the mechanism of excitation, the luminescence is classified in different types, as described in Table 2.1. Luminescent processes can be observed

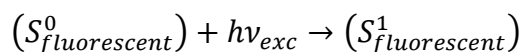
in aromatic hydrocarbons (perylene, porphyrins, pyrene, etc.), lanthanide ions, semiconductor nanocrystals, fullerenes, porphyrin metal complexes, and ruthenium complexes.<sup>32, 57</sup>

**Table 2.1.** Different types of luminescence.

Type of luminescence	Condition of excitation
Photoluminescence (fluorescence, phosphorescence, delayed fluorescence)	Absorption of light (photons)
Thermoluminescence	Occurrence of heating after storage of energy (e.g., radioactive irradiation)
Electroluminescence	Electric field
Cathodoluminescence	Cathode rays (electron beams)
Radioluminescence	Ionizing radiation (X-rays, $\alpha$ , $\beta$ , $\gamma$ )
Bioluminescence	Biochemical reaction
Chemiluminescence	Chemical reaction (e.g., oxidation)
Triboluminescence	Frictional and electrostatic forces
Sonoluminescence	Ultrasound

Photoluminescence is the process of spontaneous emission of photons accompanying the de-excitation which occurs by the interaction of light with matter. According to Stokes' rule, the fluorescent emitted light has a longer wavelength than that of the absorbed radiation.

The mechanism of absorption of photons in the ground state ( $S_{fluorescent}^0$ ) and excited to an electronic excited state ( $S_{fluorescent}^1$ ) is called photoluminescence (fluorescence and phosphorescence) and is the typical case of the luminescence. The process of excitation of a fluorescent molecule is represented as:



where  $h$  is Planck's constant and  $\nu_{exc}$  is the frequency of the excitation light.

A molecule in the state  $S_{fluorescent}^1$  can relax to the ground state via different pathways:<sup>17, 32, 57</sup>

- a. *Fluorescence*: a spin-allowed radiative transition from an excited state to the ground state (of same multiplicity) of the fluorescent molecule. It could be  $S_n^* \rightarrow S_0 + h\nu_{em}$  or  $T_n^* \rightarrow T_{n-1} + h\nu_{em}$ , where  $h$  is Planck's constant and  $\nu_{em}$  is the frequency of the emission light.

- b. A non-radiative relaxation process in which the excitation energy is dissipated as heat to the solvent.
- c. *Phosphorescence*: spin-forbidden radiative transition from excited triplet state ( $T_{fluorescent}^1$ ) to the ground state (of different multiplicity) of the fluorescent molecule.
- d. *Quenching*: molecular oxygen is a well-known quencher of the fluorescence and occurs generally in the triplet states.
- e. Collision fluorescence quenching can also occur during the process of relaxation from the singlet state to the ground state by interacting with a second molecule.

The efficiency of the fluorescence process is calculated by the fluorescent quantum yield ( $\Phi$ ), which is defined as the ratio of the number of photons emitted to the number of photons absorbed:

$$\Phi = \frac{\text{Number of photons emitted}}{\text{Number of photons absorbed}}$$

The emission of a photon is as fast as the absorption of a photon ( $\approx 10^{-15}$  s). However, before emitting a photon or undergoing other de-excitation process, an excited molecule stays in the excited state for a certain time (depending on the type of molecule and the medium, from a few tens of picoseconds to a few hundreds of nanoseconds).<sup>17, 58</sup>

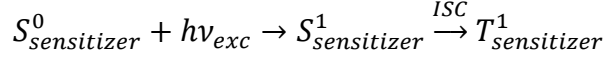
### 2.1.1. Basic principles and mechanism of triple–triplet annihilation upconversion (TTA-UC) process

Generally, TTA-UC process occurs by the involvement of two organic molecules dissolved in an organic solvent. The molecule that absorbs the optical energy and uses it for later on transformations is denoted as *sensitizer*. The other type of molecule present in the system and possessing a high fluorescent quantum yield ( $\Phi$ ), is stated as *emitter*. The TTA-UC process is based on a series of connective processes including intersystem crossing (ISC), triplet energy transfer (TET), triplet-triplet annihilation (TTA), and delayed fluorescence.<sup>59-60</sup> The energetic scheme of the process is represented in Figure 2.1.

The sensitizer absorbs the optical energy and the excitation of photon occurs from the ground state to the singlet state (Q-band) of the sensitizer ( $S_{sensitizer}^1$ ). Further, the photon is relaxed to the metastable sensitizer triplet state ( $T_{sensitizer}^1$ ) via intersystem crossing (ISC). In general, intermolecular transitions between states with different multiplicity are prohibited.



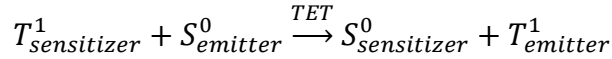
Nonetheless, the probability of the ISC process can be strongly strengthened by spin-orbit coupling with a heavy metal atom. Thus, using atoms like palladium or platinum with ISC efficiency closer to unity can reinforce the ISC process in the TTA-UC system:



where  $h$  is Planck's constant and  $\nu_{exc}$  is the frequency of excitation light.

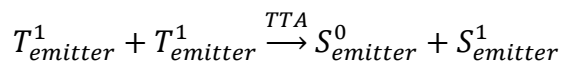
Four types of processes can occur from the  $T_{sensitizer}^1$  state:

- Emission of phosphorescent photon to the ground state of the sensitizer molecule ( $S_{sensitizer}^0$ ).
- Non-radiative triplet state relaxation, dissipating the optical energy as heat.
- The process of quenching of the metastable sensitizer triplet state ( $T_{sensitizer}^1$ ) by molecular oxygen and the generation of singlet oxygen.
- Triplet energy transfer (TET) between the optically created triplet ensembles of the sensitizer molecules to accessible triplet states of the emitter molecules ( $T_{emitter}^1$ ):

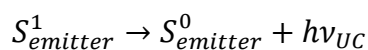


The excited triplet state of the emitter molecule can store the energy for a longer duration without any energy dissipation or phosphorescent photon emission. The reason behind this is that the emitter molecule has a negligible small ISC coefficient. If the same energy transfer process occurs within another pair of sensitizer and emitter molecules then one more emitter molecule is transferred into the excited triplet emitter state. Three types of process or energy dissipation can occur:

- A TTA process between two triplet excited emitter molecules  $T_{emitter}^1$ .
- The process of quenching of the emitter triplet state by molecular oxygen or a non-radiative relaxation to the ground state emitter molecule  $S_{emitter}^0$ .
- Out of the two triplets excited emitter molecules, one molecule returns to the ground state and the other molecule assembles the total energy and populates the excited emitter singlet state:



Finally, the delayed fluorescent photon is relaxed from the singlet state of the emitter molecule because of the high fluorescence ability:



where,  $\nu_{UC}$  is the frequency of the emitted delayed fluorescence (upconversion).

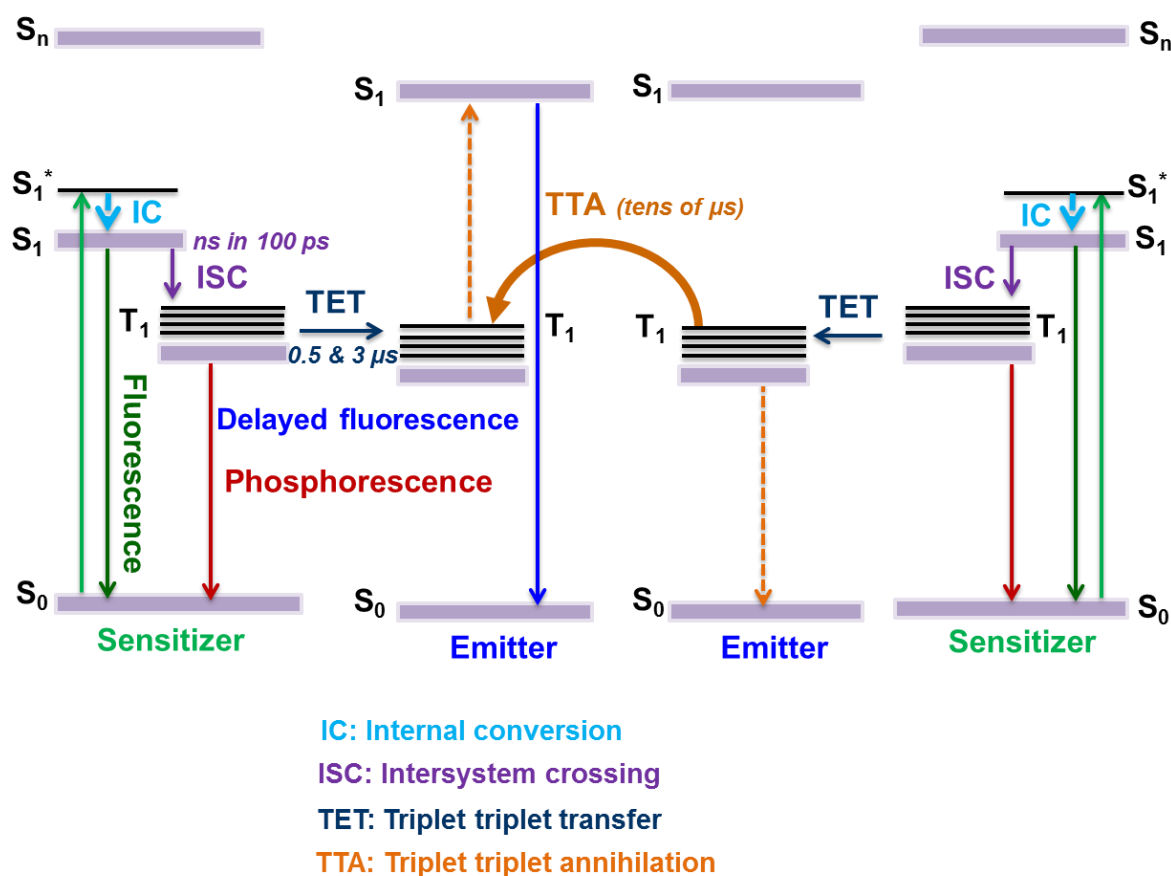


**Figure 2.1.** Simplified energetic scheme of the TTA-UC process: the green arrow represents excitation, the red represents the residual phosphorescence of a sensitizer, the orange represents the triplet-triplet annihilation, the blue represents the upconversion (delayed fluorescence of an emitter).

### 2.1.1.1. Factors required for an efficient TTA-UC process

To observe an efficient TTA-UC process, the series of the connective processes intersystem crossing (ISC), triplet energy transfer (TET), triplet-triplet annihilation (TTA) and delayed fluorescence should be maximized or efficient enough.<sup>61</sup> The process of intersystem crossing should be efficient to transfer the photon from the singlet state to the triplet state of sensitizer. To achieve this, the sensitizer molecule should have a high ISC coefficient. In parallel, the ISC coefficient for the emitter molecule should be very low, which prohibits the radiative decay process (phosphorescence) from the triplet state of emitter molecule:

$$C_{Sensitizer}^{ISC} \gg C_{emitter}^{ISC}$$

In the UC system, sensitizer and emitter molecules contain both triplet and ground states in which both have the capability to reabsorb the emitted UC photons by the emitter molecule. In order to reduce the reabsorption, the emission of UC photons should take place in a region of the spectrum free from the sensitizer and emitter ground state absorption. The process of reabsorption can be avoided once the concentration of the used emitter molecule is lower and has a large Stokes shift. The process of reabsorption occurs in the system with low efficiency of TTA-UC based systems, such as fac-(tris-(2,2'-phenylpyridine))iridium ( $\text{Ir}(\text{ppy})_3$ ). In such systems the strong reabsorption of emitted UC photons takes place when the strong absorption band of the sensitizer molecule overlaps completely with the fluorescent spectrum of the emitter.<sup>62</sup>

For example, systems with high TTA-UC efficiency such as porphyrins and phthalocyanines avoid the process of reabsorption. These metallated macrocycles have a band-like absorption spectrum, consisting of two strong bands – the Soret (absorption from  $S^0 \rightarrow S^2$ ) and the Q-band ( $S^0 \rightarrow S^1$ ). No optical absorption is observed for wavelengths lower than the Q-band and higher than the Soret band. Those wavelengths represent a so-called transparency window in which the efficient TTA-UC process occurs:

$$E(S_{Sensitizer}^0 \rightarrow S_{Sensitizer}^2) > E(S_{emitter}^1 \rightarrow S_{emitter}^0) \gg E(S_{Sensitizer}^0 \rightarrow S_{Sensitizer}^1)$$

The TTA-UC process is efficient once the combined energy of two emitter triplet states is greater than that of the excited emitter singlet state:

$$2 \times E(T_{emitter}^1) \geq E(S_{emitter}^1)$$

The triplet energy transfer between the triplet states of the sensitizer and the emitter molecule is efficient once the triplet states have similar level and overlap with each other.<sup>63-64</sup>

$$E(T_{Sensitizer}^1) \cong E(T_{emitter}^1)$$

### **2.1.1.2. Role of molecular oxygen on the TTA-UC process**

The TTA-UC process occurs by the involvement of triplet states of the sensitizer and emitter molecules. The energy transfer process from the triplet state of the sensitizer to the emitter takes place in times of the order of microseconds. This time is more than enough for the molecule of oxygen to occupy the energy from the sensitizer molecule during the TET



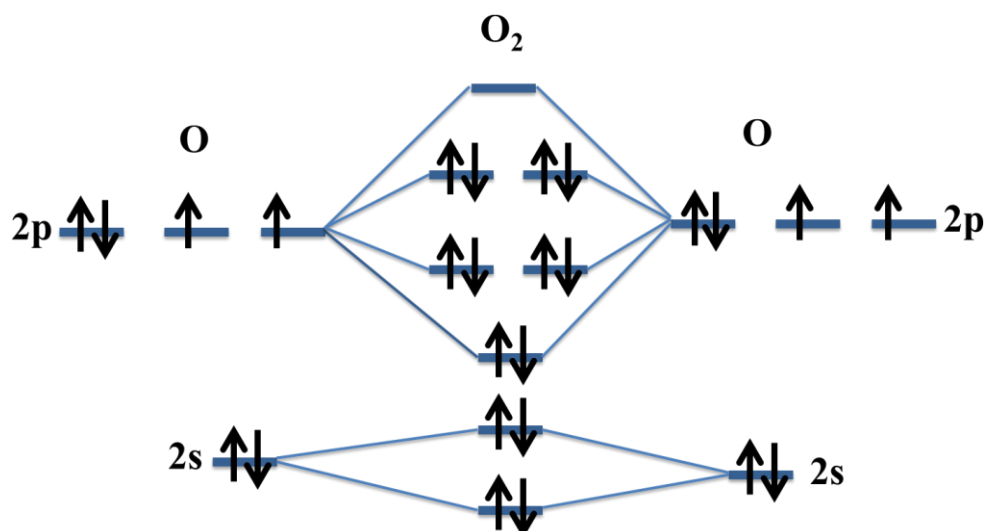


Figure 2.3. Molecular orbital diagram of oxygen.

## 2.2. Colloidal systems

A colloidal system is a heterophase mixture system composed of two immiscible phases: a discontinuous phase (dispersed phase) is distributed uniformly in a dispersion medium (continuous phase).<sup>65-66</sup> The colloidal size range of the dispersed phase in the continuous phase is defined as extending over a range from a few nanometer to few tens micrometers. Both phases are generally differentiated from each other and, depending on their specific physical states, different names are proposed for colloidal systems, as given in Table 2.2.<sup>66</sup> Some of the colloidal states do not accomplish thermodynamic equilibrium but the state may be long lived, which is theoretically or practically difficult to differentiate from an equilibrium phase.

Table 2.2. Examples typical colloidal systems.

Dispersed phase	Continuous phase		
	Gas (fluid)	Liquid	Solid
Gas (bubbles)	---	Foam	Solid foam
Liquid (droplets)	Liquid aerosol	Liquid emulsion	Solid emulsion
Solid (particles)	Solid aerosol	Suspension	Solid suspension

### 2.2.1. Stability of colloids

Colloidal stability is achieved only when both phases are well dispersed and evenly distributed. It can be defined in terms of the capability of the colloidal system not to aggregate or sediment under the influence of gravity. In the absence of any stabilization mechanism, colloidal particles are likely to aggregate due to the attractive interaction between particles arising from van der Waals forces. The stabilization between two similar charged particles occurs when the repulsive forces overcome the van der Waals attraction. The balance between the van der Waals interaction and the repulsion between electrical double layers surrounding charged particles can be controlled to provide an energetic barrier to the coagulation of particles.

Three main types of processes are involved in stabilization of colloidal dispersions: *electrostatic stabilization* refers to the Coulombic repulsion between two similarly charged particles and *steric stabilization* refers to a dense amphiphilic polymer adsorbed or chemically attached to the surface of colloidal particles (entropic and enthalpic hindrance of polymer chains). If the particles contain functional groups with charge, both electrostatic repulsion and steric hindrance will simultaneously occur and which is known as *electrosteric stabilization* (see Figure 2.4).

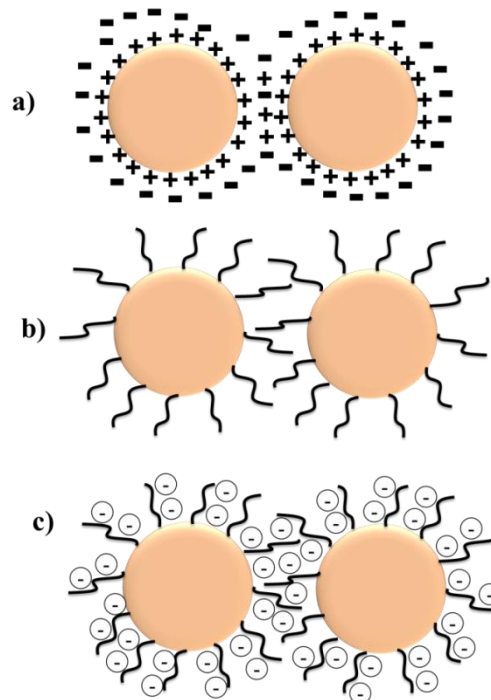


**Figure 2.4.** Stability of colloidal particles is depended on three main types: a) electrostatic stabilization b) steric stabilization and c) electrosteric stabilization.

The addition of charged surfactants is useful to achieve electrostatic stabilization. When two droplets stabilized with charged surfactants at the liquid/liquid interface approach each other, the droplet collision is avoided due to Coulomb repulsion. A large number of differently functionalized inorganic stabilizers can be also useful to achieve the stabilization of colloidal droplets. The combination and balance of electrostatic attractive forces with repulsive forces is described on the basis of the DLVO (Derjaguin, Verwey, Landau and Overbeek) theory between a pair of colloidal particles and denoted as:<sup>67</sup>

$$V_T = V_A + V_R$$

where  $V_T$  is the total potential energy of the colloidal particles interaction,  $V_A$  the attractive potential energy, and  $V_R$  the repulsive interaction:

$$V_A = \frac{-A}{12} \left[ \frac{1}{x(x+2)} + \frac{1}{(x+1)^2} + 2 \ln \frac{x(x+2)}{(x+1)^2} \right]$$

where  $x = \frac{D}{2r}$ .

The attractive potential energy  $V_A$  is directly proportional to the particle radius ( $r$ ) and to a material constant called Hamaker constant ( $A$ ), and is inversely proportional to the distance of separation ( $D$ ). The Hamaker constant is a function of both the electronic polarizability and the density of the material.<sup>68</sup> When the distance between two particles is small ( $D \ll 2r$ ), the above equation can be simplified as:

$$V_A = -\frac{Ar}{12D}$$

The electrostatic repulsive interaction  $V_R$  could be given as:

$$V_R = \psi_0 \cdot \exp(-kD)$$

with  $k = \sqrt{\frac{2c_0e^2}{\epsilon\epsilon_0k_B T}}$ .

where  $\psi_0$  is the Stern potential,  $k$  is a constant,  $c_0$  is the ion concentration,  $k_B$  the Boltzmann constant,  $D$  is the interparticle distance and dielectric constants of the bulk electrolyte solution  $\epsilon$ , and of vacuum  $\epsilon_0$ . The constant  $k$  is usually denoted as the reciprocal of the Debye length ( $\kappa$ ) which is expressed as the distance to which the electrostatic potential is decayed to the  $1/e$  of the surface potential.

## 2. Theoretical background

The total energy potential of the charge-stabilized colloidal particles of same charge with a radius  $D$  of identical particles could be denoted as follows:

$$V_T = V_A + V_R + V_B = \frac{-AR}{12D} + \psi_0 \cdot \exp(-kD) + \frac{1}{D^{12}}$$

The total electrostatic potential curve for two charge-stabilized systems including van der Waals attraction, electrostatic repulsion, and Bonn repulsion is shown in Figure 2.5-a.<sup>66, 69</sup> The electrostatic repulsion will prevent the two similar charged particles to get attracted to each other. The colloidal dispersion is stable when the particles can overcome the energy barrier ( $V_m$ ), below which the particles have no sufficient energy to contact with each other. The height of the energy barrier, illustrated in Figure 2.5-a, represents the stability of the colloids and could be easily altered by the concentration of ions in the dispersion. The energy barrier of the system decreases or disappears once the electrolyte concentration in the dispersion is increased (see Figure 2.5-b). Nonetheless, an irreversible coagulation process (primary minimum) occurs when the strong van der Waals attractive force draws the two particles together and also once the energy barrier is overcompensated. In a few systems, a reversible process of aggregation occurs, yielding a secondary minimum at longer distances known as flocculation.<sup>66</sup>

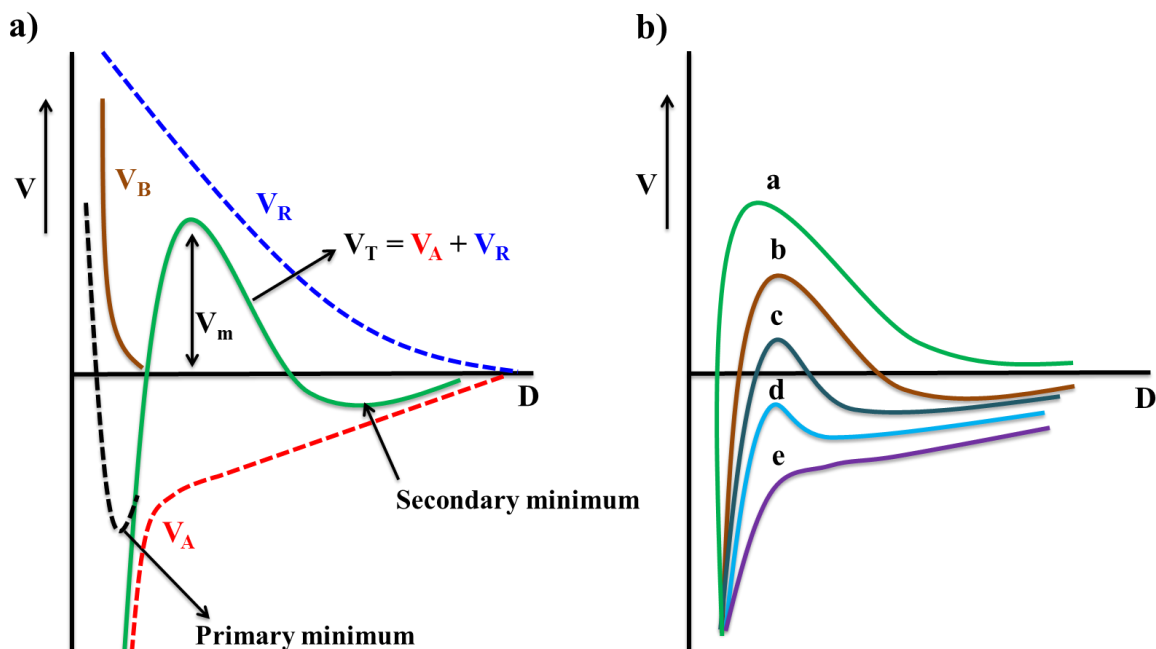


**Figure 2.5.** a) Interaction potential of two particles with different distances according to DLVO theory and b) effect of electrolyte concentration (increased from a to e) on the energy barrier. Adapted with permission from Napper. Copyright (1970) American Chemical Society.<sup>71</sup>



As indicated above, the other mechanism to improve colloidal stability is the steric stabilization, which refers to the steep repulsion between two particles in a good solvent as a result of a stabilizing polymer on the surface.<sup>70</sup> A number of factors are involved in the achievement of an effective steric stabilization. For adsorbing amphiphilic polymers, we require:<sup>66</sup>

- High surface coverage of the particle,  $\Gamma$
- Strong adsorption,  $\chi_s > \chi_{sc}$
- Good solvent for stabilizing chain,  $\chi < 0.5$
- Low free polymer concentration,  $c_{eq} \approx 0$

A protective layer of dense polymer chains is covered on the surface of colloidal particles with thickness  $\delta$  (see Figure 2.6-a). The covered polymer chains will overlap once the interparticle distance  $D$  is closer than  $2\delta$  and leads to increase in the chain density with the decrease of chain movement in the region between two particles. The steric potential ( $V_S$ ) then raises to resist the van der Waals attraction potential ( $V_A$ ) (see Figure 2.6-b).

The theory of solubility of polymers based on net solvent-polymer interaction energy is developed by Flory and Huggins. It is defined as:

$$x \left[ \left( u_{12} - \frac{1}{2}(u_{11} + u_{22}) \right) \right] \frac{z}{k_B T} = \frac{\Delta u}{k_B T}$$

where 1 refers to solvent and 2 to a polymer segment;  $T$  is the absolute temperature;  $z$  is a coordination number; and  $k_B$  is the Boltzmann constant. The strong steric potential for stabilization is obtained in a good solvent when the repulsive forces between the polymer segments makes the polymer coils to swell (Flory-Huggins parameter  $\chi < 0.5$ ). However, the process of destabilization is occurred when the solvent is not good enough for the polymer (Flory-Huggins parameter  $\chi > 0.5$ ), and the polymer coils will then shrink.

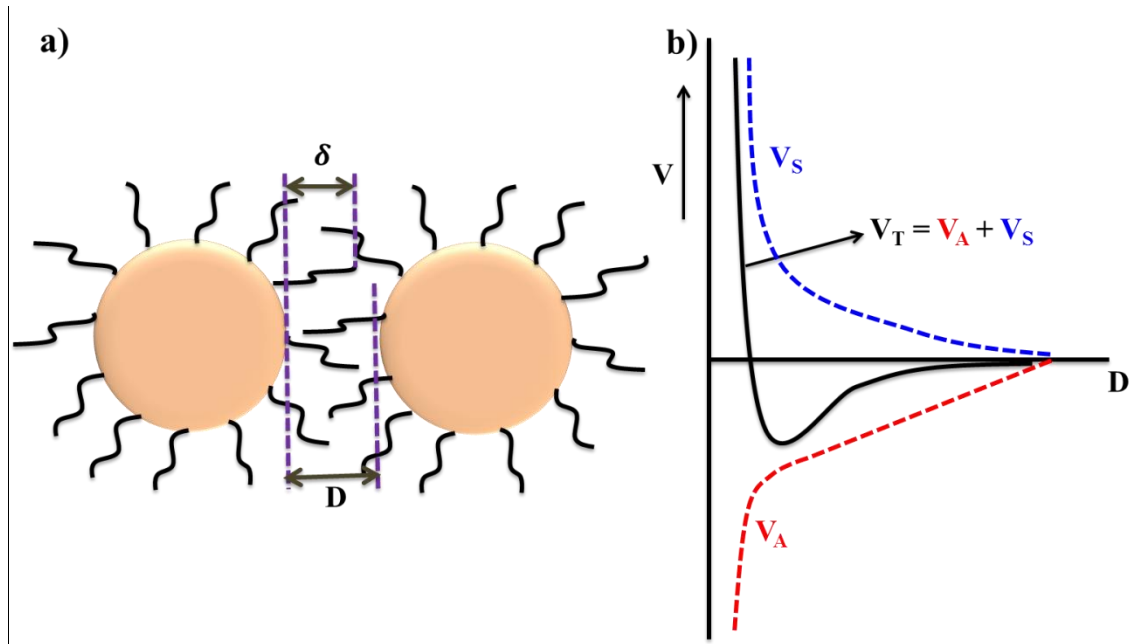


**Figure 2.6.** Schematic representation of steric stabilization of colloidal particles by non-ionic polymer.

### 2.2.2. Emulsions

Emulsions are dispersions of liquid droplets (dispersed phase) in another liquid (continuous phase); the two liquid phases are essentially immiscible to each other. In principle, the emulsions are classified into two types: oil/water (O/W) or direct emulsions and water/oil (W/O) or inverse emulsions.<sup>71-74</sup>

Depending on their size and stability, emulsions are classified into three types: macroemulsions, microemulsions and miniemulsions.<sup>71</sup>

- The size of droplets with 1-100  $\mu\text{m}$  is referred to as macroemulsions. Normally, in macroemulsions, when  $\gamma_{12}$  is around a few tens of  $\text{mN m}^{-1}$  then the  $\Delta S_{conf}$  term is much lower in magnitude than the  $\Delta A\gamma_{12}$  term and thus, the value of  $\gamma_{12}$  is controlled by the addition of surfactants which makes the macroemulsions kinetically stable. This type of emulsion system needs external energy interference, such as stirring or shaking.<sup>25</sup>
- The size of droplets with 10 to 100 nm is denoted as microemulsions and the term was first used by Schulman et al.<sup>75</sup> Microemulsions are thermodynamic stable emulsions and are formed once the  $\Delta G_{form}$  is negative. In general, they are observed when the interfacial tension ( $\Delta\gamma_{12}$ ) between two liquids is sufficiently low ( $\sim 10^{-4}$  to  $10^{-2}$   $\text{mN m}^{-1}$ ) and the  $\Delta S_{conf}$  term is greater in magnitude than the  $\Delta A\gamma_{12}$  term. Depending on the

nature, the formation of stable microemulsions is obtained by using a concentration of surfactant higher than the critical micellar concentration (CMC) and a co-surfactant is added in addition to the surfactant. High shear force is not required and general mixing is enough to obtain microemulsions.

- Miniemulsions have typical droplet sizes between 50 to 500 nm and were originally reported by Ugelstad et al.<sup>76-77</sup> In these kind of emulsions the  $\Delta G_{form}$  is considered as net positive rather than net negative when the  $\Delta S_{conf}$  term is smaller than the  $\Delta A\gamma_{12}$  term. The surfactant concentration is lower than the CMC and a costabilizer with low molecular weight are commonly used to stabilize the miniemulsions.<sup>78</sup> These kinds of emulsions are kinetically stabilized and that high shear forces are necessary.

### 2.2.2.1. Surfactants

A surfactant is a substance that decreases the surface tension of the medium in which has been dissolved, and/or the interfacial tension with other phases; accordingly, it is positively adsorbed at the liquid/vapor interface and/or at other interfaces.<sup>66</sup>

The physical properties of the interfaces (liquid/liquid, solid/liquid, and gas/liquid systems) on which the surfactants molecules are adsorbed are altered once they are dissolved in a solvent at low concentration. The surfactant molecules are surface-active agents or amphiphilic molecules (both oil- and water-loving). The surfactant molecule stays at the interfaces to keep the lyophilic part in the solution and to reduce the strong interaction of the lyophobic part with the solvent. The amphiphilic molecules consist of hydrophilic and hydrophobic units, typically named as ‘head’ and ‘tail’, respectively. The adsorption and aggregation of surfactant molecules can be determined by their hydrophobic nature when the tail part is dissolved in a solvent (for instance, water is the most common solvent).<sup>79</sup> The aggregation of surfactant molecules depends on their aqueous concentration. If the concentration is above CMC, then they tend to form well organized large structures which are liquid crystalline. The factors influencing the critical micellar concentration (CMC) of a surfactant are:<sup>66</sup>

- Length of the hydrocarbon chain
- Temperature
- Hydrophilic groups
- Counterion effect
- External additives (salt addition)

Surfactants are classified into three basic classes, depending on the nature or structure of both the head and tail groups. They are:<sup>66</sup>

1. Anionic surfactants: These surfactants contain anionic functional groups at their head group. Examples of these surfactants are sodium dodecyl sulfate (SDS), ammonium lauryl sulfate, alkylbenzene sulfonates, alkyl ether sulfates, and phosphate esters.
2. Cationic surfactants: These surfactants contain cationic functional groups at their head group. Examples: cetyl trimethylammonium bromide (CTAB), cetyl trimethylammonium chloride (CTAC), and benzalkonium chloride (BAC).
3. Non-ionic surfactants: These are surfactants with no charge at their head group. The most commonly used non-ionic surfactants in miniemulsion polymerization are alkyl poly(ethylene glycol ethers) and alkylene oxides.
4. Zwitter-ionic surfactants: These surfactants contain both positive and negative groups, that is, they are amphoteric. The positive charge is often an ammonium group and the negative charge is a carboxylate.

### 2.2.3. Emulsion polymerization

Emulsion polymerization can be classified in three types: macroemulsion, miniemulsion, and microemulsion polymerization.<sup>72, 80-81</sup> This classification is based on the mechanism of polymerization and the mechanisms of stability.

The microemulsion system occurs when an amount of surfactant or surfactant/cosurfactant mixture is used to obtain a thermodynamically stable emulsion. In microemulsion systems, the interfacial tension between two liquid phases is close to zero because of the presence of high amounts of surfactant. The initiator radicals can be in the continuous phase or in the dispersed phase. In this kind polymerization process, the initiation process does not occur at the same time in all microdroplets leading to a final state containing polymer particles in coexistence with empty micelles.

In the macroemulsion polymerization, the monomer is present in an aqueous solution containing surfactant micelles. The surfactant concentration is above the critical micellar concentration (CMC). The polymerization process starts by the water soluble initiator which is dissolved in the continuous phase. Big monomer droplets with diameter of  $\sim 1-10 \mu\text{m}$  and empty or swollen monomer micelles are present in the initial stage of the macroemulsion polymerization process. The initiator radicals in the continuous phase react with the monomer

molecules and create oligoradicals. These oligoradicals migrate to micelles and increase in amount when compared to those of monomer droplets present in the continuous phase. The polymer particles are formed inside the micelles when the monomer diffuses through the continuous phase from the reservoir droplets to micelles. This polymerization method is limited to monomers that have sufficient water solubility.

The size of the droplets is smaller in miniemulsion system when compared to the other two types of emulsion polymerization methods. To adjust the droplet size, high shear forces such as ultrasound or high-pressure homogenization are generally used. In this kind of system, free surfactant micelles are not available, and the polymerization step occurs when the initiator radicals enters the monomer droplets. The initiator radicals can be in the continuous or in the dispersed phase. During the polymerization step, micron-sized droplets are formed when the monomer is soluble in the continuous phase. In miniemulsion polymerization, the ratio of number of initial droplets to the polymer particles is 1:1.

### ***2.2.3.1. Nucleation mechanisms***

Essentially, the three main mechanisms involved in particle nucleation mechanism for emulsion polymerization are: the micellar nucleation, the homogeneous nucleation and the droplet nucleation.

- **Micellar nucleation:** In this mechanism, the chain propagation of a polymer chain occurs once the initiator radicals enters into a swollen monomer surfactant micelle and reacts with the monomer. The process of micellar nucleation can be only achieved above the critical micellar concentration (CMC) of the used surfactant in the system. This is observed in usual microemulsion polymerization. In microemulsion polymerizations, the monomer diffuses from other monomer swollen micelles, which serve as monomer reservoirs. In miniemulsions the overall concentration of surfactant might be larger. However, due to the interfaces, surfactant concentration of free surfactant molecules in water below the level of CMC.<sup>82</sup>
- **Homogeneous nucleation:** This mechanism is important for surfactant-free emulsion polymerization, but it has less significance in miniemulsion polymerization of styrene. Water-soluble oligomers are generated when the initiator radicals attacks the monomer units and further acts as nucleating sites. The polymer chain propagation and

termination occurs when the monomer units moves to the nucleating sites by diffusion.<sup>72, 83-84</sup>

- Droplet nucleation: This is the main mechanism in miniemulsion polymerization. The droplets formed during the emulsification step are polymerized via radicals who enter the monomer droplets. In the case of batch miniemulsion polymerizations, the monomer diffusion to the reaction sites is of no kinetic importance because there are already the maximal concentration of monomer at all reaction sites. In general, the nucleation of every single droplet depends on the statistics of radical entry and overall size. During this polymerization process the particle number does not change.<sup>71-72, 84</sup>

### 2.2.4. Stability of emulsions

In the emulsion system, stability of emulsions is an important factor to consider and is controlled by the process involved in the growth of droplets. The growth of droplets in emulsions occurs by two processes: coalescence and Ostwald ripening (see Figure 2.7).<sup>78, 85</sup> Kinetically stabilized emulsions, stable for up to several months, are obtained by suppressing the process of coalescence and Ostwald ripening. The process of coalescence occurs by collision of two droplets with each. This kind of collision results in the formation of larger droplets, which leads to destabilization of emulsion system. The coalescence of the particles is generally avoided by the addition of surfactants.<sup>85-86</sup>

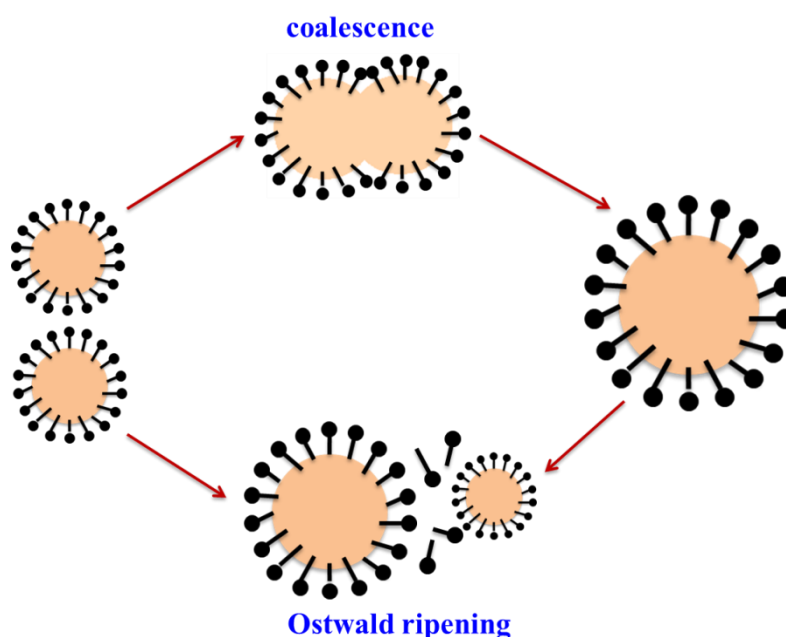


**Figure 2.7.** Schematic representation of coalescence and Ostwald ripening process of colloidal particles in a miniemulsion system.

Ostwald ripening refers to a process of diffusion of smaller droplet to a bigger one due to the difference in Laplace pressure and chemical potential. The Laplace pressure is depending on the radius of the droplet, so that it is different for droplets with different sizes. The pressure difference across a liquid/liquid interface is expressed by the Laplace equation:<sup>78, 87</sup>

$$\Delta p = \frac{2\gamma}{r}$$

where  $r$  is the radius of curvature and  $\gamma$  is the interfacial tension.  $\Delta p$  is smaller for large droplets than for small ones. The total energy of the system is reduced by the process of migration of molecules from the smaller droplets, across the continuous phase, into the larger droplets.

Ostwald ripening is not observed in ideally well monodispersed emulsions. The important factor that contributes the Ostwald ripening is:<sup>66</sup>

The solubility, in the continuous phase, of the molecules comprising the droplets increases; this will enhance the rate of transfer between droplets. Indeed, it is sometimes observed that the presence of surfactant (above the CMC) enhances the rate further. This is achieved by an overall increase of the effective concentration in the continuous phase, because the molecules from droplets will be solubilized in the surfactant micelles.

The reduction of Ostwald ripening is possible by adding a component to the droplet phase with a lower solubility in the continuous phase than in the disperse phase, which is commonly called costabilizer.<sup>72</sup> In water-in-oil emulsions, the costabilizer should be water-insoluble and monomer-soluble, i.e. hydrophobe and in oil-in-water emulsions, salts are used as costabilizer. The most common costabilizer used in direct miniemulsions are hexadecane, and inorganic salts, such as sodium chloride in inverse miniemulsion.<sup>82</sup> Polymers with hydrophobic nature have also used to reduce Ostwald ripening, for instance, styrene emulsions are stabilized by using polystyrene<sup>88</sup> and MMA emulsions are stabilized by poly(methyl methacrylate).<sup>89</sup> The concentration of costabilizer in the shrinking droplet would increase once the diffusion from a smaller droplet to a bigger one occurs, and further cause an increase in the osmotic pressure  $\Pi_{\text{Osm}}$  within the droplet, represented as:<sup>87</sup>

$$\Pi_{osm} = \frac{R \cdot T \cdot C}{M}$$

where;  $M$  is the molecular weight of costabilizer,  $R$  the universal gas constant,  $T$  the temperature, and  $C$  the concentration of costabilizer. The osmotic pressure counteracts the Laplace pressure and prohibits the inter-droplet diffusion.

### 2.2.5. Emulsion stabilization via solid particles: Pickering emulsions

An alternative method to stabilize emulsions is the use of small solid particles instead of surfactant molecules. This type of emulsion is stabilized by the adsorption of small solid particles at the oil-water interface. The most common materials used to stabilize the emulsion system are clay minerals. This effect was first proposed by Pickering in 1907. Therefore, these emulsions are known as Pickering emulsions.<sup>90-91</sup> Due to the absence of conventional surfactants, Pickering emulsions are particularly used for cosmetic and pharmaceutical applications. Emulsions are more stable once the droplets are covered by solid nanoparticles. The solid particles used for the process of stabilization are smaller (sub-micron, < 100 nm) than the emulsion droplets. Droplets for Pickering emulsions are usually larger than 100 nm, the droplets are not necessarily completely covered with solid particles. In Pickering emulsions, the adsorption of solid particles helps in the reduction of bare oil-water interface and stabilizes the complete system.<sup>91-93</sup> Pickering droplets with the absence of solid particles at the surface leads to coalescence/flocculation, which minimizes the total interfacial area of the oil-water interface.<sup>95</sup> The stabilization of these emulsions can be achieved by different kinds of solid particles made of organic compounds, polymers, clays (montmorillonite, laponite) or metal oxides.<sup>94</sup>

The partial wetting of the solid by water and oil results in the adsorption of particles at the oil-water interface. The three interfaces present in the system are oil-water, solid-oil and solid-water, and the corresponding interfacial energies are represented as  $\gamma_{O-W}$ ,  $\gamma_{S-O}$ , and  $\gamma_{S-W}$ .<sup>95</sup> The wetting process of the solid by the oil inside a water medium results in the occurrence of a negative spreading coefficient  $S(O/W)$  of oil, and the adhesion energy of the oil,  $E_{Adh}(O/W)$  is positive:

$$S(O/W) = -E_{Adh}(W/O) = \gamma_{S-W} - \gamma_{O-W} - \gamma_{S-O} < 0$$

$$E_{Adh}\left(\frac{W}{O}\right) = -S\left(\frac{W}{O}\right) = \gamma_{S-W} + \gamma_{O-W} - \gamma_{S-O} > 0$$



The spreading coefficient of water,  $S(W/O)$ , is negative and the adhesion energy of water,  $E_{Adh}(W/O)$ , is positive when the partial wetting of the solid by water inside an oil medium is obtained:

$$S(W/O) = \gamma_{S-o} - \gamma_{O-w} - \gamma_{S-w} < 0$$

$$E_{Adh}(W/O) = \gamma_{S-o} + \gamma_{O-w} > 0$$

If the solid particles are too hydrophobic, they would be totally wet by the oil in the system, and if they are too hydrophilic, they would be totally wet by the water. This effect leads the solid particles not to adsorb and remain separately dispersed in the aqueous phase of the emulsion. By using Young's law, under partial wetting conditions, the contact angle in oil,  $\theta_o$ , and in water  $\theta_w$ , is expressed as ( $\theta_o = \pi - \theta_w$ ):

$$\cos(\theta_o) = \frac{\gamma_{S-w} - \gamma_{S-o}}{\gamma_{W-o}}$$

$$\cos(\theta_w) = \frac{\gamma_{S-o} - \gamma_{S-w}}{\gamma_{W-o}}$$

The process of adsorption of solid particles at the oil-water interface is very strong under partial wetting conditions. The two main parameters involved in the free energy of adsorption are size and interfacial tensions of the solid nanoparticles. The free energy of adsorption for spherical particles with radius 'r' is:<sup>96</sup>

$$\Delta_{ads}F = -\pi r^2 \gamma_{O-w} (1 - \cos(\theta_w)) \text{ for } \theta_w < 90^\circ$$

$$\Delta_{ads}F = -\pi r^2 \gamma_{O-w} (1 + \cos(\theta_w)) \text{ for } \theta_w > 90^\circ$$

The adsorption of solid nanoparticles is stronger when the contact angle is  $90^\circ$ , which results in a higher stability of the emulsions. Hydrophilic solid particles with a contact angle  $\theta < 90^\circ$  form direct emulsions, and systems with hydrophobic particles with a contact angle  $\theta > 90^\circ$  form inverse emulsions.<sup>94</sup> In some cases, if  $\theta = 90^\circ$ , then the formation of bicontinuous emulsions can occur.<sup>97</sup> The adsorption free energy per unit interfacial area covered by adsorbed particles is  $\Delta_{ads} \frac{F}{\pi R^2}$ , which is not depended on the particle size.<sup>98-99</sup>

### 2.2.6. Capsule formation

Polymeric nanocapsules are comprised of a liquid core surrounded by a (thin) layered solid shell. The solid shell can be composed by the polymeric materials or inorganic components and the liquid core can be composed by hydrophobic and hydrophilic liquids, water, and aqueous solutions. According to the model described by Torza and Mason, the morphology of emulsion system containing three immiscible liquids, where two immiscible liquids are dispersed in a third immiscible liquid with a spreading coefficient  $S_i$ . This coefficient depends on the interfacial tensions between each phase  $i, j$  and  $k$  ( $\gamma_{ij}, \gamma_{jk}, \gamma_{ik}$ ) and is expressed as:<sup>100</sup>

$$S_i = \gamma_{jk} - (\gamma_{ij} + \gamma_{ik})$$

In this kind of system, the hydrophobic liquid phases (oil) 1 and 3 are suspended in a third immiscible liquid phase 2. The three possible configurations that can be obtained when the interfacial tension was estimated as  $\gamma_{12} > \gamma_{23}$ , i.e.  $S_1 = \gamma_{23} - (\gamma_{12} + \gamma_{13}) < 0$  and clearly explained below (Figure 2.8):

- Two possible configurations can occur when the hydrophobic natures of oil 1 and 3 are similar ( $\gamma_{12} \approx \gamma_{23}$ ):
  - a) The surface tension between the two oil phases can get high ( $\gamma_{31} > (\gamma_{12} + \gamma_{13})$ ). This results in the formation of two separated droplets with spreading coefficient  $S_1 < 0, S_2 > 0, S_3 < 0$ .
  - b) The surface tension between the two oil phases can get low ( $\gamma_{31} < (\gamma_{12} + \gamma_{13})$ ). This results in the partial engulfment of oil 1 with spreading coefficient  $S_1 < 0, S_2 < 0, S_3 < 0$ .
- A third possible configuration can occur if the hydrophobic nature of oil 3 is higher than that of the oil 1 ( $\gamma_{12} > \gamma_{23}$ ) and lowers the surface tension between the two oil phases ( $\gamma_{31} < (\gamma_{12} + \gamma_{13})$ ). This kind of effect results in the core-shell morphology with spreading coefficient  $S_1 < 0, S_2 < 0, S_3 > 0$ .

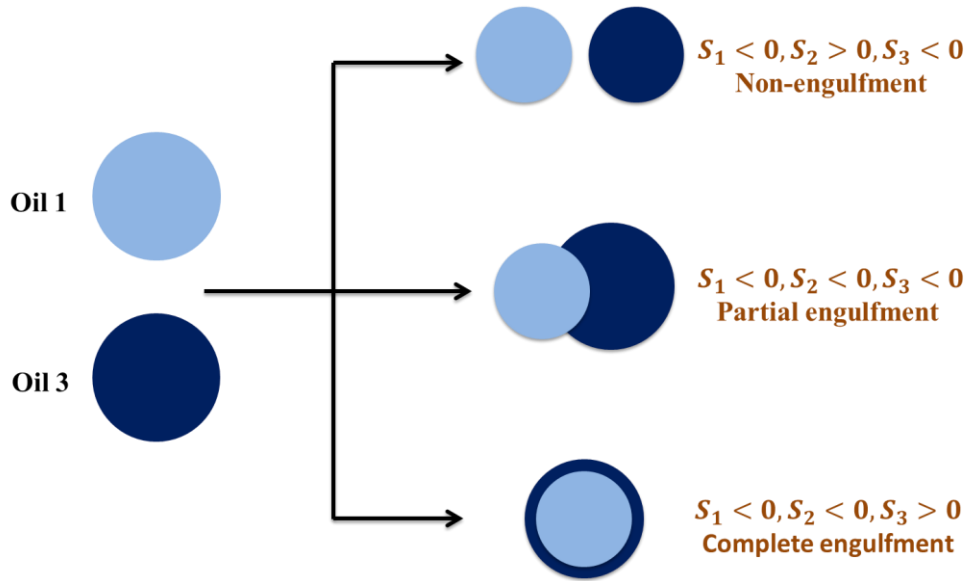


**Figure 2.8.** Illustration of possible morphologies occurred in accordance to different spreading coefficients  $S_i$ : immiscible droplets liquid 1 and liquid 3 are dispersed in immiscible medium liquid 2. Copyright (1970), with permission from Elsevier.<sup>101</sup>

The model mentioned above is mainly applied for immiscible compounds with low molecular weight. The equilibrium morphologies are not obtained when compounds with high molecular weight are involved in the system. In the emulsion system, the phase separation occurs because of the size of the polymer chains with respect to their mobility. The main driving force to be considered in these systems for final configuration is the variation of free energy. In an emulsion system with polymer 1 and 2, and water, the total free energy ( $\Delta G$ ) for all kind of morphologies is proposed by Chen et al. and described by the following equation:<sup>101</sup>

$$\Delta G = \sum \gamma_{ij} A_{ij} - \gamma_0 A_0$$

where  $\gamma_0$  and  $A_0$  are the initial interfacial tension and the area of the system, respectively, and  $\gamma_{ij}$  and  $A_{ij}$  are the interfacial tension and the interfacial area between  $i$  and  $j$ . The configuration with a minimal free energy change will be the thermodynamically favored one.

Several factors such as the chain mobility of the polymer phases,<sup>102</sup> temperature during the preparation of capsules or particles,<sup>103</sup> the rate of solvent evaporation,<sup>104</sup> reaction kinetics,<sup>105</sup> the interfacial tension between the phases which depends on the nature of the phases and the surfactant used<sup>106</sup> influence the final morphologies of an emulsion system with multiple phases.

In inverse miniemulsions, the formation of capsules is governed by two component reaction at the liquid/liquid interface and by the hydrophilic liquid that is encapsulated in the nanocapsule. In direct miniemulsions, core and shell materials are generally present inside the droplet before the phase separation forms the capsule morphology. Direct miniemulsions allows the encapsulation of hydrophobic liquids. The phase separation occurs either during a polymerization step or during evaporation of solvent. The two approaches used to produce hybrid nanocapsules are described in the following.

### 2.2.6.1. Nanocapsule formation by miniemulsion polymerization method

The formation of capsules occurs by the phase separation between the solvent and the formed polymers during the miniemulsion polymerization step.<sup>82</sup> As shown in Figure 2.9, the continuous phase at the beginning contains surfactant and water, and the dispersed phase is composed of monomer, hydrophobic oil, and a hydrophobic initiator. The dispersed phase form droplets after the process of ultrasonication and is stabilized by surfactant molecules present in the water phase. Before the polymerization step, the monomer and the initiator are dissolved within the hydrophobic oil. Once the polymerization starts, the formed polymers become immiscible within the hydrophobic oil and phase separation in the droplets occurs. One common example is the formation of polystyrene capsules via polymerization method. The dispersed phase contains styrene (St) as a monomer, hexadecane as a hydrophobic liquid, and 2,2'-azobis(2-methylbutyronitrile) as a hydrophobic oil-soluble initiator. The shell formation is possible because the interfacial energy between the polymer and water is lower than between the hydrophobic core liquid and water.

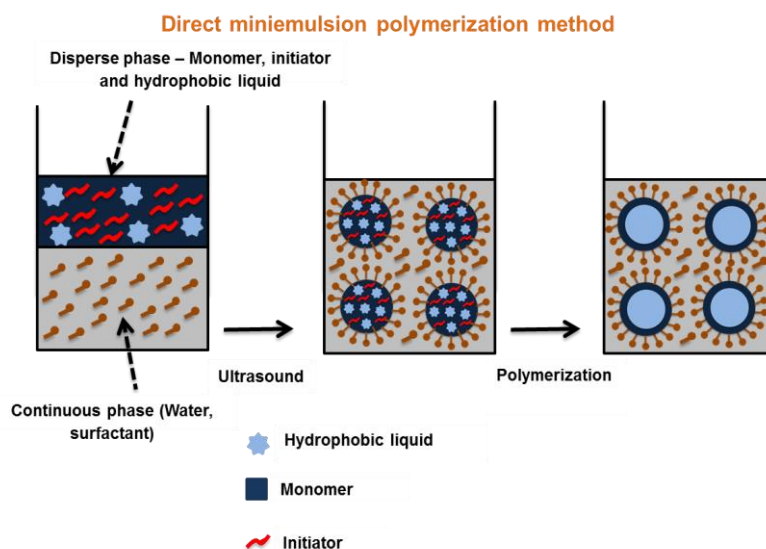


**Figure 2.9.** Schematic representation of the capsule formation by miniemulsion polymerization.

### 2.2.6.2. Nanocapsule formation by solvent evaporation method

The solvent evaporation method allows for the encapsulation of hydrophobic upconversion dyes, antiseptic agents, drugs in a hydrophobic liquid core and is useful for life science applications.<sup>107-109</sup> The formation of capsules by this method is obtained by using pre-synthesized polymers dissolved in a good solvent and mixed with a non-solvent. The phase separation between the polymer and its non-solvent in the dispersed droplets occurs during the slow evaporation of the solvent. The process of formation of nanocapsules by solvent evaporation is shown in Figure 2.10.

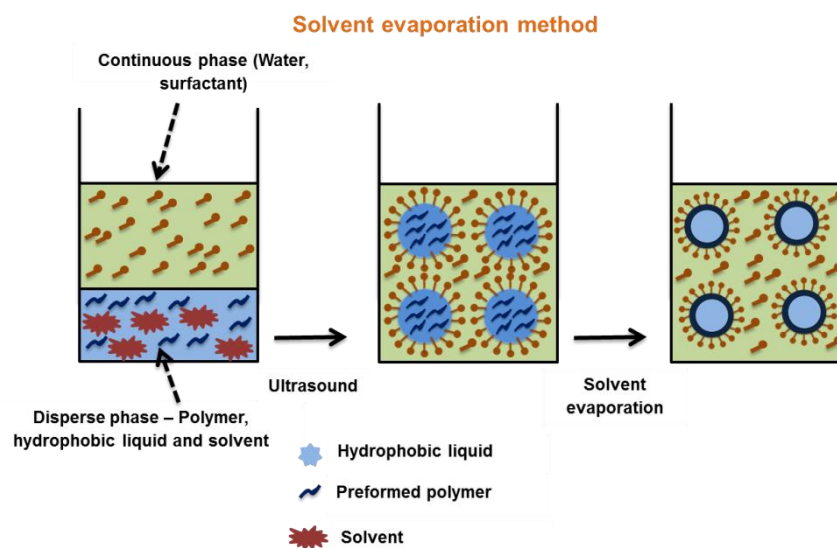


**Figure 2.10.** Schematic representation of capsules formation via solvent evaporation method.

## 3. Characterization techniques

### 3.1 Transmission electron microscopy (TEM)

TEM is a microscopic technique in which an accelerated electron beam transmits through a thin specimen and interacts with it. The generation occurs through a thermal emission at a thermionic cathode at an acceleration voltage of 50-200 kV and the transmitted electrons are detected. Scattering of the beam results after the interaction of electrons on to the specimen and the image is detected by using electromagnetic lenses. The transmitted electrons are detected under the specimen by a CCD chip, which gives a clear picture of the specimen. The ratio of scattered-to-transmitted light varies due to the dependence of the thickness and properties of the observed specimen. The density of electrons which transmit through specimen varies in difference to contrast of the sample, i.e. fewer electrons are transmitted when the dark areas of the image (denser areas in the sample) are observed.<sup>110</sup>

### 3.2 Scanning electron microscopy (SEM)

The working mechanism of SEM is equivalent to that happening in TEM. When the electron beam is scanned and focused on the surface of specimen, Auger, backscattered and secondary electrons, X-rays are generated. The emission of secondary electrons depends on the surface region of the specimen. Thus, the morphology of the specimen is obtained by collecting the information of secondary electrons and transferred to image. The acceleration voltage used is generally smaller in contrast to TEM, which is in the range of 0.1-30 kV and is scanned line by line. This usage of low voltage in SEM is a prominent way to observe the surface morphology of the polymeric nanocapsules with different inorganic particles deposited on the surface which are presented in this thesis work.

### 3.3 Dynamic light scattering (DLS)

In this thesis, dynamic light scattering is used to measure the size and size distribution of nanoparticles and nanocapsules. The light is scattered to all directions by the particles when a laser beam passes through the highly diluted dispersion. The principle of DLS is based on the effect of Brownian motion of the particles and due to the occurrence of changes in density and concentration of the sample, it results in the fluctuation of intensity of the scattered light.<sup>111-112</sup> The slower movement of larger particles leads to less fluctuation of the signal and is contrary

observed for smaller particles. The scattered light can be detected in different angles in response to the laser beam. The scattered light can be recorded using a photomultiplier detector (PMT). The particle movement depends on the hydrodynamic radius ( $R_h$ ). The  $R_h$  can be obtained in accordance to the Stokes-Einstein equation by calculating the translation diffusion coefficient  $D$  of the particles using the autocorrelation function and is expressed as:<sup>113</sup>

$$R_h = \frac{k_B T}{6\pi\eta D}$$

Where,  $\eta$  is the shear viscosity,  $k_B$  the Boltzmann constant and  $T$  is the temperature of the solvent.

## 4. Results and discussion

### 4.1. Influence of molecular oxygen on the fluorescence and TTA-UC process

An important factor influencing the degradation of fluorescence and TTA-UC efficiency is the presence of oxygen. The main reason behind this influence is that the ground state of the molecular oxygen has a triplet multiplicity that involves in all triplet-energy transfer processes of TTA-UC. Due to the small size and high diffusion, oxygen efficiently quenches the populated triplet states of the fluorophore in the fluorescent process and sensitizer molecules in the TTA-UC process, creating extremely reactive singlet oxygen, which leads to degradation of active dyes molecules. The reaction of perylene with the singlet oxygen results in the formation of different perylene quinones,<sup>114-116</sup> and is explained in Section 4.1.1.

#### 4.1.1. Photooxidation of perylene

Generally, photo-oxidation of perylene by oxygen occurs in two different ways. The first way is by reacting the perylene with singlet oxygen that has been photochemically generated. The second one is a photo-oxidation by photoinduced electron transfer to produce radical ions followed by reaction with oxygen species ( $O_2$ ,  $^1O_2$  or  $O_2^-$ ).<sup>115</sup> “White and coworkers”<sup>117</sup> proposed that the quenching of excited naphthalene by oxygen produces singlet oxygen, which then reacts with perylene. However, perylene is sensitive to singlet oxygen and leads to a photooxidation process. Perylene degradation is also solvent sensitive whereas rapid in acetone, moderate in DMF and DMSO, but slow in THF.<sup>115</sup>

The accelerated oxidation of perylene under moderate optical excitation and in presence of molecular oxygen and an effective singlet oxygen generator (such as PdOEP, acting as a sensitizer molecule) is demonstrated in this work. The chemical structure of the specific sensitizer molecule (PdOEP) and emitter molecule (perylene) is shown in Figure 4.1.



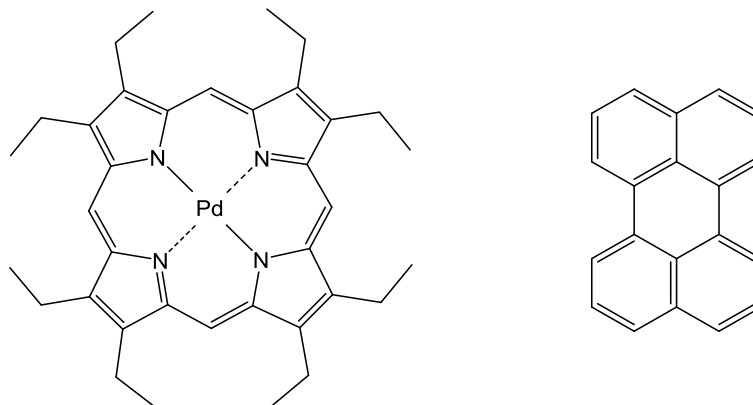


**Figure 4.1.** Structures of the a) sensitizer (Palladium (II) 2,3,7,8,12,13,17,18-octaethyl-21H,23H-porphyrin, PdOEP) and b) Dibenz[de,kl]anthracene (perylene).

The mass spectrum of the non-irradiated sample with PdOEP ( $1 \times 10^{-4}$  M) and perylene ( $1 \times 10^{-3}$  M) in tetrahydrofuran, revealed the peak of perylene molecular ion, but no peaks of its oxidation products (see Figure 4.2). After 24 h of irradiation with a daylight simulator, peaks corresponding to one (MW=268 g/mol), two (MW=282 g/mol), three (MW=298 g/mol) and four additional oxygen atoms (MW=314 g/mol) in perylene molecule are clearly seen in Figure 4.3.

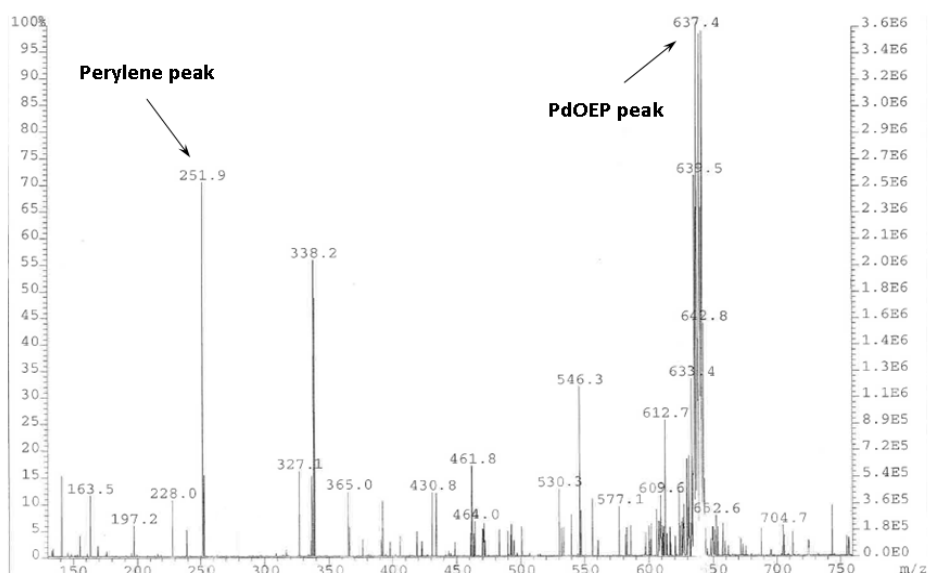


**Figure 4.2.** Field desorption (FD) - mass spectrum for sample measured before irradiating with a sunlight simulator. Concentration for PdOEP:  $1 \times 10^{-4}$  M; MW: 639.18 g/mol and perylene:  $1 \times 10^{-3}$  M; MW: 252.31 g/mol.

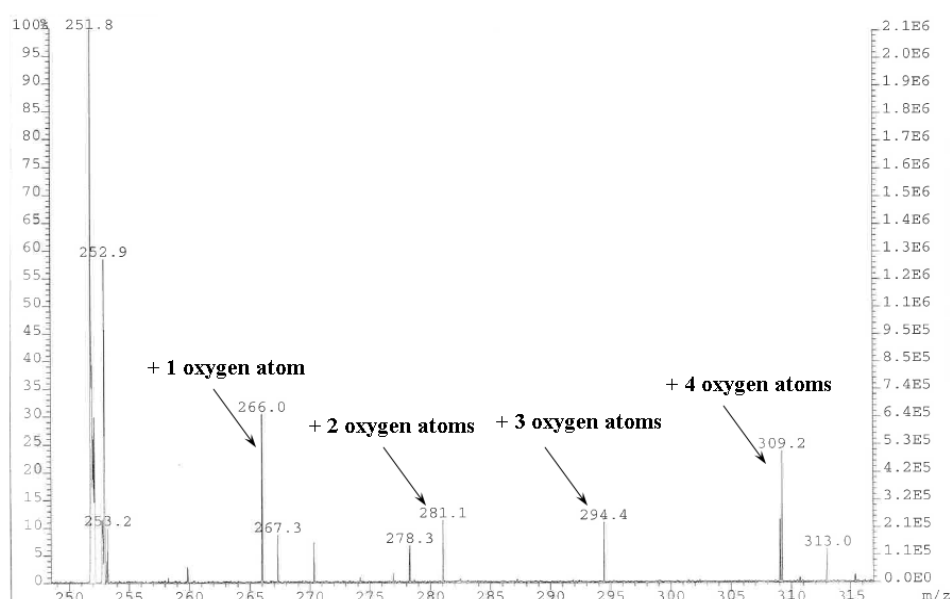


**Figure 4.3.** FD - mass spectrum for sample measured after irradiation with a sunlight simulator (AM1.5) for 1 h. The double oxidated perylene (see Figure.4.4-2), 1,12-perylenedione and 3,10-perylenedione, and tetraoxidated perylene (see Figure. 4.4-4) are described in literature,<sup>114</sup> mono and trioxidated compounds (see possible structures in Figure. 4.4-1 and 4.4-3) are unknown. However, similar structures were described as photooxidation products for other polycyclic aromatic hydrocarbons.<sup>118</sup> Therefore, we can consider them as synthetic intermediates in the photooxidation to more stable di- and tetraoxidized derivatives.

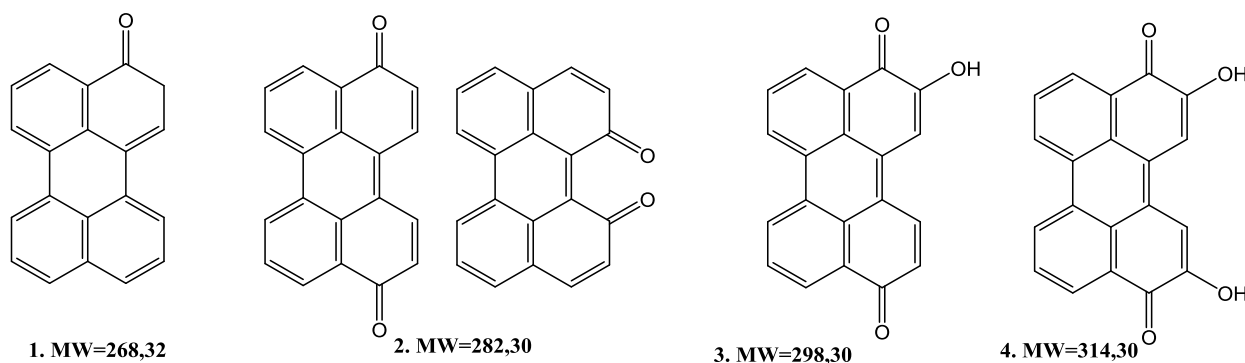


**Figure 4.4.** Possible structures of the oxidized perylene molecules.

To avoid these unwanted reactions, the bulk fluorescent or upconversion solutions are usually deoxygenated by a suitable method, such as purging by an inert gas, freeze-pump-thaw procedure, or sealing of the UC samples in a glove box.

#### 4.1.2. Different approaches to improve the luminescence efficiency (fluorescence and TTA-UC process)

As discussed in the motivation part, the main aim of this work is to protect the luminescent materials from the process of degradation caused by the presence of molecular oxygen. This thesis describes different approaches to obtain sustainable and reproducible luminescence efficiency in polymeric nanocapsules:

1. Synthesis of nanocapsules using different polymer materials as shell.
2. Synthesis of encapsulated triplet-triplet annihilation photon upconversion nanocapsules under protective conditions.
3. Improving the efficiency of encapsulated fluorophores with ceria/polymer hierarchical nanocapsules.
4. The improvement in efficiency of upconversion process by deposition of different inorganic materials on the surface of polymeric nanocapsules.
5. Deposition of silicate clay particles on surface of polystyrene nanocapsules by Pickering miniemulsion method.

#### 4.2. Synthesis of nanocapsules using different polymer materials as shell

In this section we describe the change in the upconversion properties by varying the shell type. Polymeric nanocapsules were synthesized using different types of monomers in order to obtain sustainable, reproducible upconversion properties. This is because, every polymer has a certain oxygen permeability coefficient and the oxygen permeability of a polymer decreases with the increasing degree of crystallinity (see Table 4.1). The capsules were synthesized using two methods: solvent evaporation method and free radical miniemulsion polymerization method. The capsules in this section are labelled as **KK-SE-XX** and **KK-MP-XX**, where **XX** is the number of the sample (see details Table 4.2).

#### 4. Results and discussion

**Table 4.1.** The degree of crystallinity and oxygen permeability coefficient of different polymers which are used for the synthesis of nanocapsules.<sup>119</sup>

Polymer	Crystallinity	O <sub>2</sub> permeability ( <i>P</i> ) / <i>cm</i> <sup>3</sup> × 10 <sup>13</sup>
Polystyrene (PS)	Amorphous	1.9
Poly(methyl methacrylate) (PMMA)	Amorphous	0.116
Poly(acrylonitrile) (PAN)	Semi-crystalline	0.00015
Poly(acrylonitrile-co-styrene) (66/34 wt.-%)	Semi-crystalline	0.036
Poly(L-lactide) (PLLA)	Semi-crystalline	0.00012

**Table 4.2.** Characteristics of the different samples presented in this section.

Sample name	Shell material	Synthesis method	Diameter (nm) <sup>[a]</sup>	Core/shell ratio (in weight) <sup>[b]</sup>	Solid content (wt.-%)
KK-SE-01	PMMA	Solvent evaporation	170 nm (± 25%)	2:1	15 ± 2
KK-SE-02	PLLA	Solvent evaporation	190 nm (± 30%)	1:1	10 ± 2
KK-MP-01	PS	Free-radical miniemulsion polymerization	160 nm (± 32%)	1.8:1	15 ± 3
KK-MP-02	PMMA	Free-radical miniemulsion polymerization	150 nm (± 45%)	2:1	14 ± 2
KK-MP-03	PAN	Free-radical miniemulsion polymerization	470 nm (± 38%)	2:1	11 ± 3
KK-MP-04	P(AN-co-S)	Free-radical miniemulsion polymerization	130 nm (± 37%)	2:1	13 ± 2

[a] As obtained by DLS

[b] Core/shell ratio: hexadecane/polymer ratio

#### **4.2.1. Synthesis of poly(methyl methacrylate) and poly(L-lactic acid) nanocapsules via solvent evaporation polymerization method**

Poly(methyl methacrylate) (sample **KK-SE-01**) and poly (L-lactic acid) (sample **KK-SE-02**) polymeric hybrid luminescent nanocapsules with upconversion dyes encapsulated in the hydrophobic core material were synthesized via solvent evaporation.<sup>109</sup> The sensitizer and emitter concentration in the hydrophobic phase was equal to  $1 \times 10^{-4}$  M and  $1 \times 10^{-3}$  M in both samples. The procedure to prepare PMMA and PLLA capsules is described in the experimental section (Section 7.2). The obtained nanocapsules consist of a polymeric shell and organic liquid core with UC dyes. Capsules by this method are obtained from the pre-synthesized polymers (PMMA and PLLA) dissolved in a required solvent. In our case, chloroform which can easily dissolve both polymers is used as an organic solvent for the pre-polymer (PMMA and PLLA). The capsules are formed when the chloroform is slowly evaporated at room temperature, which results in a phase separation between the polymer and the non-solvent in dispersed droplets. The formation of capsules occurs when the polymer chains are precipitated at the interface of droplets and solidify the pre-synthesized polymer as a shell around the liquid core, which is dissolved in the aqueous phase (non-solvent). The size of the obtained PMMA nanocapsules were in the range of 170 nm ( $\pm 25\%$ ), as measured by dynamic light scattering (DLS). The solid content of the dispersions was 15–20 wt.-%. The size of obtained obtained PLLA nanocapsules were in the range of 190 nm ( $\pm 30\%$ ) and the solid content of the dispersions was  $10 \pm 2$  wt.-%. Figures 4.5a-d, shows the SEM and TEM images of the obtained PMMA and PLLA nanocapsules.

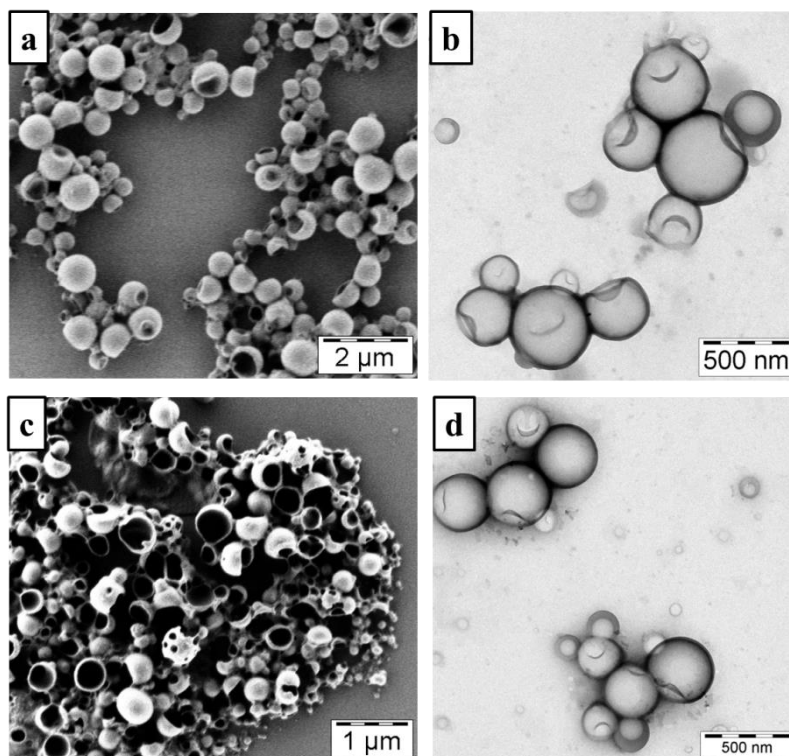


**Figure 4.5.** Electron microscopy images of nanocapsules synthesized via solvent evaporation method. a) SEM and b) TEM images of poly(methyl methacrylate) hybrid nanocapsules, c) SEM and d) TEM images of poly(L-lactic acid) hybrid nanocapsules.

The samples were placed in argon atmosphere after the synthesis of nanocapsules. Further for luminescence measurements, the latex dispersion was transferred in to quartz vials and sealed. The luminescence spectra of PdOEP and perylene encapsulated in PMMA (**KK-SE-01**) and PLLA (**KK-SE-02**) capsules synthesized by solvent evaporation method are observed upon excitation with a 532 nm laser (intensity  $1 \text{ W cm}^{-2}$ ) (see Figure 4.6). Intensive UC fluorescence of perylene with  $\lambda_{\text{max}} = 470 \text{ nm}$  and residual phosphorescence of sensitizer molecule (PdOEP) with  $\lambda_{\text{max}} = 670 \text{ nm}$  are seen only in the PMMA capsules (see Figure 4.6-a). In PLLA capsules, we observed only the residual phosphorescence of the sensitizer molecule (PdOEP) with  $\lambda_{\text{max}} = 670 \text{ nm}$  (see Figure 4.6-b). The phosphorescence emission in nanocapsules prepared with PLLA shell is nearly 20 times higher than in PMMA due to the presence of strong triplet states. The absence of UC fluorescence of perylene in PLLA capsules can be explained by the formation of a polymer coagulum during preparation of the capsules, which contains most of the dye and is filtrated from the samples during purification. Thus, the remaining perylene content in the suspension is very small. The strong reduction of perylene concentration does not support the transfer of triplet-triplet electron exchange from sensitizer to emitter molecules. These experiments conclude that TTA-UC emission is observed in nanocapsules with PMMA as shell material, but not in those prepared with PLLA.

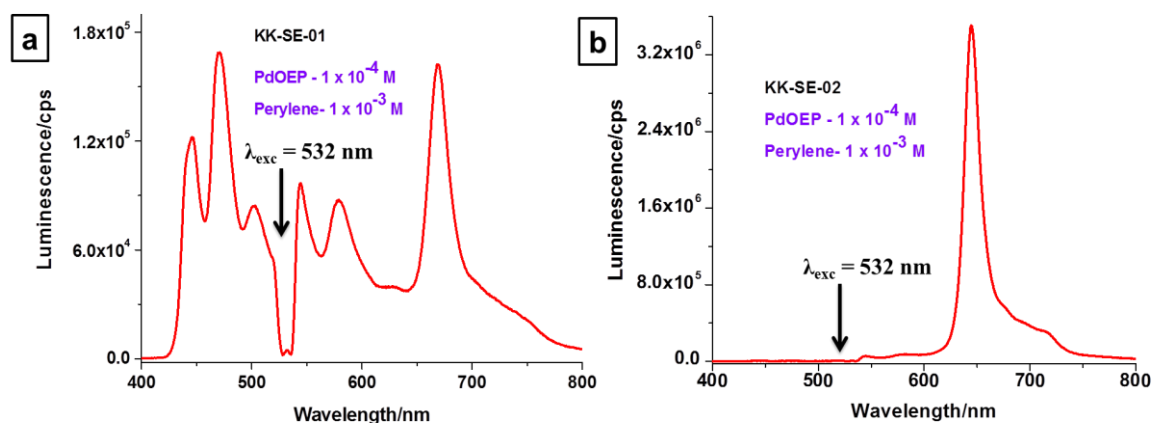


**Figure 4.6.** Luminescence emission spectra of TTA-UC encapsulated nanocapsules synthesized via solvent evaporation method. a) Upconversion fluorescence (perylene) and phosphorescence (PdOEP) spectrum of PMMA nanocapsules and b) residual phosphorescence (PdOEP) spectrum of PLLA nanocapsules. Excitation intensity of 532 nm laser is  $1 \text{ W cm}^{-2}$ . The sensitizer and emitter concentration in the hydrophobic phase was equal to  $1 \times 10^{-4} \text{ M}$  and  $1 \times 10^{-3} \text{ M}$  in all samples.

#### 4.2.2. Free-radical miniemulsion polymerization method

Polystyrene (sample **KK-MP-01**), poly(methyl methacrylate) (sample **KK-MP-02**), poly(acrylonitrile) (sample **KK-MP-03**), and poly(acrylonitrile-co-styrene) (66/34 wt.-%) (sample **KK-MP-04**) polymeric nanocapsules were synthesized by free radical miniemulsion polymerization.<sup>120</sup> The experimental details are explained in Section 7.2.4. The sensitizer and emitter concentration in the hydrophobic phase was equal to  $1 \times 10^{-4} \text{ M}$  and  $1 \times 10^{-3} \text{ M}$  in all samples. The obtained nanocapsules consist of a polymeric shell and an organic liquid core with the UC dyes. The capsules are formed when the polymer chains are precipitated at the interface of droplets. The formation of a shell is only possible when the interfacial energy between the polymer and water is lower than between the hydrophobic core liquid and water.<sup>121</sup> In the case of PS nanocapsules, acrylic acid (AA) was added as a comonomer to increase the hydrophilic nature within the system. The size of the obtained PS nanocapsules were in the range of 160 nm ( $\pm 32\%$ ), PMMA nanocapsules were in the range of 150 nm ( $\pm 45\%$ ), PAN nanocapsules were larger than  $1.5 \mu\text{m}$  and P(AN-co-S) were in the range of 130 nm ( $\pm 37\%$ ) as measured by dynamic light scattering (DLS) and the solid content of the dispersions was 15–20 wt.-%. The formation of nanocapsules was clearly confirmed by the corresponding SEM and TEM images (see Figure 4.7 a-b for **KK-MP-01**, Figure 4.7 c-d for **KK-MP-02**, Figure 4.7 e-f for **KK-MP-03** and Figure 4.7 g-h for **KK-MP-04**).

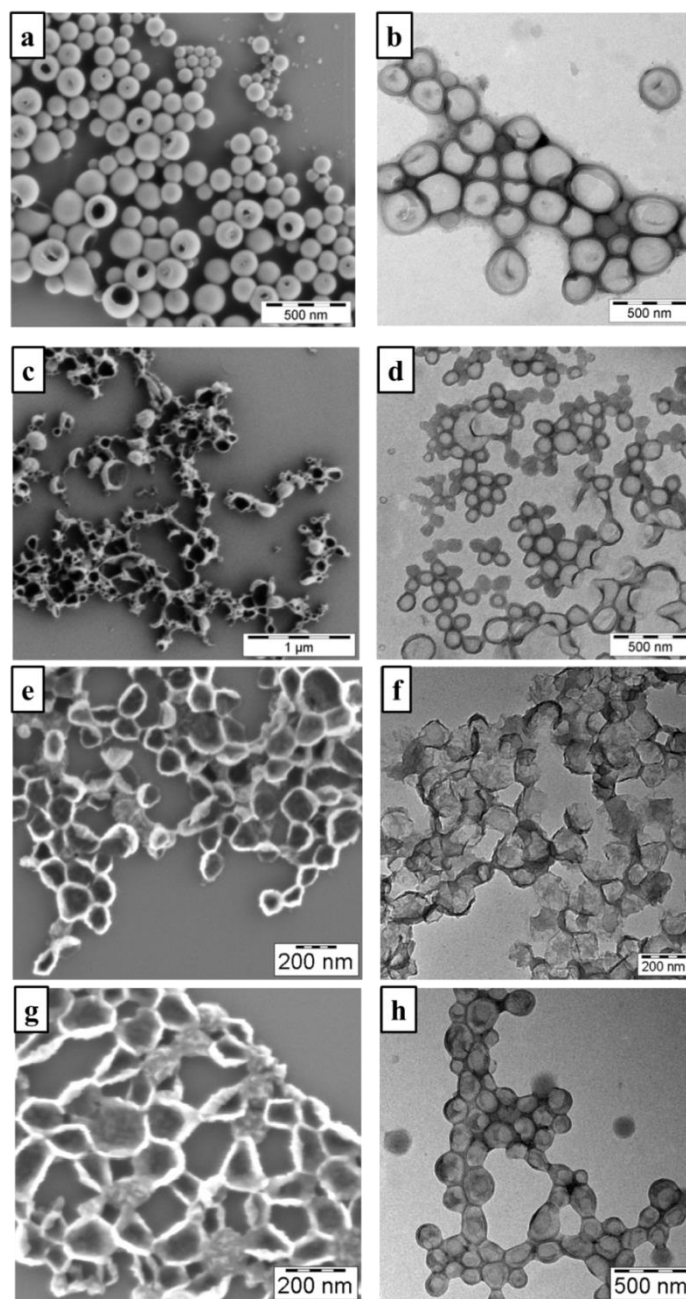


**Figure 4.7.** Microscopic images of encapsulated UC dyes (PdOEP and perylene) synthesized via free radical miniemulsion polymerization. a) SEM and b) TEM images of polystyrene hybrid nanocapsules, c) SEM and d) TEM images of poly(methyl methacrylate) hybrid nanocapsules, e) SEM and f) TEM images of poly(acrylonitrile) hybrid nanocapsules and g) SEM and h) TEM images of poly(acrylonitrile/styrene) hybrid nanocapsules.

The luminescence spectra of PdOEP and perylene encapsulated in PS (**KK-MP-01**), PMMA (**KK-MP-02**) and (**KK-MP-03**) nanocapsules synthesized via free radical miniemulsion polymerization method were recorded upon excitation with a 532 nm laser (intensity  $1 \text{ W cm}^{-2}$ ). Intensive UC fluorescence of perylene with  $\lambda_{\text{max}} = 470 \text{ nm}$  and residual phosphorescence of the sensitizer molecule (PdOEP) with  $\lambda_{\text{max}} = 670 \text{ nm}$  are observed in PS and PMMA samples except in PAN sample (see Figure 4.8).



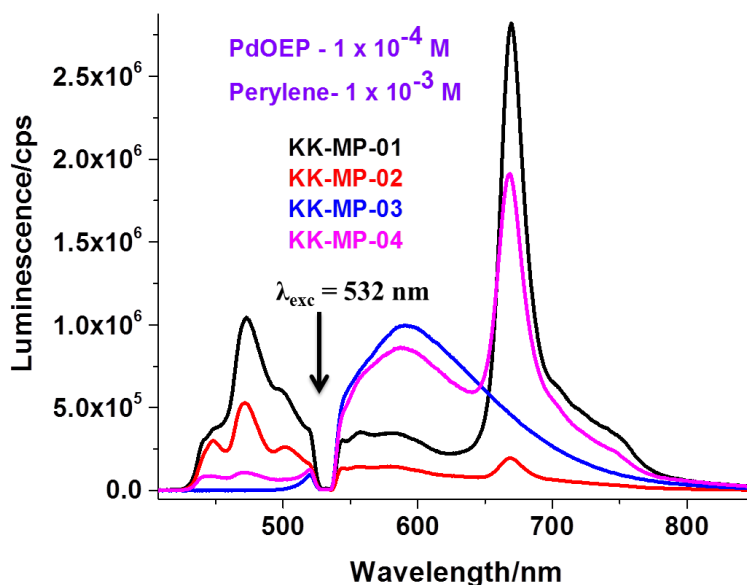


**Figure 4.8.** Luminescence spectra of TTA-UC encapsulated nanocapsules synthesized via free radical polymerization method. The sensitizer and emitter concentration in the hydrophobic phase was equal to  $1 \times 10^{-4}$  M and  $1 \times 10^{-3}$  M in all samples. Excitation intensity of 532 nm laser is  $1 \text{ W cm}^{-2}$ .

The luminescence emission spectra clearly denote that the UC fluorescence intensity is higher for the case of **KK-MP-01** (black line) than for sample **KK-MP-02** (red line). An absence of UC fluorescence and residual phosphorescence was observed in the PAN system (blue line). In contrast to **KK-MP-01** and **KK-MP-02**, the formation of UC nanocapsules with PAN shell was not fully efficient, because acrylonitrile is hydrophilic in nature and poorly miscible in the hexadecane solution containing UC dyes. PdOEP molecules are separated from the PAN latex system after filtration as a consequence of the formation of a coagulum, but small amounts of the perylene molecules remain in the suspension system. The corresponding luminescence emission spectra (blue line) **KK-MP-03** clearly shows an emission centered at 570 nm with high intensity, which can be due to the formation of molecular dimers from the emitter molecules (perylene). Thus, to improve the UC process in the PAN system, we synthesized the P(AN-co-S) nanocapsules, and the corresponding luminescence emission spectrum (magenta line) is shown in Figure 4.8. A clear core/shell morphology was observed for the P(AN-co-S) nanocapsules to that of the pure PAN latex dispersion system. Thus, the UC fluorescence of perylene and residual phosphorescence of PdOEP was observed in sample **KK-MP-04**, in contrast to the sample **KK-MP-03**.

### 4.2.3. Conclusions

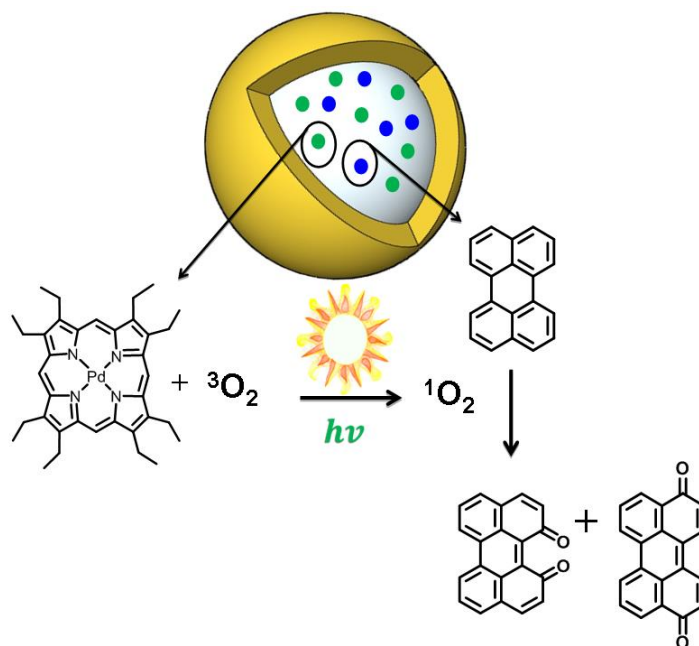
Upconversion dyes (PdOEP and perylene) were successfully encapsulated into polymer nanocapsules using two methods: solvent evaporation method and free radical miniemulsion polymerization. The synthesized nanocapsules show intense fluorescence emission of TDI with  $\lambda_{\text{max}} = 670$  nm upon low excitation intensity of 630 nm laser (intensity is  $0.2 \text{ W cm}^{-2}$ ). Poly(methyl methacrylate) and poly(L-lactic acid) nanocapsules were synthesized by using the solvent evaporation method. The process of upconversion was observed only in PMMA nanocapsules in contrast to the PLLA nanocapsules. Furthermore, polystyrene, poly(methyl methacrylate), poly(acrylonitrile) and poly(acrylonitrile-co-styrene) nanocapsules were synthesized by using free radical polymerization. The upconversion process was observed only in PS and PMMA nanocapsules, but not in PAN and P(AN-co-S) nanocapsules. Therefore, we can conclude that efficient upconversion properties has been observed in nanocapsules prepared with polystyrene and poly(methyl methacrylate).

### 4.3. Synthesis of nanocapsules containing TTA-UC dyes under protective conditions<sup>1</sup>

In Section 4.2 we had observed the change in the upconversion efficiency of encapsulated TTA-UC dyes in different polymeric nanocapsules. For further investigation of the improvement in upconversion efficiency, in this section we synthesize polymeric nanocapsules containing TTA-UC dyes under protective conditions. Nanocapsules containing TTA-UC dyes are synthesized under oxygen-protective conditions (i.e., complete darkness and argon atmosphere) by free-radical miniemulsion polymerization. These conditions help to exclude the oxidation of the emitter molecules caused by singlet oxygen, generated during the synthesis at daylight conditions and oxygen-rich environment. Subsequently, keeping all the other experimental conditions the same, samples synthesized under protective conditions demonstrate substantially increased upconversion efficiency. These experimental facts strongly support the hypothesis that posterior removing of oxygen from TTA-UC nanocapsules is not sufficient to obtain reproducible and sustainable upconversion results.

---

<sup>1</sup> This section is based on the publication “Synthesis of Triplet-Triplet Annihilation Upconversion Nanocapsules Under Protective Conditions” by Kartheek Katta, Dmitry Busko, Yuri Avlasevich, Rafael Muñoz-Espí, Stanislav Balushev and Katharina Landfester, published 2015 in *Macromolecular Rapid Communications*, volume 36 on the pages 1084-1088. © 2015, with kind permission from John Wiley and Sons.



**Scheme 4.1.** Schematic representation showing influence of sunlight on the formation of singlet oxygen and its effect on triplet-triplet annihilation upconversion process.<sup>121</sup> Copyright 2015, John Wiley and Sons.

The TTA-UC process is based on triplet-triplet energy transfer (TTT) between the optically created triplet ensembles of the sensitizer molecules to accessible triplet states of the emitter molecules, combination of triplet energies of two emitters via triplet-triplet annihilation (TTA) and the subsequent delayed emission of a photon with a higher energy, than the absorbed ones. It is important to notice that metallated macrocycles such as porphyrins or phthalocyanines, which are usually used as sensitizers, are also known as good singlet oxygen generators. With other words, in presence of molecular oxygen and light, absorbed by the sensitizer, a remarkable amount of singlet oxygen can be created. In its turn, the singlet oxygen is known as a very aggressive species and can lead to remarkable oxidative damage of the used emitter or sensitizer molecules.<sup>54-56</sup>

In this section, it is explained for the first time that even during the synthesis of UC nanocapsules oxidative damaging of the UC active dyes occurs, leading to substantial and arbitrary changes in UC characteristics, if no protective environment is used. Therefore, in order to obtain reproducible UC properties of the nanocapsules, the oxidative damage cannot be neglected and special attention must be paid on the elimination of this type of photo-induced oxidation. The capsule samples presented in this section are listed in Table 4.3.

**Table 4.3.** Characteristics of the different samples presented in this section.

Sample name	Material	Atmosphere	Daylight/darkness	Diameter (nm) <sup>[a]</sup>
NC1	PS	Air	Daylight	175 ( $\pm$ 28%)
NC2-A	PS	Argon	Daylight	182 ( $\pm$ 22%)
NC3-D	PS	Air	Darkness	160 ( $\pm$ 34%)
NC4-AD	PS	Argon	Darkness	189 ( $\pm$ 31%)

[a] As obtained by DLS

#### 4.3.1. Study of TTA-UC properties in nanocapsules synthesized under different conditions

The polymeric nanocapsules presented in this section were synthesized by free-radical miniemulsion polymerization. The experimental procedure for the synthesis is presented in Section 7.3. The nanocapsules are formed by phase separation of the copolymer being formed between styrene and acrylic acid in a dispersed organic liquid droplets (hexadecane) containing the upconversion dyes.<sup>72, 122</sup> The shell formation is possible when the interfacial energy between the polymer and water is lower than between the hydrophobic core liquid and water.<sup>30</sup> In our case, the interfacial tension was decreased by the addition of acrylic acid as a hydrophilic comonomer. The formation of nanocapsules can be clearly observed in the SEM and TEM images (Figure 4.10 a-b). Figure 4.10-c shows luminescence spectra (black line) upon excitation with a  $\lambda = 532$  nm laser (intensity  $1 \text{ W cm}^{-2}$ ) of the sample **NC1**, synthesized under daylight, dispersed in water. Intensive UC fluorescence of perylene with  $\lambda_{\text{max}} = 470$  nm and residual phosphorescence of sensitizer molecule (PdOEP) with  $\lambda_{\text{max}} = 670$  nm are seen.

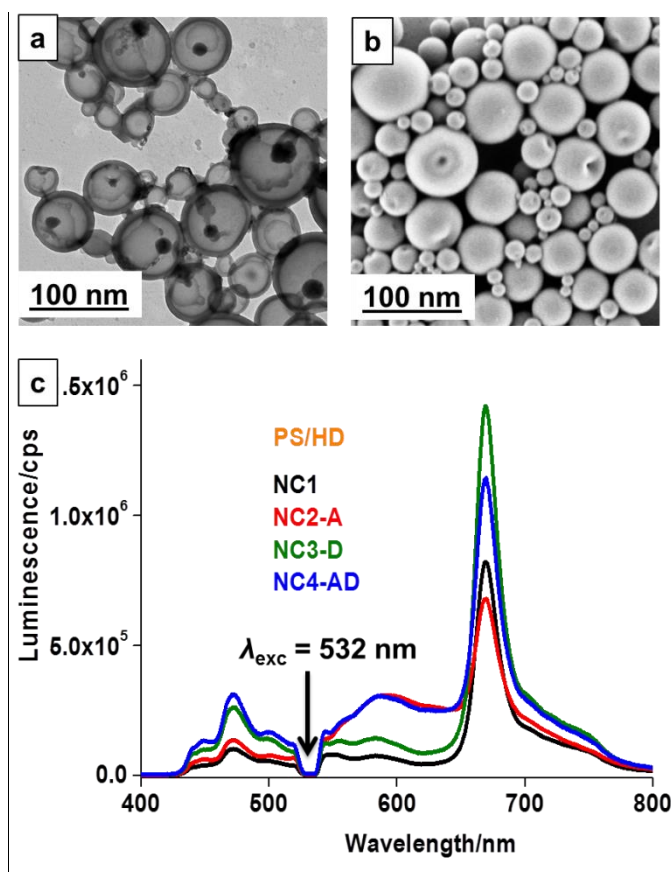


**Figure 4.10.** a) TEM and b) SEM images of polystyrene/hexadecane nanocapsules synthesized by free-radical miniemulsion polymerization. c) Luminescence spectra of nanocapsules synthesized at different conditions, as follows: **NC1** (black line, in day light), **NC2-A** (red line, in day light under argon atmosphere), **NC3-D** (green line, in darkness) and **NC4-AD** (blue line, in darkness under argon atmosphere). Excitation intensity of 532 nm laser is  $1 \text{ W cm}^{-2}$ . The sensitizer and emitter concentration in the hydrophobic phase was equal to  $1 \times 10^{-4} \text{ M}$  and  $1 \times 10^{-3} \text{ M}$  in all samples.<sup>121</sup> Copyright 2015, John Wiley and Sons.

An important factor influencing the TTA-UC efficiency is the presence of oxygen. The main reason behind this influence is that the ground state of the molecular oxygen has a triplet multiplicity that involves in all triplet-energy transfer processes of TTA-UC. Due to the small size and high diffusion, oxygen efficiently quenches the populated triplet states of the sensitizer molecules, creating extremely reactive singlet oxygen, which leads to degradation of active dyes molecules. For instance, the reaction of perylene with the singlet oxygen was studied and used for the synthesis of different perylene quinones.<sup>114-116</sup> The accelerated oxidation of perylene under moderate optical excitation and presence of molecular oxygen and effective singlet oxygen generator (such as PdOEP) is demonstrated in Section 4.1. To avoid these unwanted reactions, the UC solution is usually deoxygenated by a suitable method such as purging by an inert gas, freeze-pump-thaw procedure, or sealing of the UC samples in a glove box. However, the stock solutions for UC experiments are usually prepared in ambient conditions, which include the presence of oxygen and daylight, neglecting the fact

that the generation of singlet oxygen still occurs in the solution, resulting in degradation of compounds.

To overcome the limitations caused by oxygen influence, the nanocapsule synthesis was carried out in a closed flask under argon atmosphere under daylight (sample **NC2-A**). The corresponding luminescence spectrum is shown in Figure 4.10-c (red line). UC efficiency and residual phosphorescence is enhanced in comparison to **NC1** (black line), that can be explained by the decrease of the concentration or total absence of the oxygen inside the capsules during polymerization step, which in its turn resulted in decreased rate of photo degradation of the dyes.

With the aim of increasing the upconversion effect, the nanocapsules were synthesized in dark conditions under oxygen (**NC3-D**) and under argon (**NC4-AD**) atmospheres. Luminescence spectra (see Figure 4.10-c) of samples **NC3-D** (green line) and **NC4-AD** (blue line) show that both UC efficiency and phosphorescence emission are strongly enhanced. Surprisingly, the capsules synthesized in darkness under argon did not show noticeable cumulative effect of both factors. This can be explained partially by the favorable formation of molecular dimers of perylene during the synthesis under argon atmosphere, the directly excited emission of which is seen around 570 nm for **NC2-A** and **NC4-AD**. Argon and darkness have a clear effect, as indicated by the increased rate of triplet-triplet transfer (the phosphorescence of PdOEP is slightly lower than for **NC3-D**) and increased UC emission.

The dependence of luminescence signal on the excitation intensity for the samples **NC1**, **NC2-A**, **NC3-D** and **NC4-AD** are shown in Figure 4.11 a-d. It should be noted that the upconversion has been observed at much lower excitation intensities ( $0.006 \text{ W cm}^{-2}$ ) (Figure 4.11) for **NC3-D** and **NC4-AD** when compared to those of **NC1** and **NC2-A**. The dependence of the UC fluorescence on the excitation intensity is also shown. The region of excitation intensities, where the UC nanocapsules (especially, sample **NC4-AD** in Figure 4.12) demonstrate an intensity dependence that is well approximated with a sub-linear function, is more than 3 orders of magnitude broad. These measurements strongly indicate that the upconversion efficiency was increased in nanocapsules that were synthesized under protective conditions.

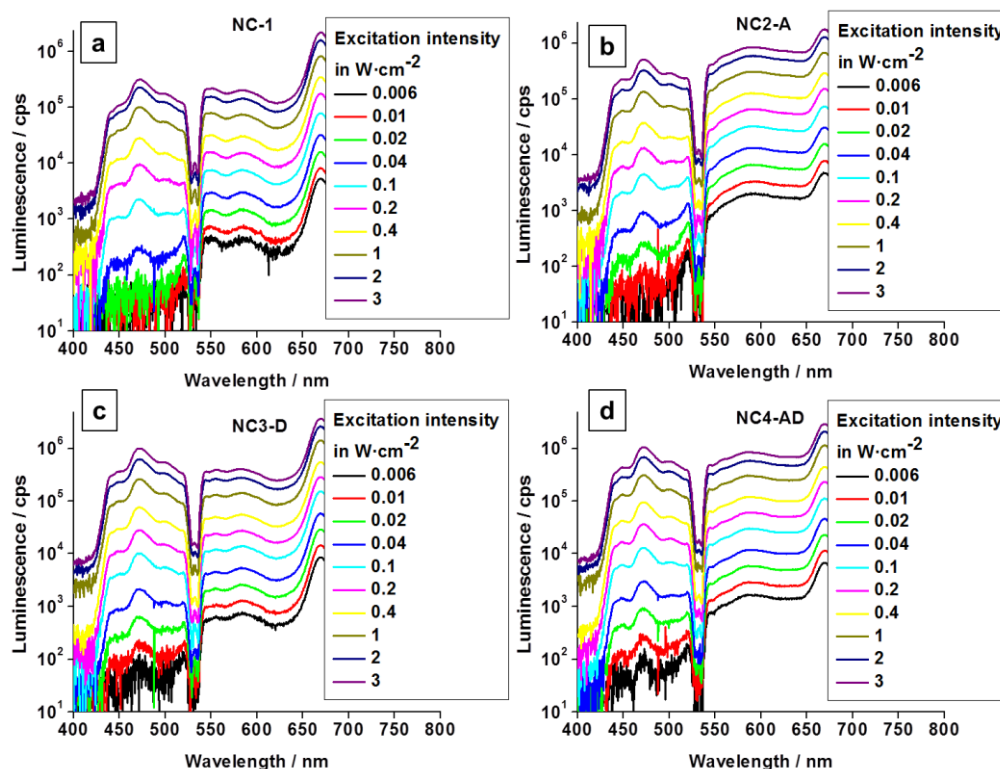


**Figure 4.11.** Luminescence emission spectra of synthesized polystyrene/hexadecane nanocapsules at different conditions upon various excitation intensities of a 532 nm laser (violet line at 3 W cm<sup>-2</sup> and black line at 0.006 W cm<sup>-2</sup> – top to bottom) a) **NC1** (in day light), b) **NC2-A** (in day light under argon atmosphere), c) **NC3-D** (in darkness) and d) **NC4-AD** (in darkness under argon atmosphere).<sup>121</sup> Copyright 2015, John Wiley and Sons.

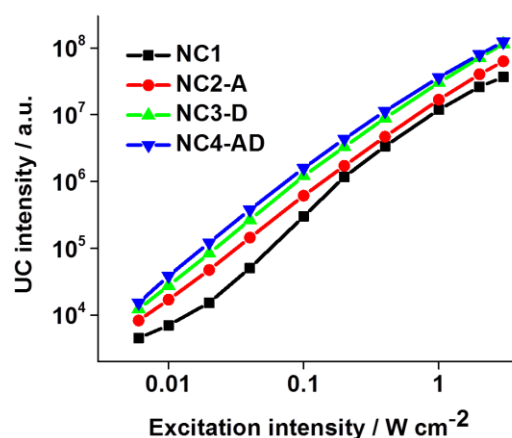


**Figure 4.12.** Dependence of the integral upconversion fluorescence intensity on the excitation intensity. The TTA-UC nanocapsules (**NC1**, **NC2-A**, **NC3-D** and **NC4-AD**) were synthesized at different conditions, as described in **Figure 4.10**. The UC measurements are conducted in samples, sealed in nitrogen-filled glove box.<sup>121</sup> Copyright 2015, John Wiley and Sons.

The absorption spectra of upconversion dyes dissolved in THF under daylight and darkness conditions after 24 and 48 h. of irradiation with a daylight simulator is shown in Figure 4.13.

The absorption spectrum clearly shows that the emission intensity of perylene molecule (emitter) is decreased under daylight conditions when compared to that of the darkness conditions. This result also proves that the complete upconversion efficiency is not observed under daylight conditions.

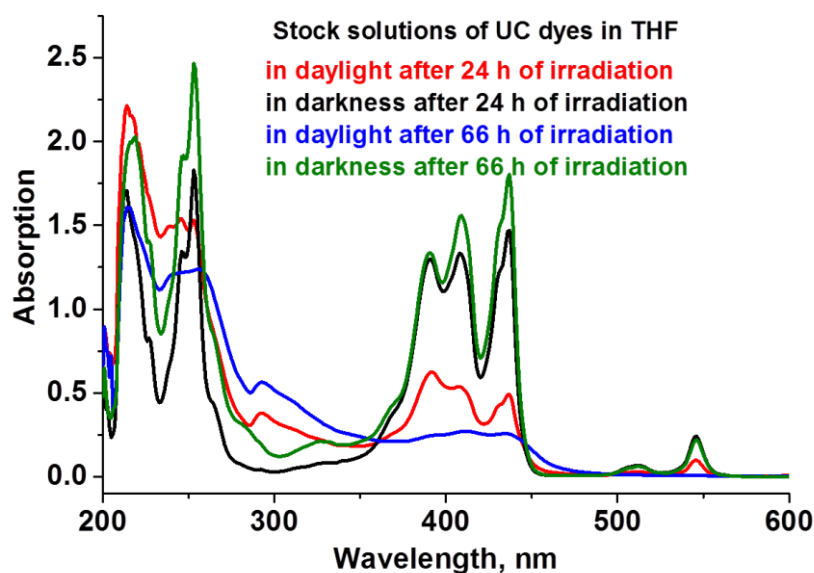


**Figure 4.13.** Absorption spectra of the upconversion dyes (PdOEP as sensitizer and perylene as emitter), dissolved in THF under daylight (red and blue line) and darkness (black and green line) conditions after 24 h and 48 h. of irradiation with a sunlight simulator.

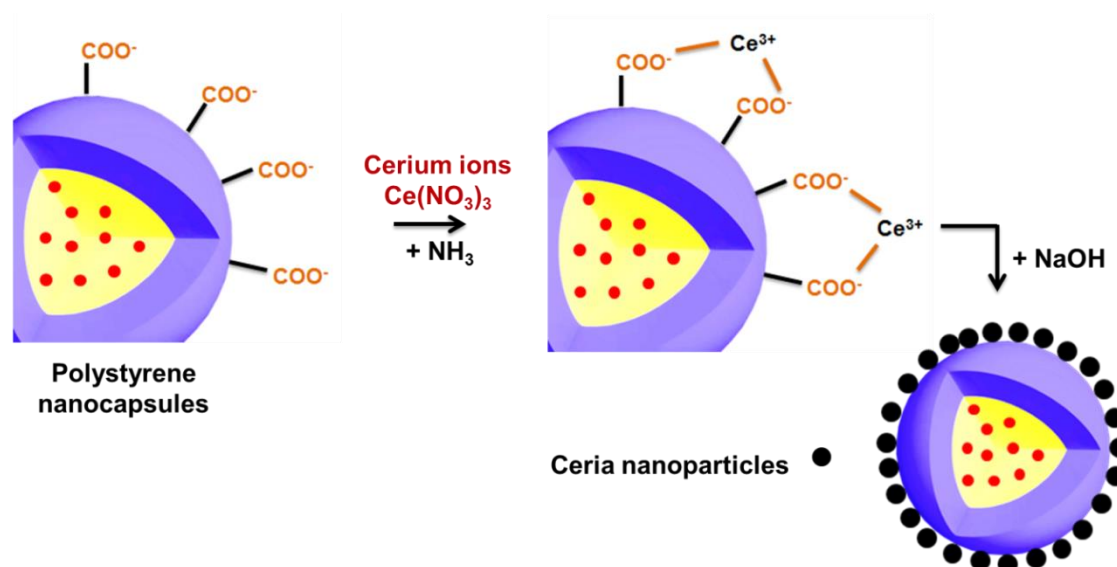
### 4.3.3. Conclusions

The crucial role of molecular oxygen during the nanocapsules synthetic procedure on the TTA-UC efficiency was studied. Polystyrene nanocapsules with TTA-UC system were synthesized by free-radical miniemulsion polymerization in darkness and under argon atmosphere. The synthesized nanocapsules show intensive UC fluorescence of perylene with  $\lambda_{\max} = 470$  nm and residual phosphorescence of PdOEP with  $\lambda_{\max} = 670$  nm upon low excitation intensity of  $\lambda = 532$  nm laser (intensity is tens of  $\text{mW cm}^{-2}$ ). The luminescence spectra of nanocapsules synthesized in protective conditions shows that both UC fluorescence and residual sensitizer phosphorescence has been strongly enhanced.



#### 4.4. Improving the efficiency of encapsulated fluorophores with ceria/polymer hierarchical nanocapsules<sup>123</sup>

In the section 4.2 and 4.3 we had observed the change in the upconversion efficiency in different polymeric nanocapsules, and in nanocapsules synthesized under protective conditions. In this section, we report the other approach to achieve high efficiency of fluorescence properties is deposition of ceria on the surface of carboxylate functionalized polymeric nanocapsules. The high performance functionalized organic–inorganic hybrid fluorescent nanocapsules, comprised of a polymer shell armored with an inorganic layer and a liquid core containing a fluorophore. The polymeric capsules are synthesized by free-radical miniemulsion polymerization with covalently bound carboxylate surface functionalities, which help to bind metal ions through electrostatic interactions between opposite charges. A cerium(IV) oxide nanoparticle layer, formed in situ at the surface of the hybrid nanocapsules, act as oxygen scavenger and avoid the reactive molecular oxygen from the external environment to enter into capsules, eventually resulting in a reduction of the photo-oxidation of encapsulated fluorescent molecules. This approach shows an increase in the fluorescence of a model organic fluorophore (i.e., terrylene diimide) by avoiding the ground state molecular oxygen to react with electronically excited states (triplet or singlet) of the fluorescent hydrocarbon molecule.



**Scheme 4.2.** Schematic representation of the formation of cerium(IV) oxide on the surface of carboxylate functionalized fluorescent nanocapsules.

### 4.4.1. Encapsulation of terrylene diimide (TDI) in hybrid nanocapsules: State of the art

Hybrid polymeric core–shell nanoparticles with encapsulated fluorescent dye molecules are frequently used for life-science applications, such as cell labeling and drug delivery.<sup>2-3, 6, 9</sup> Polymeric hybrid nanoparticles and nanocapsules with tailored inorganic components on the surface have attracted great interest in recent years because of the ability to tune size, composition, porosity, stability, surface functionality, or colloidal stability, among other properties.<sup>124-129</sup> Generally, fluorescent dye molecules are sensitive to the external environment, which leads to unwanted chemical reactions.<sup>17</sup> Molecular oxygen is a well-known quencher of fluorescence. Therefore, the shell properties of the nanocontainers are often customized to protect the fluorophore encapsulated into a liquid core.<sup>130</sup>

The higher lying singlet state of a fluorophore  $^1\Sigma$  is relatively short living and its fast relaxation creates the lowest excited singlet state  $^1\Delta$ , relaxing further to the excited triplet state via an intersystem crossing process. The ground state of oxygen molecule is a triplet state ( $^3\Sigma$ ) and has the capability to occupy the energy at the excited triplet state of the fluorophore. Thus, singlet oxygen ( $^1\Sigma$ ) is the product obtained during the process of fluorescence quenching.<sup>17, 56, 131-132</sup>

For the optical response, photooxidation represents significant changes in the emission properties of fluorophores because of an irreversible chemical reaction. In a simple description, the longer the fluorescence lifetime and the lower the fluorescence quantum yield of the fluorophore is, the stronger is the sensitivity to the presence of oxygen quenching.<sup>17</sup> The solubility of oxygen in organic solvents is also an important factor involved in the quenching process of a fluorescent molecule. The solubility of oxygen in organic solvents decreases with increasing alkyl chain length of the alkanes.<sup>133-134</sup> Furthermore, the process of involvement of oxygen quencher is less efficient in high viscosity liquids or media.<sup>17</sup> In bulk fluorescent samples with dye content on the level of  $10^{-4}$ – $10^{-5}$  M, the oxygen quenching effect does not play a significant role: by applying standard degassing techniques such as nitrogen or argon bubbling and/or freeze-pump-thaw cycles, the oxygen amount can be lowered. As a consequence, these techniques are efficient enough to suppress the oxygen quenching of the sample fluorescence.<sup>17</sup> The case of fluorescent samples containing dyes encapsulated in nanoconfined materials becomes more complicated: generally, the encapsulation process of the dye leads usually to a drastic reduction of the total dye

concentration in the sample and increases the amounts of dissolved molecular oxygen and encapsulated fluorescent dye. A variety of methods have been applied to encapsulate the fluorescent materials into micro- and nanocapsules,<sup>135-136</sup> with an hydrophobic dye concentration in the order of  $10^{-4}$ M and a total solid content on the level of 1–5 wt. -%. Accordingly, in bulk fluorescent samples the oxygen/dye molar concentration ratio is typically about 10:1 and, in contrast, in nanoconfined materials it is of about 200:1. Such a relative quencher excess will affect the optical response of the studied nanosized sample, causing pronounced oxygen quenching of fluorescence signal, and simultaneously effective photo-oxidation of the used organic dye. This effect could be an additional source of uncertainty when the fluorescence signal is used as a quantitative measure at field of theranostics.<sup>137-138</sup>

In comparison to visible light, the near-infrared (NIR) light undergoes less diffuse scattering, causes less photodamage, and can penetrate deeper into tissues, being therefore preferred for life science applications. In general, organic dyes excited above 600 nm are highly favorable for live-cell imaging experiments, because the background signal obtained from the autofluorescence of living cells is negligible in the near infrared region.<sup>139-140</sup> In this work, we have chosen a specific fluorescent dye molecule (i.e., terylene diimide, TDI, which shows intense fluorescence in the NIR spectral region of the electromagnetic spectrum) to be encapsulated in polymeric nanocapsules.<sup>141-142</sup> TDI, which is excited with red light ( $\lambda_{\text{exc}} = 633$  nm, from a HeNe laser, for instance) and shows bright fluorescence at  $\lambda_{\text{max}} = 670$ –690 nm, is a suitable organic dye for patterning or imaging of biomaterials. This dye belongs to the rylene-family,<sup>143</sup> which is formed by extending the core  $\pi$ -conjugated system of highly fluorescent perylene-3,4:9,10-tetracarboxdimides. The rylene-family has unique optical properties, such as high extinction coefficients, high thermal, chemical and photochemical stabilities, and exhibit brilliant color.<sup>144-145</sup> Furthermore, in bulk samples, TDI demonstrates an excellent fluorescence quantum yield ( $\sim 90\%$ ),<sup>139</sup> less affected by the presence of molecular oxygen. Using the example of TDI, we aim to demonstrate that in nanoconfined geometries, quenching of the fluorescence of a dye becomes an important issue that needs to be taken into account. To obtain sustainable and reproducible results, the efficient protection against oxygen quenching cannot be neglected because the fluorescent response is used as a quantitative measure. To avoid this problem, herein we focus on the development of an oxygen protection strategy, applicable for a broad range of encapsulated materials.

The core–shell structure of the hybrid organic–inorganic nanoparticles allows independent molecular design of each part, in order to protect the encapsulated dye from fluorescence quenching by oxygen. For instance, the oxygen permeability of the shell material can be lowered drastically by using semicrystalline nanocellulose.<sup>51</sup> Furthermore, bovine serum albumin (BSA) film at the oil–water interface<sup>146</sup> or rose bengal embedded in a microcapsule shell<sup>147</sup> can also be used to protect the encapsulated dye from the molecular oxygen. Incorporating oxygen scavenging materials such as WO<sub>3</sub> photocatalysts loaded with Pt,<sup>148</sup> phosphonate coatings,<sup>149</sup> organophosphates<sup>150</sup> or polyoxyethanyl  $\alpha$ -tocopheryl sebacate<sup>49</sup> reduces the oxygen quenching significantly. Last but not least, another possibility is to attach an oxygen scavenger (e.g., diphenylanthracene moieties) to the emissive dye itself.<sup>151</sup> Decoration of the molecular structure of cyanine dyes including a cyclodextrin complex, acetyl modification, fluoro- and cyano-substitution leads to increased photostability of the fluorophore.<sup>3</sup> However, unfortunately, all these oxygen-protective strategies affect in general the properties of core and shell materials that are used to form nanoconfined materials.

Our main goal is to develop a strategy to avoid the reactive oxygen impact by applying an additional synthetic step, while keeping unchanged all parameters involved in the synthesis of the original nanoconfined materials. Exemplarily, polystyrene nanocontainers with a liquid core (i.e., hexadecane) synthesized by using the miniemulsion techniques will be protected by depositing metal oxide particles on the surface.

Deposition of metal oxide particles on the surface of polymer hybrid nanoparticles via controlled surface crystallization was shown in previous work of our group.<sup>126-128</sup> The regular arrangement of functional groups on the nanocapsule surface can provide nucleation and structure-directing centers for controlled crystallization of metal oxide particles. We have chosen cerium(IV) oxide nanoparticles to be deposited on the nanocapsule surface in order to combine biocompatibility with a high oxygen scavenging ability. Cerium oxide is a lanthanide metal oxide with a redox potential behavior that can easily switch between cerium(IV) and cerium(III) and has capability to leave oxygen vacancies in the crystal lattice.<sup>152</sup> Cerium(IV) oxide exhibits prominent antioxidant properties, ideal for applications such as water-gas shift catalysis,<sup>153</sup> combustion catalysis,<sup>154</sup> oxygen ion conductors and solid oxide fuel cells.<sup>155</sup> Due to the valence and oxygen defect properties of cerium(IV) oxide, nanoparticles of this material are also used as efficient free radical scavengers in biomedical applications as a potent therapeutic option for the treatment of ROS (reactive oxygen species) generated disorders such as neurodegenerative disorders, retinal disorders and cancer.<sup>156-158</sup>

In this section, we report the process of armoring anionically functionalized nanocontainers, loaded with TDI, by crystallizing cerium(IV) oxide nanoparticles on the nanocontainer surface. As a result, we obtain reproducible and sustainable fluorescent properties of the nanocapsules, independently from oxygen contamination of the external environment. The capsules in this section are described in Table 4.4.

**Table 4.4.** Characteristics of the different samples presented in this section.

Sample name	Material	Atmosphere	CeO <sub>2</sub> on nanocapsule surface	Diameter (nm) <sup>[a]</sup>
NC	PS	Air	No	140 nm ( $\pm$ 23%)
NC(Ar)	PS	Argon	No	153 nm ( $\pm$ 29%)
NC-CeO <sub>2</sub>	PS	Air	Yes	146 nm ( $\pm$ 30%)
NC(Ar)-CeO <sub>2</sub>	PS	Argon	yes	159 nm ( $\pm$ 18%)

[a] As obtained by DLS

### Polystyrene-based hybrid nanocapsules prepared by miniemulsion polymerization

The target of the work presented in this section was to design colloiddally stable polystyrene-based hybrid nanocapsules containing the fluorescent dye terrylene diimide (TDI) and armored with metal oxide nanoparticles on the polymer shell surface. Polymeric nanocapsules (labeled as sample **NC**) were prepared under ambient conditions by free-radical miniemulsion polymerization of styrene and acrylic acid (AA) (see experimental Section 7.4.1). The thickness of the shell of the formed nanocapsules was of ca. 20 nm in average and the weight ratio polymer/hexadecane was of ca. 1:2. The high mobility of the fluorescent dye was acquired by dissolving in liquid core (hexadecane), and ensuring effective fluorescence. The surface of the nanocapsules was negatively charged, as proven by polyelectrolyte titration, as a result of the used anionic surfactant and the hydrophilic comonomer (acrylic acid). Acrylic acid plays a crucial role in binding the cerium ions to the surface of nanocapsules and is also helpful to increase the hydrophilic nature in the system.<sup>159</sup> The obtained nanocapsules consist of a polymeric shell and an organic liquid core containing the fluorophore. The shell formation is likely to occur when the interfacial energy between the monomer and water is lower than between the hydrophobic core liquid and water. The nanocapsules are formed by phase separation of the copolymer being formed between styrene and acrylic acid in dispersed organic liquid droplets (hexadecane).<sup>121</sup> The pH value was adjusted to pH 10 for ensuring the

deprotonation of the carboxylic groups at the surface, required for an efficient binding of the metal ions.

#### 4.4.2. Protecting the nanocapsules from oxygen: Crystallization of cerium(IV) oxide on the nanocapsule surface

The crystallization of cerium(IV) oxide nanoparticles is carried out on the surface of the polymer nanocapsules (see experimental Section 7.4.3). First, the cerium ions from the precursor are complexed by the carboxylate functional groups and the crystallization occurs upon addition at a controlled rate of a base (NaOH), acting as a precipitating agent. SEM and TEM images, presented in Figure 4.14, demonstrate that the inorganic ceria nanoparticles were efficiently crystallized on the surface (Figure 4.14 a–b show pristine sample **NC** and Figure 4.14 c–d the hybrid sample **NC-CeO<sub>2</sub>**). The X-ray diffraction (XRD) pattern of the hybrid sample, shown in Figure 4.15, was unambiguously assigned to crystalline CeO<sub>2</sub> (ceria, JPCD card No. 34-0394). Elemental mapping by EDX also confirmed the presence of cerium in the investigated areas (see Figure 4.16). TEM images of ceria hybrid nanocapsules in Figure 4.17 indicate a homogeneous distribution of ceria nanocrystals on the capsules surface. The presence of bright spots on the dark field images (Figure 4.17b) confirms crystalline domains lying in the detection plane. A corresponding high resolution image of the hybrid sample **NC-CeO<sub>2</sub>** is shown in Figure 4.17 c–d. The ceria content for this sample was determined to be about 44 wt.% by thermogravimetric analysis (see Figure 4.18).

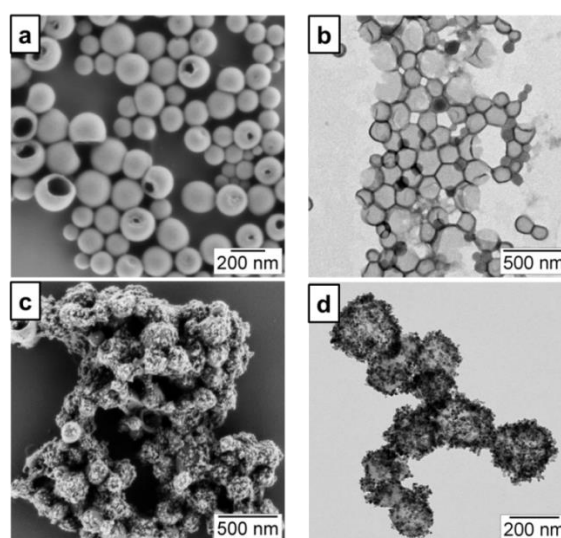


**Figure 4.14.** Electron micrographs the prepared capsules: a) SEM and b) TEM of carboxylate functionalized polystyrene hybrid nanocapsules (sample **NC**); c) SEM and d) TEM of ceria/polymer hybrid samples (sample **NC-CeO<sub>2</sub>**).<sup>123</sup>

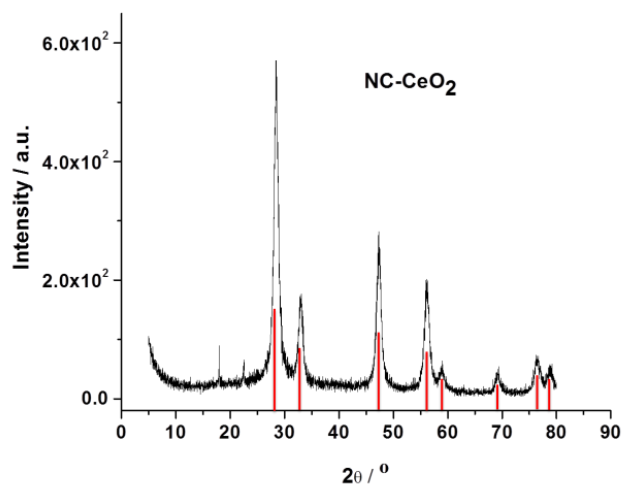


**Figure 4.15.** XRD pattern of hybrid polystyrene nanocapsules with cerium(IV) oxide on the surface (NC-CeO<sub>2</sub>). Vertical lines indicates the position and relative intensity of cubic cerium(IV) oxide crystal phase (JPCD card No. 34-0394).<sup>123</sup>

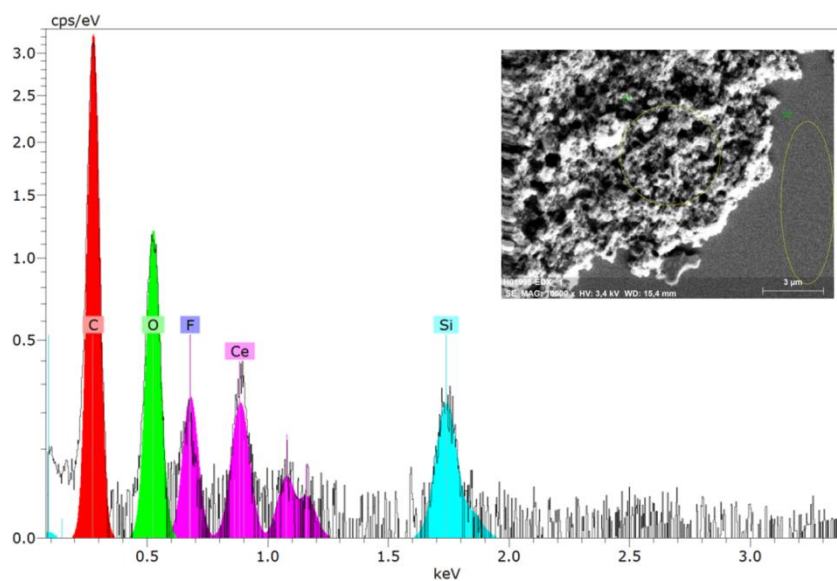


**Figure 4.16.** EDX spectrum and corresponding SEM picture of hybrid polystyrene nanocapsules with cerium(IV) oxide on surface (NC-CeO<sub>2</sub>).<sup>123</sup>

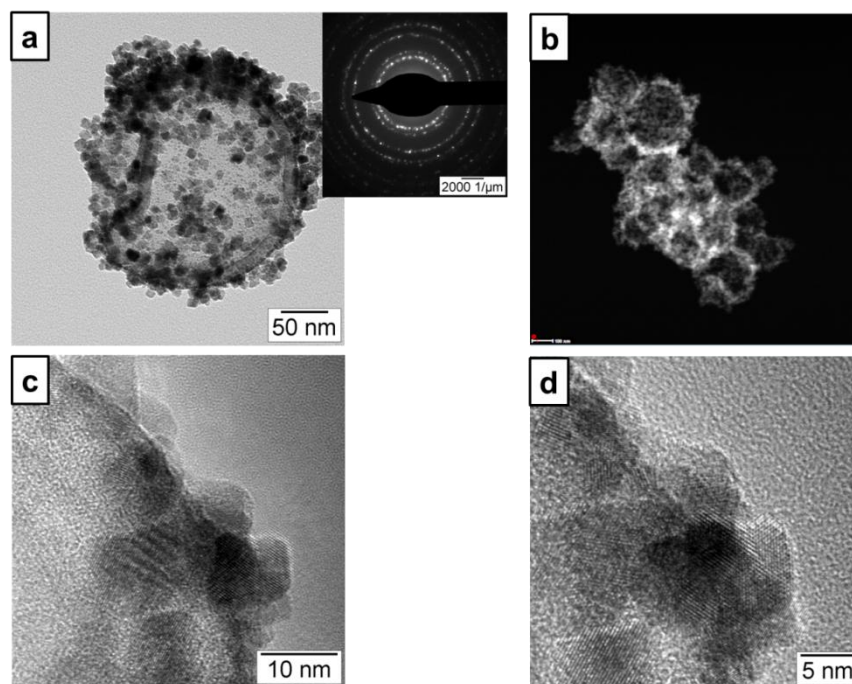


**Figure 4.17.** TEM images of  $\text{CeO}_2$ /polystyrene hybrid nanocapsules (sample:  $\text{NC-CeO}_2$ ): a) bright field image (inset shows the electron diffraction of the shown capsule), b) dark field image; and c) and d) high resolution images at different magnification.<sup>123</sup>

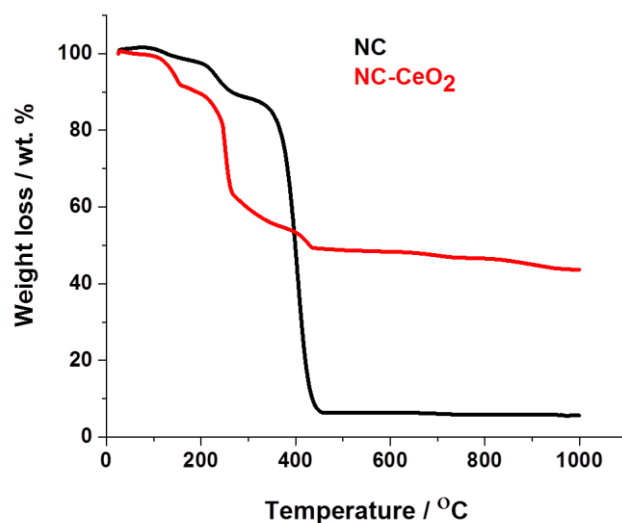


**Figure 4.18.** Thermogravimetric analysis curves of **NC** (black line, ambient conditions without cerium oxide) and **NC-CeO<sub>2</sub>** (red line, ambient conditions with cerium oxide).<sup>123</sup>

#### 4.4.3. Fluorescent properties of the nanocapsules

The fluorescence spectrum measured under ambient conditions for the pure polymer nanocapsules (sample **NC**) is shown in Figure 4.19 (black line). An intense fluorescence emission from terylene diimide (TDI) with  $\lambda_{\text{max}} = 685 \text{ nm}$  is observed. An important factor



influencing the decrease of fluorescence efficiency is the photo-oxidation. This kind of photochemical reaction is observed as a result of the interaction of the sample with singlet oxygen, which converts a fluorescent molecule into a state in which no longer absorbs and fluoresces. A possible explanation for the process of photo-oxidation in aromatic hydrocarbons is that non-zero probability for intersystem crossing always exists (e.g., the energy of an excited singlet state is transferred to the excited triplet state). The excited triplet state is relatively long-lived, even at room temperature, and can serve as a source for singlet oxygen generation.

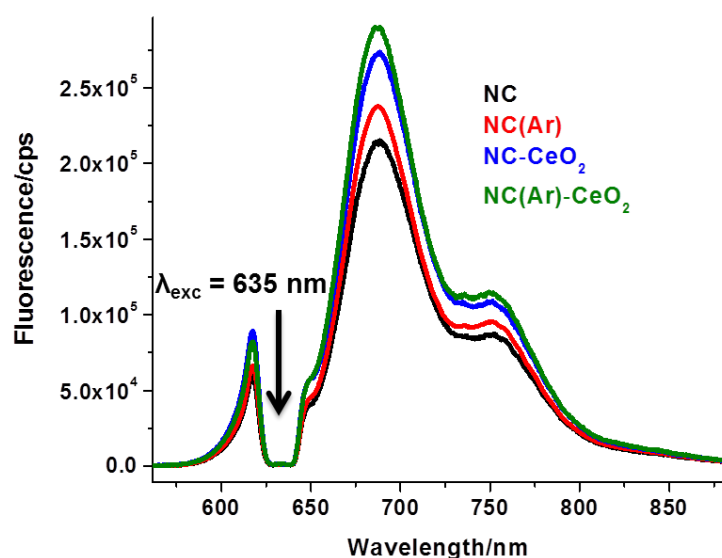


**Figure 4.19.** Fluorescence spectra of terylene diimide encapsulated in nanocapsules: **NC** (black line, ambient conditions without cerium oxide), **NC(Ar)** (red line, argon conditions without cerium oxide), **NC-CeO<sub>2</sub>** (blue line, ambient conditions with cerium oxide) and **NC(Ar)-CeO<sub>2</sub>** (green line, argon conditions with cerium oxide). The excitation intensity of 635 nm laser is  $0.2 \text{ W cm}^{-2}$ .<sup>123</sup>

In our case, during the encapsulation of TDI molecules, the molecular oxygen present in the external environment (e.g., in the water phase) can enter into already formed polymer nanocapsules due to the permeability of the thin polymer shell. Thus, singlet oxygen is created by the process of interaction between the electronic excited state of TDI and the ground state of molecular oxygen within the fluorescent encapsulated materials, which results in a photooxidation process. To overcome the limitations caused by oxygen influence, a sample named as **NC(Ar)** was prepared in a closed flask under argon atmosphere. The sample from the closed flask was transferred to a quartz cuvette under ambient conditions for further fluorescence measurements. The corresponding fluorescent spectrum measured under ambient

conditions is shown in Figure 4.19 (red line). The fluorescence efficiency is enhanced in comparison to the sample prepared under ambient conditions **NC** (black spectrum), which can be explained by the decrease of the concentration or total absence of the oxygen inside the capsules during polymerization step of sample **NC(Ar)**. This decrease resulted also in a decreased rate of photo degradation of the TDI molecule.

To further minimize the effect of fluorescence quenching, cerium(IV) oxide was crystallized on the surface of polymer sample **NC**, which yielded the hybrid sample **NC-CeO<sub>2</sub>**. The corresponding fluorescent spectrum is shown in Figure 4.19 (blue line). The fluorescence efficiency of **NC-CeO<sub>2</sub>** is enhanced in comparison to nanocapsules synthesized under ambient conditions without cerium(IV) oxide on surface (sample **NC**, black line), but also when compared with nanocapsules synthesized under argon atmosphere without cerium(IV) oxide on surface (sample **NC(Ar)**, red line). The improvement of the fluorescence in the presence of cerium(IV) oxide can be explained by a further reduction of the photo-oxidation process in the dye TDI.

Oxygen vacancies present in the structure of cerium(IV) oxide nanoparticles are the most likely origin of the enhancement of the fluorescence, since they can scavenge oxygen molecules of the environment and prohibit molecular oxygen to enter into nanocapsule. For a further improvement of the fluorescence emission, the deposition of cerium(IV) oxide was also carried out on nanocapsule samples prepared under inert atmosphere (the resulting sample is labeled as **NC(Ar)-CeO<sub>2</sub>**). The corresponding fluorescence spectrum is shown by the green curve in Figure 4.19. Control experiments were carried to confirm that the improvement of fluorescence efficiency originates from the formed cerium oxide and not from the cerium(III) precursor itself or any of the precipitating agent (see spectra in Figure 4.20). An enhancement of the fluorescence intensity took place only in the presence of the crystallized cerium(IV) oxide.

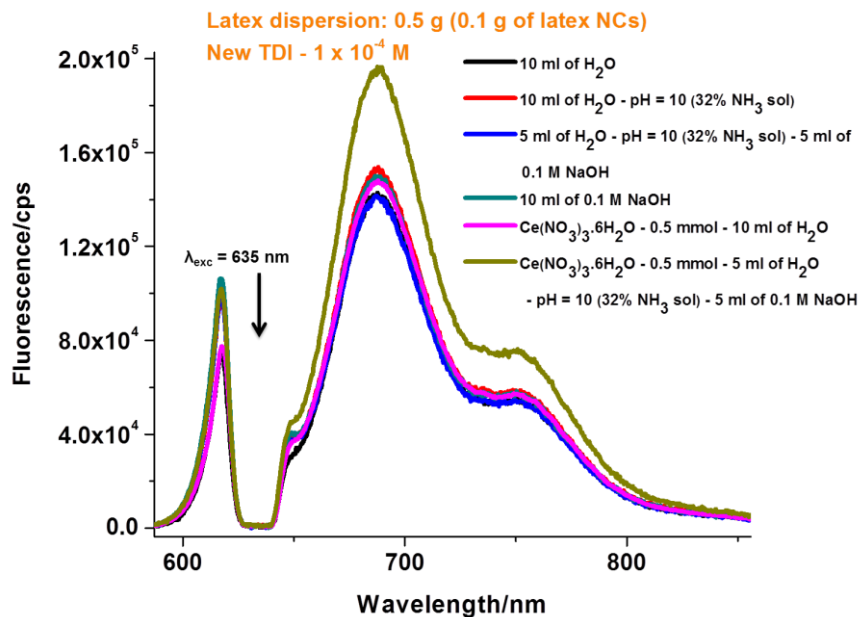


**Figure 4.20.** Luminescence spectra of terylene diimide encapsulated nanocapsules in various conditions with 635 nm laser using excitation intensity of  $0.2 \text{ W cm}^{-2}$ .<sup>123</sup>

To investigate that the effect of external oxygen, we recorded again the fluorescence emission spectra for all synthesized samples after having sealed the samples with argon in the gloves box (see Figure 4.21). The spectra did not show any significant difference when comparing samples prepared in an oxygen-free atmosphere.

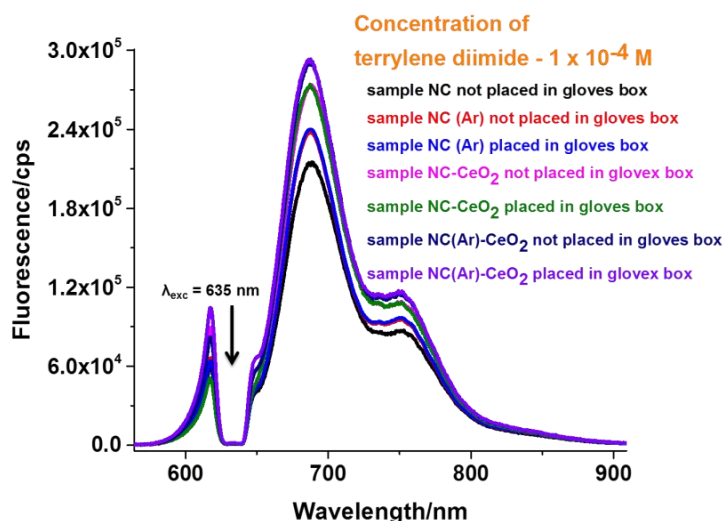


**Figure 4.21.** Luminescence spectra of terylene diimide encapsulated nanocapsules placed in gloves box and not in gloves box, NC (ambient conditions without cerium oxide), NC (Ar) (argon conditions without cerium oxide), NC-CeO<sub>2</sub> (ambient conditions with cerium oxide) and NC(Ar)-CeO<sub>2</sub> (argon conditions with cerium oxide). Excitation intensity of 635 nm laser is  $0.2 \text{ W cm}^{-2}$ .<sup>123</sup>

Finally, photodegradation experiments were carried out to investigate the stability of the fluorescence emission of pure polymer nanocapsules synthesized under ambient conditions (NC) and argon conditions NC(Ar) in comparison to the analogous hybrid nanocapsules with cerium(IV) oxide crystallized on the surface (NC-CeO<sub>2</sub>). The recorded spectra, shown in Figure 4.22, indicate that the emission is significantly higher and more stable in the hybrid CeO<sub>2</sub>-containing samples.

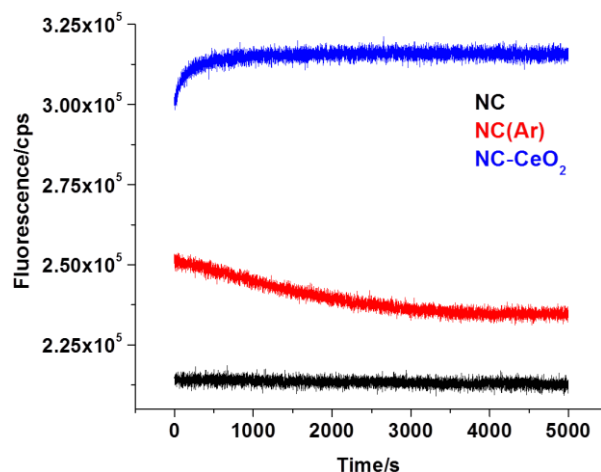


**Figure 4.22.** Photodegradation measurements of nanocapsules synthesized under different conditions without cerium oxide (sample NC in black, ambient conditions; sample NC(Ar) in red, under argon) and with cerium oxide on the surface (sample NC-CeO<sub>2</sub> in blue, ambient conditions).<sup>123</sup>

### 4.4.3. Conclusions

In this section, we have demonstrated that the armoring with CeO<sub>2</sub> of polystyrene nanocapsules containing a model fluorophore molecule (i.e., terrylene diimide) results in a significant enhancement of the fluorescence. The *in situ* crystallization of the metal oxide on the surface of the nanocontainers suppresses the photobleaching process of the fluorescent molecule by molecular oxygen. Hybrid CeO<sub>2</sub>/polymer samples simply prepared at ambient conditions under air are even more efficient in terms of fluorescence intensity than pure polymer nanocapsules carefully prepared under oxygen-free, inert atmosphere. The enhancement effect can be explained by the trapping of the quenching oxygen molecules on the metal oxide surface, which results in a reduction of the photo-oxidation process.

## 4.5. Inorganic protection of polymer nanocapsules: Screening of different materials on polystyrene capsules

In the section 4.4 we had observed the improvement in the fluorescence efficiency of encapsulated fluorophores with ceria/polymer hierarchical nanocapsules. Taking into consideration this effect, the upconversion efficiency is investigated herein by depositing different inorganic nanoparticles on the surface of polymeric nanocapsules. In this section, we report how to achieve sustainable UC properties by the synthesis of organic/inorganic hybrid nanocapsules encapsulated with triplet-triplet annihilation upconversion (TTA-UC) materials. Different inorganic materials are deposited on the surface of functionalized polymeric nanocapsules which are synthesized by free-radical polymerization in miniemulsion. The nanocapsules with varying amounts of surface-bound functional groups are produced by using different types of surfactants. Laponite clay  $[\text{Si}_8(\text{Mg}_{5.45}\text{Li}_{0.4})\text{O}_{20}(\text{OH})_4]\text{Na}_{0.7}$  is deposited on the surface of positively charged polystyrene nanocapsules via layer-by-layer deposition. Surfactant-free polystyrene nanocapsules are prepared by using the Pickering miniemulsion method. The controlled *in situ* mineralization of hydroxyapatite and the crystallization of cerium(IV) oxide are carried out on the surface of negatively charged polystyrene nanocapsules. The inorganic materials on the nanocapsules surface act as a scavenger and eventually avoid the entry of oxygen from external environment into nanocapsules encapsulated with TTA-UC materials. By avoiding the entry of oxygen, the photo-oxidation process of perylene molecules is avoided within the system, and an increase in the TTA-UC properties occurs.

### 4.5.1. Overview of different strategies for deposition of inorganic materials

The synergy of organic and inorganic components in hybrid nanoparticles has become a very active field of research, which has become a “meeting point” for physicists, polymer and colloid chemists, material scientists, and even physicians and biotechnologists. Among many others, hybrid particles find their application in catalysis, optoelectronics, cell imaging, or targeting drug delivery systems.<sup>122, 128, 160-161</sup> In particular, incorporation of inorganic materials *in* and *on* polymer substrates is of significance importance because of low density, large specific area, mechanical and thermal stabilities, and surface permeability. Polymeric materials can act as scaffolds or templates for the formation of inorganic materials, which yields in many cases nanoparticles with a core-shell structure.<sup>128, 162-163</sup> In such structures, the

surface properties of the final materials are varied by tuning the properties of the shell surrounding the core material. In the present work, we focus on polymer nanocontainers with an inorganic shell on the surface.

A first approach for deposition of inorganic components on the surface of polymer nanoparticles is to start with inorganic materials and polymer nanoparticles formed *ex situ* and combine them by using heterocoagulation and layer-by-layer strategies. Layer-by-layer deposition is simple and has been widely used, because of the ability to control precisely shape, composition, thickness, and properties of the shell material. In the context of hybrid particles, most typically, negatively charged inorganic materials are deposited on the polymer component through electrostatic interactions with positively charged polyelectrolytes.<sup>164-168</sup> By using this method, armored polymer nanoparticles with clay platelets were prepared by miniemulsion polymerization.<sup>169</sup> This approach will be shortly discussed in the next section (Section 4.6).

The second possible approach is to start with nanoparticles formed *ex situ*, and then conduct the polymerization *in situ*. This is exactly what occurs in the so-called Pickering emulsions.<sup>170</sup> Pickering emulsions are stabilized by adsorption of small colloidal particles at the oil-water interface and are thermodynamically stable through reduction of bare oil-water interface. Although the initial aim is not necessarily the preparation of hybrid materials, the resulting particles are certainly hybrid.<sup>90, 171-172</sup>

Finally, a third possibility for the inorganic deposition on polymer particles is the controlled *in situ* crystallization of the inorganic material. The regular arrangement of functional groups on the polymeric nanoparticles surface can provide nucleation and structural directing centers for the controlled crystallization of the inorganic component. Crystallization starts by addition of a precipitating agent. Here, we have chosen hydroxyapatite and cerium(IV) oxide (similarly to previous Section 4.4) as inorganic materials to be deposited on the surface of our nanocontainers.<sup>126, 173</sup> Hydroxyapatite (HAP) has been mainly chosen as a representative biomaterial due to its similarity to bone material, which is useful for biomedical applications in implant coatings.<sup>174-176</sup> The other model inorganic material chosen has been cerium(IV) oxide because the capability to leave oxygen vacancies in the crystal lattice,<sup>152</sup> which is the origin of its prominent antioxidant properties, ideal for applications in water-gas shift catalysis,<sup>153</sup> combustion catalysis,<sup>154</sup> oxygen ion conductors and solid oxide fuel cells.<sup>155</sup>

In this section, we aim to compare and evaluate the application of each of these strategies for the preparation of polymer/inorganic hybrid nanocapsules containing optically active molecules, namely upconversion dyes. In Section 4.3, we have reported that the properties of triplet-triplet annihilation upconversion (TTA-UC) can be enhanced by synthesizing the nanocapsules with upconversion dyes under protective conditions.<sup>121</sup> In recent years, nanocapsules containing upconversion dye molecules were used in biological applications, such as genetic detection and cell labeling.<sup>177-178</sup> An important factor influencing the decrease in efficiency of the TTA-UC process is the presence of oxygen.<sup>179</sup> Molecular oxygen is involved in triplet-energy transfer processes of TTA-UC because of the occurrence of ground state triplet multiplicity.<sup>38, 46</sup> Due to the small size and high diffusion, oxygen quenches efficiently the populated triplet states of the sensitizer molecules in TTA-UC processes and creates extremely reactive singlet oxygen, which leads to degradation of active dye molecules.<sup>54, 56</sup> By synthesizing hybrid organic-inorganic nanocapsules containing upconversion dyes, the singlet oxygen generation is reduced and results in the improvement of upconversion properties.

Herein, we target on the fabrication of hybrid polymeric nanocapsules with encapsulated UC dyes by the deposition of Laponite RD, hydroxyapatite, and cerium(IV) oxide on the surface of polystyrene nanocapsules. As a result, we obtain efficient and sustainable upconversion properties of the nanocapsules by suppressing the oxidative degradation from the external environment.

We synthesized polystyrene nanocapsules containing upconversion dyes with either cationic or anionic surface functionalization (see experimental Section 7.5.1). The encapsulated dyes were palladium(II) 2,3,7,8,12,13,17,18-octaethyl-21H,23H-porphyrin (abbreviated as PdOEP) as a sensitizer and perylene as an emitter, dissolved in hexadecane. The capsules were prepared by free-radical miniemulsion copolymerization of styrene and a second functionalizing comonomer. A cationically functionalized sample (labeled as sample **PS1**, cf. Table 4.5) was prepared by using 2-aminoethyl methacrylate hydrochloride (AEMH) as a comonomer and cetyltrimethylammonium bromide (CTAB) as a surfactant, while acrylic acid as a comonomer and sodium dodecyl sulfate (SDS) as a surfactant were used for the preparation of an anionically functionalized sample (labeled as sample **PS2**). SEM and TEM images of the prepared nanocapsules are shown in Figure 4.23. A complete shell formation is possible only when the interfacial energy between the monomer and water is higher than between the hydrophobic core liquid and water.<sup>30, 121</sup> The nanocapsules are generated by

#### 4. Results and discussion

---

phase separation between the forming copolymer and the dispersed organic liquid (hexadecane).<sup>159</sup>

**Table 4.5.** Characteristics of the different samples presented in this section.

---

<b>Sample name</b>	<b>Type of surfactant</b>	<b>Surface functionalization</b>	<b>Inorganic shell</b>	<b>Deposition method</b>
PS1	CTAB	-NH <sub>2</sub>	None	---
PS2	SDS	-COOH	None	---
PS3	CTAB	-NH <sub>2</sub>	Clay	Layer-by-layer
PS4	SDS	COOH	Hydroxyapatite	In situ crystallization
PS5	SDS	-COOH	CeO <sub>2</sub>	In situ crystallization

---

To enhance the TTA-UC properties of the encapsulated dyes in the nanocapsules, we deposited inorganic materials on the surface of polystyrene nanocapsules by either (i) starting from ex-situ formed materials (namely silicate clay platelets) or (ii) by in-situ formation of inorganic nanoparticles (namely ceria and hydroxyapatite). The inorganic components cover the polymer shell and play an important “protecting” role by avoiding the entry of molecular oxygen into the nanocapsules.



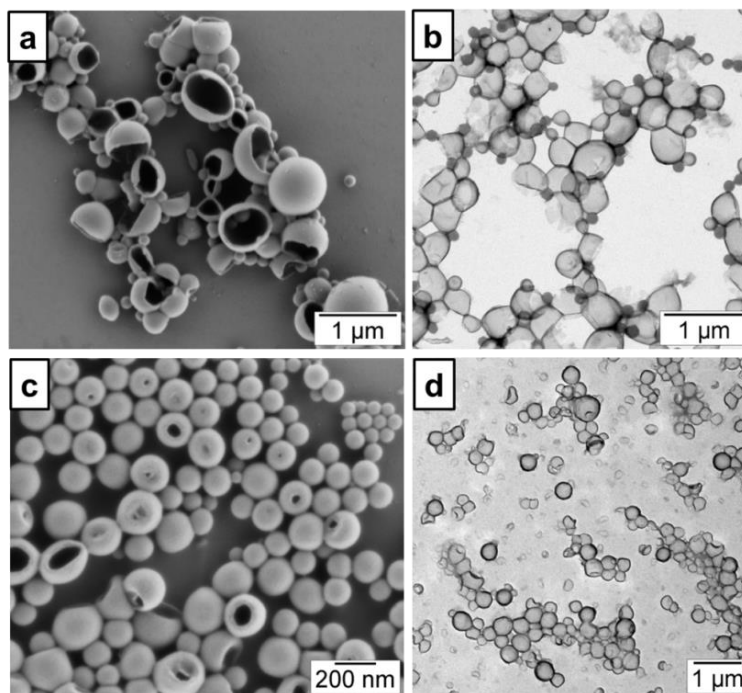


**Figure 4.23.** Microscopic images of encapsulated TTA-UC dyes: a) SEM and b) TEM images of amino functionalized polystyrene hybrid nanocapsules (sample **PS1**), c) SEM and d) TEM images of carboxylate functionalized polystyrene hybrid nanocapsules (sample **PS2**).

#### 4.5.2. Protection of polymer nanocapsules with silicate clay formed ex situ

A silicate clay was deposited on the surface of the amino-functionalized sample **PS1** by adapting a previously reported layer-by-layer deposition method see Figure 4.24.<sup>169</sup> The experimental details are explained in Section 7.5.2. The selected clay was Laponite RD, which is a synthetic trioctahedral hectorite clay composed of two tetrahedral silica sheets and a central octahedral magnesia sheet. Its chemical formula is  $[\text{Si}_8(\text{Mg}_{5.45}\text{Li}_{0.4})\text{O}_{20}(\text{OH})_4]\text{Na}_{0.7}$ , with a density of  $2570 \text{ kg m}^{-3}$ . These solid disk-like particles were observed by transmission electron microscopy (TEM) before deposition (see Figure 4.25). The disc like clay platelets have an overall negative charge with the rim being amphoteric and can act as individual colloids in pure water with approximately 1 nm of thickness and a lateral diameter of ca. 25-35 nm.<sup>180-182</sup> The clay sheets were dispersed in water by a high-powered homogenization step to avoid flocculation during the miniemulsion process. After addition of the clay to the polystyrene dispersion, the medium was acidified ( $\text{pH} = 3$ ) for complexation of the silicate to the nanocapsules. SEM and TEM images of the resulting clay/polystyrene hybrid nanocapsules (sample **PS3**) are shown in Figures 4.26 a-b, respectively. Elemental analysis by

energy-dispersive X-ray (EDX) spectroscopy confirmed the presence of silicate on the surface of the amino functionalized nanocapsule (see Figure 4.27).

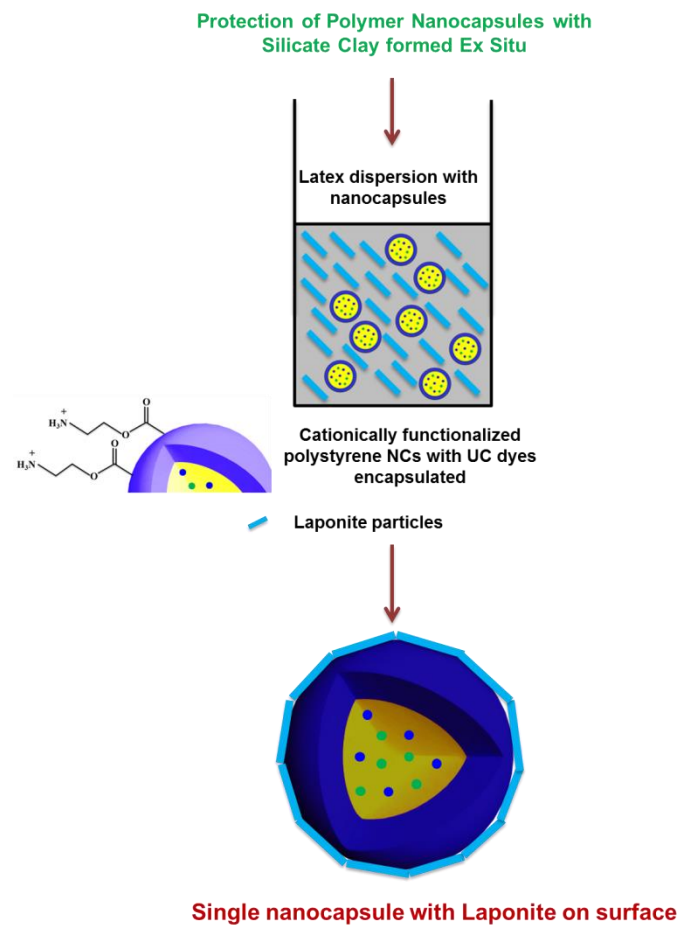


**Figure 4.24.** Schematic representation of deposition of Laponite solid particles on the surface of polystyrene nanocapsules via layer by layer deposition method (sample PS3).

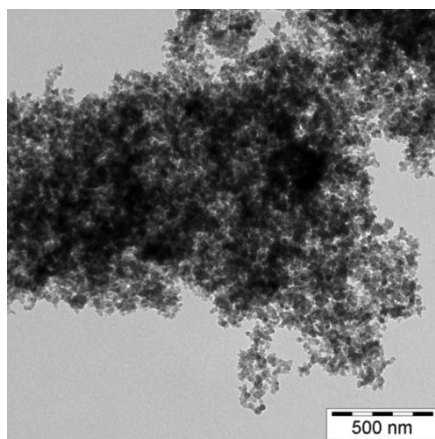


**Figure 4.25.** TEM image of only Laponite RD nanoparticles after ultrasonication process.

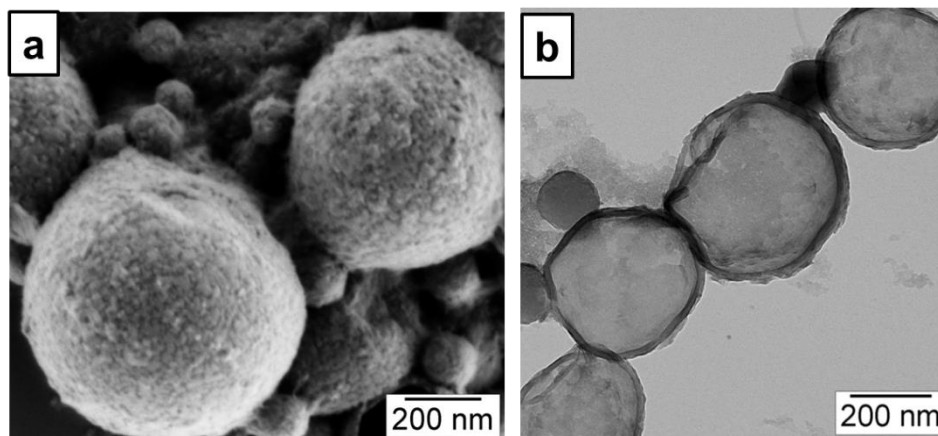


**Figure 4.26.** Microscopic images of the deposited inorganic materials on the surface of synthesized nanocapsules. a) SEM and b) TEM images of deposited Laponite RD on the surface of amino functionalized polystyrene nanocapsules by layer by layer deposition method (sample **PS3**).

As expectable, the surface charge density of the positively charged capsules changes drastically depending on the acidity of the medium:  $0.2 \text{ nm}^{-2}$  at pH 10,  $0.7 \text{ nm}^{-2}$  at pH 7, and  $1.7 \text{ nm}^{-2}$  at pH 3). The deposition of clay on the surface of functionalized nanocapsules was investigated at different pH values (see Figure 4.28 a-c), and the best results were observed at pH 3. With increase in pH the deposition of Laponite RD solid particles on the surface of amino functionalized particles was gradually decreased due to the protonation of the amino groups.

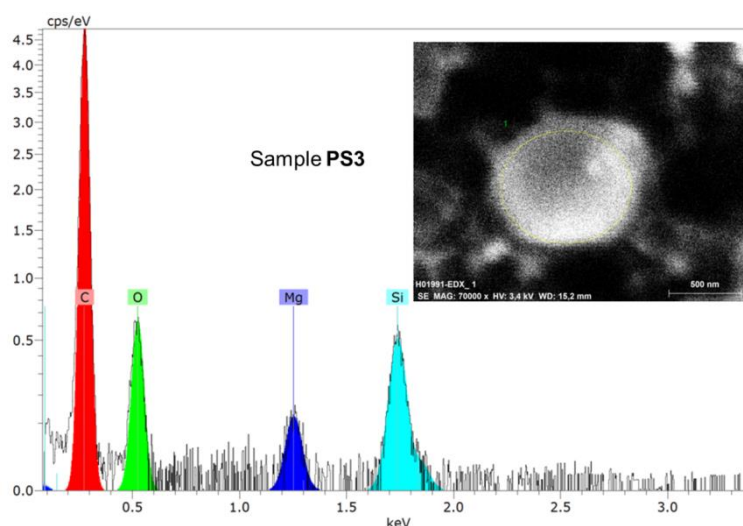


**Figure 4.27.** EDX spectrum of polystyrene nanocapsules with Laponite RD on the surface prepared by layer-by-layer deposition method (sample **PS3**). The spectrum is taken for the corresponding indicated area (spot in the SEM picture which is included on the top right side).

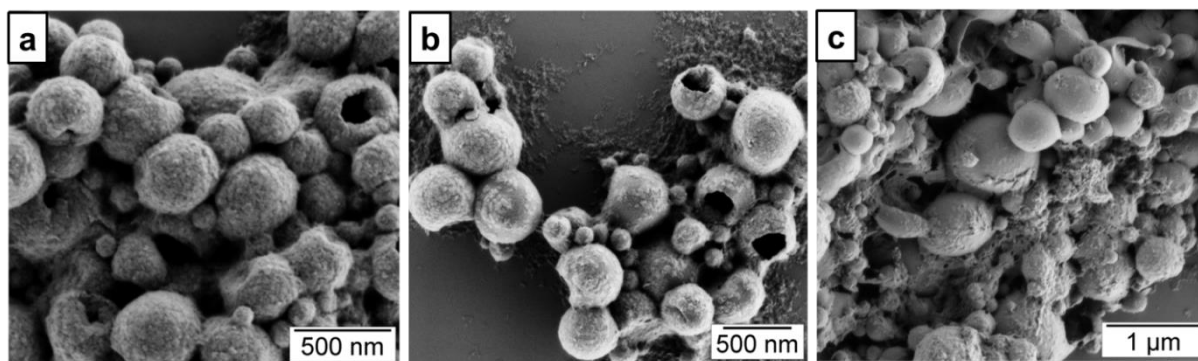


**Figure 4.28.** SEM images of polystyrene nanocapsules with Laponite RD on the surface by using layer-by-layer deposition method (sample **PS3**) at different pH: a) at pH = 3 b) pH = 7 and c) pH = 10.

### 4.5.3. In situ crystallization of hydroxyapatite and cerium oxide on the surface of polymer nanocapsules

The process of crystallization of hydroxyapatite and cerium(IV) oxide nanoparticles on the surface of carboxylate-functionalized nanocapsules occurs in a stepwise (see scheme in Figure 4.29). The experimental procedure is explained in Section 7.5.3. The pH of the nanocapsule latex dispersion (sample **PS2**) was brought to pH 10 to ensure the deprotonation of the carboxylic groups, required for an efficient complexation of the metal ions. The determined surface charge density at pH values of 3, 7, and 10 was 0.3, 0.6, and  $1.6 \text{ nm}^{-2}$ , respectively. The precipitating agent is added afterwards at a controlled rate to drive the precipitation reaction. The crystallization of the inorganic materials on the capsule surface occurs effectively when the supersaturation level is controlled by the dropping rate of precipitating agent.<sup>126, 173</sup> SEM and TEM images demonstrate clearly the crystallization of hydroxyapatite (Figure 4.30 a-b) and ceria (Figure 4.30 c-d). Elemental analyses by energy-dispersive X-ray (EDX) spectroscopy confirmed the presence of the inorganic materials.

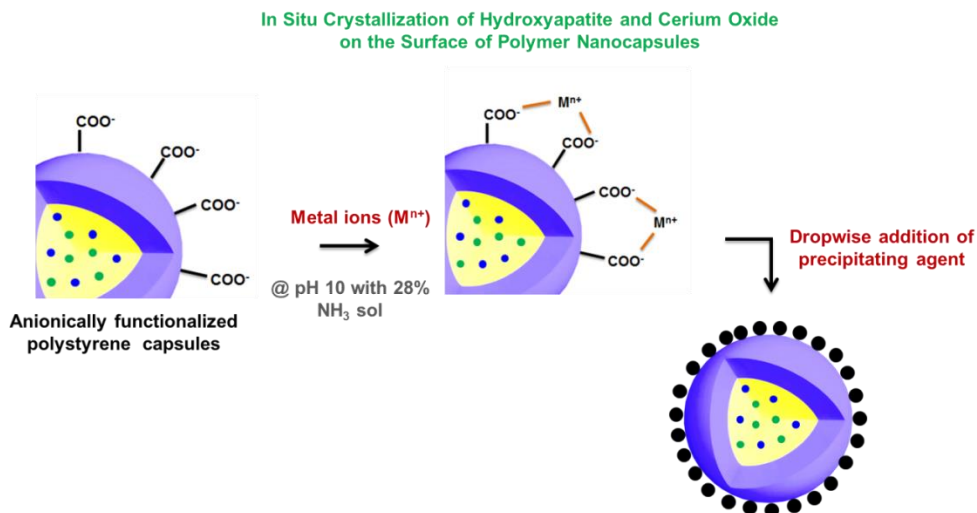


**Figure 4.29.** Schematic representation of in-situ crystallization of hydroxyapatite and cerium(IV) oxide on the surface of polymer nanocapsules (sample **PS4** and **PS5**).

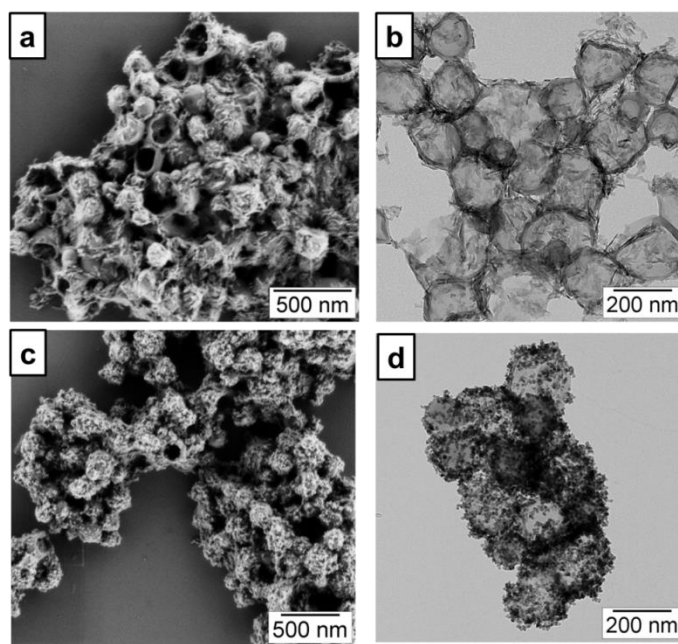


**Figure 4.30.** a) SEM and b) TEM images of carboxylate functionalized polystyrene nanocapsules with hydroxyapatite on the surface by the process of mineralization (sample **PS4**), and c) SEM and d) TEM images of cerium oxide formation on the surface of carboxylate functionalized polystyrene nanocapsules by the crystallization process (sample **PS5**).

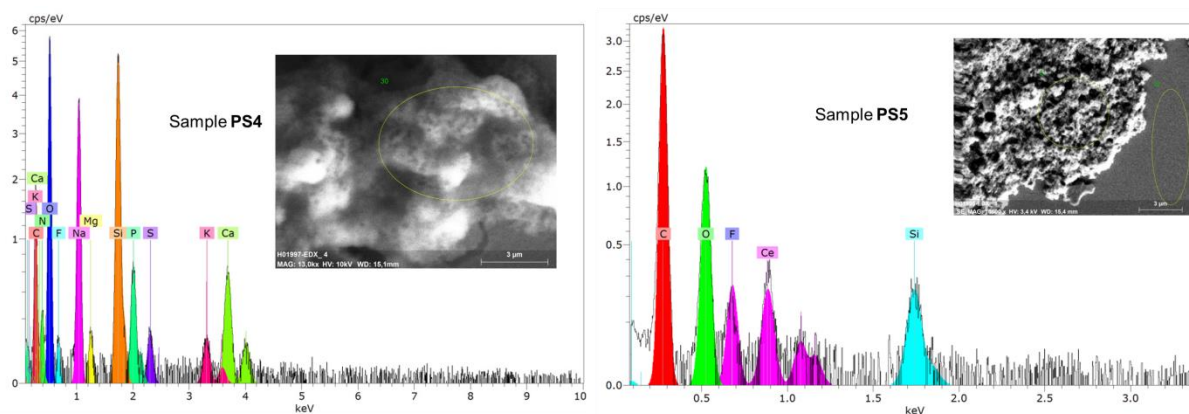


**Figure 4.31.** EDX spectrum of polystyrene nanocapsules with a) hydroxyapatite on the surface via mineralization method (sample **PS4**). The spectrum is taken for the corresponding indicated area (spot in the SEM picture which is included on the top right side), and b) ceria on the surface via crystallization method (sample **PS5**) at corresponding indicated area (spot in the SEM picture which is included on the top right side).

#### 4.5.4. Fluorescence properties of polymer and polymer/inorganic nanocapsules

The photoluminescence (PL) emission spectra of pure amino-functionalized polymeric nanocapsules with PdOEP and perylene (sample **PS1**) is shown in Figure 4.32-a (black curve), and pure carboxylate-functionalized polymeric nanocapsules (sample **PS2**) with PdOEP and perylene is shown in Figure 4.32-b (black curve). Intensive UC fluorescence of perylene with  $\lambda_{\max} = 470$  nm and residual phosphorescence of sensitizer molecule (PdOEP) with  $\lambda_{\max} = 670$  nm were observed upon excitation at 532 nm. The nanocapsules were prepared under ambient conditions by disregarding intentionally the fact that the molecular oxygen present in the external environment (e.g., in the water phase) can enter into already formed polymer nanocapsules because the thickness of the polymer shell was ca. 20 nm.

The UC efficiency for the clay/polystyrene hybrid sample **PS3** is enhanced by 41 % (excitation at 532 nm, intensity:  $3 \text{ W cm}^{-2}$ ) when compared to the sample **PS1** without clay and is shown in (Figure 4.32-a, red curve) in comparison to nanocapsules without Laponite. The inorganic materials on the surface of nanocapsules act, as mentioned above, as a protecting layer that reduces the triplet molecular oxygen of entering into nanocapsules, improving the final upconversion features.

For the samples in which the inorganic materials are prepared in situ, the UC process is enhanced up to 50% for the case of hydroxyapatite (sample **PS4** – red curve) and up to values as high as 86% (with respect to samples without inorganic material – black curve) for ceria-protected nanocapsules (sample **PS5** – blue curve) and is shown in Figure 4.32-b. Ceria

nanoparticles trap very efficiently molecular oxygen from the external environment (e.g., in the water phase) due to the presence of oxygen vacancy positions. The dependence of the luminescence signal on the excitation intensity is shown in Figure 4.33 and it should be noted that the upconversion has been observed at much lower excitation intensities. The results show that the photo-oxidation process of perylene molecules and the generation of singlet oxygen have been reduced.

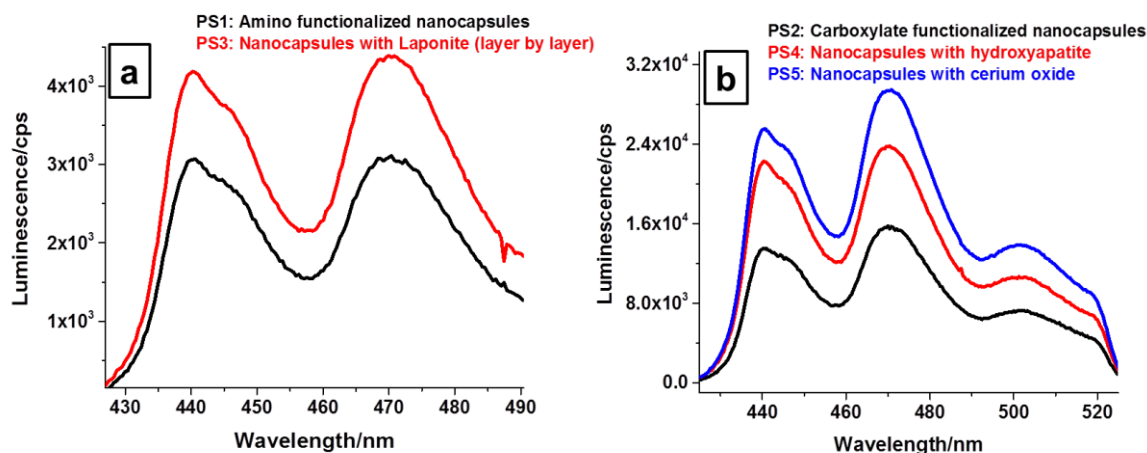


**Figure 4.32.** Luminescence spectra of TTA-UC encapsulated polystyrene nanocapsules with inorganic components on the surface using different methods, as follows: a) Protection of polymer nanocapsules with silicate clay formed ex Situ (method 1), amino functionalized nanocapsules without Laponite RD (sample **PS1** black curve) and with Laponite RD (sample **PS3** red curve), and b) in Situ crystallization of hydroxyapatite and cerium oxide on the surface of polymer nanocapsules (method 2), carboxylate functionalized nanocapsules without inorganic components (sample **PS2** black curve), with hydroxyapatite (**PS4** red curve) and cerium(IV) oxide (**PS5** blue curve). Excitation intensity of  $\lambda = 532$  nm laser is  $3 \text{ W cm}^{-2}$ .

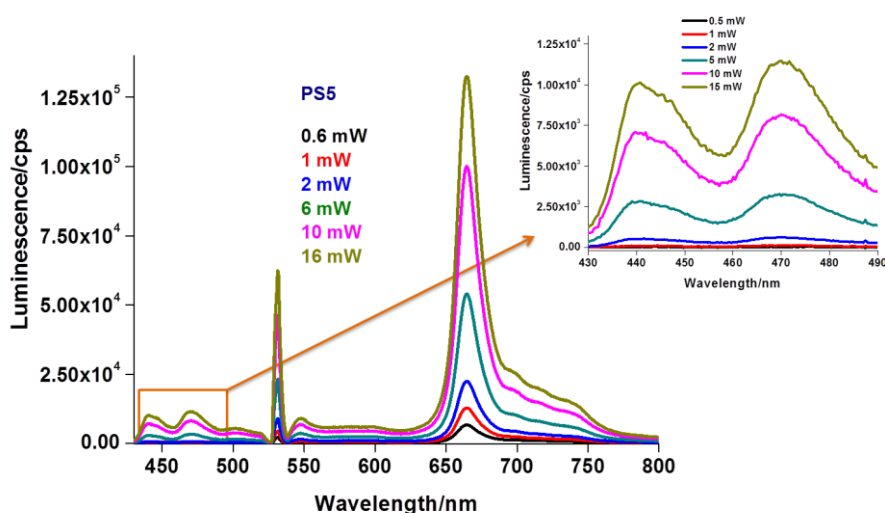


**Figure 4.33.** Luminescence spectra of synthesized polystyrene/hexadecane nanocapsules with ceria on the surface upon various excitation intensities of a 532 nm laser (from lower excitation intensity of 0.6 mW to higher excitation intensity of 16 mW).

### 4.5.3. Conclusions

A significant enhancement of the upconversion emission was successfully observed in polystyrene nanocapsules protected with inorganic components on the surface. Laponite RD solid particles were deposited via layer-by-layer deposition method. Hydroxyapatite and CeO<sub>2</sub> were deposited via in situ controlled crystallization. The inorganic materials on the surface act as a scavenging material and avoid the molecular oxygen from the external environment. This results in reduction of formation of singlet oxygen at the triplet state and further increases the triplet-triplet energy transfer in the UC system. The enhancement can be explained by suppression of the photo-oxidation of perylene molecules due to molecular oxygen.

## 4.6. Pickering miniemulsion method

In this section, we report another method to improve the upconversion properties in polystyrene nanocapsules by depositon of Laponite clay solid particles on the surface via Pickering miniemulsion method. As discussed at the beginning of the Section 4.5, the other possible method to deposit inorganic solid particles on to the surface of nanocapsules, without addition of any surfactant, is the use of the so-called Pickering emulsions.<sup>170</sup> The stabilization of the emulsion is attributed to a kinetic barrier resulting from a viscosity increase of the continuous medium between the droplets or to the mechanism of particle adsorption itself. The formation of particle film at the liquid/liquid interface occurs only when the particles have a contact angle close to 90° to both liquids. Pickering or solid stabilized emulsions have wide range of application in commercial areas such as food, cosmetics, oil refining, petrochemicals and ore purification.<sup>90, 171-172, 183-184</sup>

### 4.6.1. Deposition of silicate clay on polystyrene nanocapsules

As an alternative to the layer-by-layer method presented in Section 4.5.2, silica clay sheets (Laponite RD) can also be deposited on the surface of nanocapsules by using the Pickering miniemulsion method (see Figure 4.34). The experimental details are explained in Section 7.6. Surfactant-free clay/polymer hybrid nanocapsules labelled as (sample **PM**) were prepared in this way. Sodium chloride was added during the ultrasonication process of clay disks to induce a colloidal instability leading to the clay particle flocculation, so that the viscosity increases dramatically. This improves the extent of clay to occur Pickering stabilization of oils in water and compressing the ionic double layer around the dispersed particles. After the



addition of monomer phase to continuous phase, the overall system viscosity is lowered in comparison to that of the aqueous dispersion of clay disks in NaCl solution.<sup>185</sup> The capsule formation was clearly demonstrated by electron microscopy (Figure 4.35 a-b) and the silicate presence on the surface was proven by EDX (see Figure 4.36).

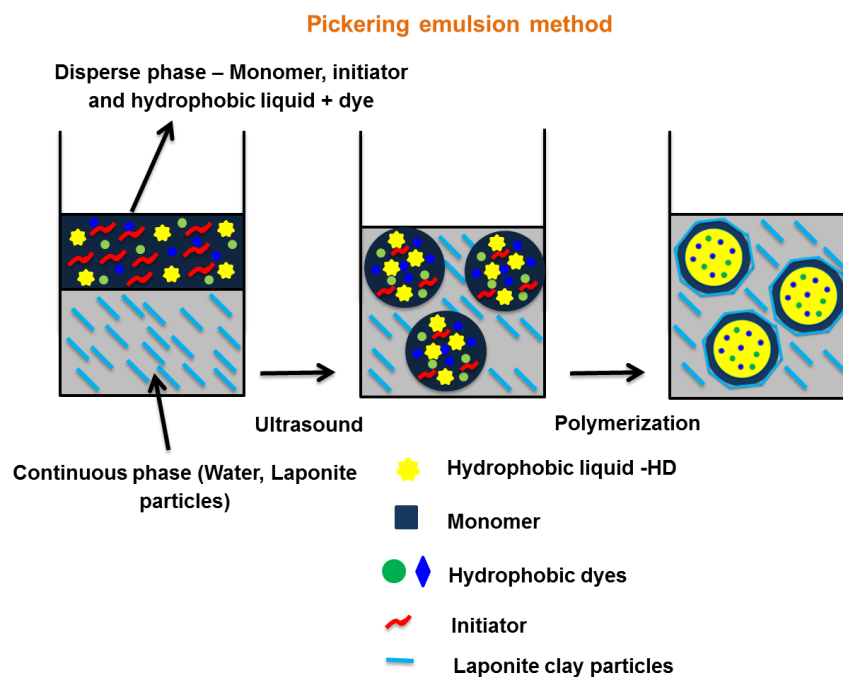


**Figure 4.34.** Schematic representation of deposition of Laponite solid particles on the surface of polystyrene nanocapsules via layer by Pickering miniemulsion method (sample **PM**).

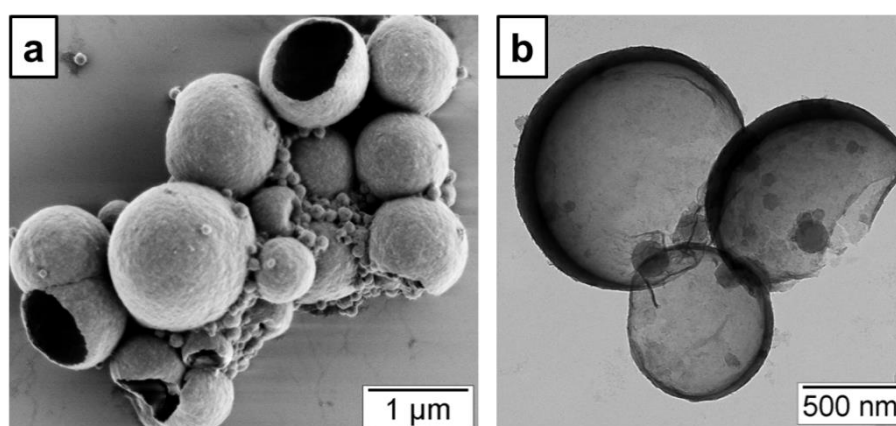


**Figure 4.35.** Microscopic images of the deposited inorganic materials on the surface of synthesized nanocapsules. a) SEM and b) TEM of nanocapsules synthesized using free surfactant Pickering miniemulsion process with Laponite RD on the surface (sample **PM**).

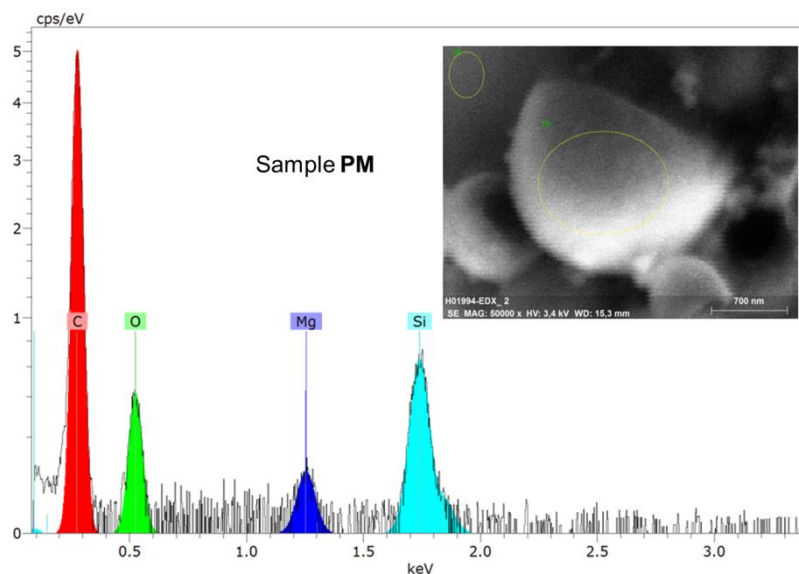


**Figure 4.36.** EDX diffraction spectrum of polystyrene nanocapsules with Laponite RD on the surface using Pickering miniemulsion method (sample **PM**) at corresponding indicated area (spot in the SEM picture which is included on the top right side).

Generally, in direct miniemulsion process the amounts of surfactant is varied to tune the size of nanoparticles or nanocapsules.<sup>186</sup> Since the small clay solid particles play the role of a surfactant in or Pickering systems, we investigated the effect of the amount of clay in a set of experiments (see Figure 4.37 a-d). Although the size of the nanocapsules was reduced with an increase in the amounts of clay particles, high amounts also resulted in the formation of solid (instead of hollow) nanoparticles and incomplete shell formation (see Figure 4.37-a). The corresponding SEM image shows that the formed polystyrene nanoparticles are covered with high amounts of clay. We also increased the amounts of clay particles above 1.4 wt% to observe the effect of deposition on the surface of capsules, but this resulted in a milky agglomeration during the ultrasonication step.

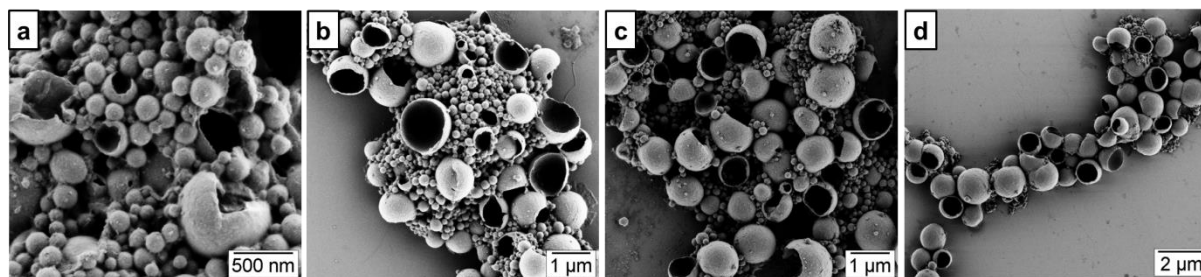


**Figure 4.37.** SEM images of polystyrene nanocapsules (sample **PM**) synthesized using Pickering miniemulsion method by varying the quantity of Laponite nanoparticles with respect to water to control the particle size and deposition on surface: a) 1.4 wt %, b) 1.2 wt %, c) 1 wt % and d) 0.8 wt %.

### 4.6.2. Fluorescent properties

The photoluminescence (PL) emission spectra of pure polystyrene nanocapsules prepared via radical polymerization method (sample **KK-MP-01** cf. Table 4.2) encapsulated with PdOEP and perylene, are shown in Figures 4.38, respectively (black curve). Intensive UC fluorescence of perylene with  $\lambda_{\text{max}} = 470$  nm and residual phosphorescence of sensitizer molecule (PdOEP) with  $\lambda_{\text{max}} = 670$  nm were observed upon excitation at 532 nm. The corresponding luminescence spectrum of sample **PM** prepared via Pickering miniemulsion is shown in Figure 4.38 (red curve). In comparison to nanocapsules without Laponite (black curve), the UC process is enhanced by 67%. The increase in the efficiency can be explained by a combination of two effects: (i) the presence of clay particles on the surface of capsules, which hinders the molecular oxygen to enter into nanocapsules; and (ii) the increase in size of the resulting capsules (see Figure 4.35 a-b). The free movement of sensitizer and emitter molecules in nanocapsules of bigger size results in more triplet energy transfer in comparison to smaller ones.

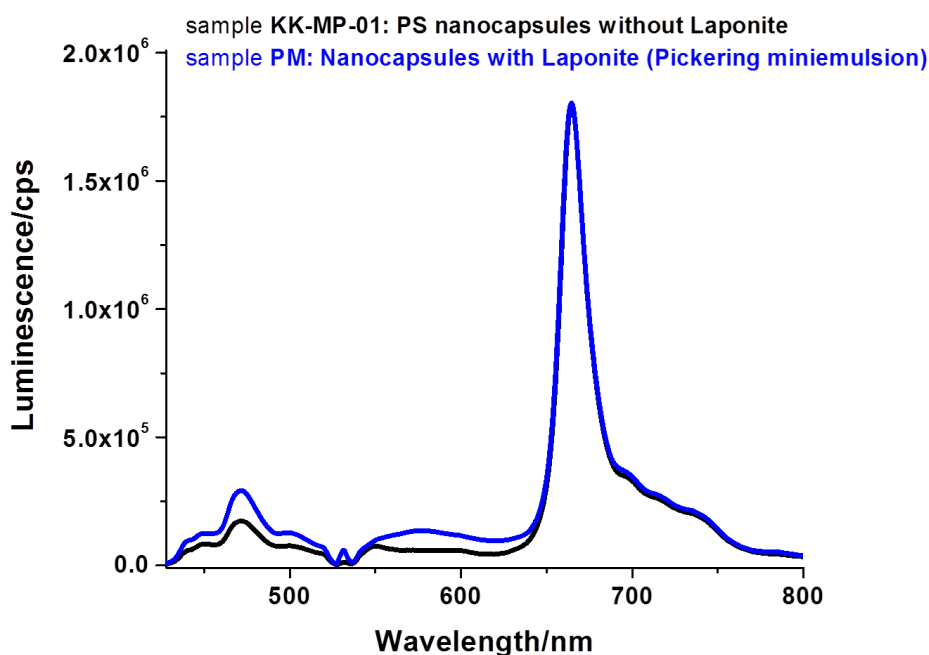


**Figure 4.38.** Luminescence spectrum of nanocapsules synthesized via free radical polymerization method with no Laponite on surface (sample **RP**) and with Laponite via Pickering miniemulsion method (the sample **PM**). The excitation intensity was 532 nm laser (power of the laser: 1 W cm<sup>-2</sup>).

### **4.6.3. Conclusions**

Laponite clay solid particles were successfully deposited on the surface of polystyrene nanocapsules via Pickering miniemulsion method. An enhancement of UC was observed in the nanocapsules with solid particles on the surface. Clay particles on the surface act as a scavenging material and avoid the molecular oxygen to enter into the nanocapsules.

## 5. General conclusions

The main focus of this thesis was to encapsulate the hydrophobic triplet-triplet annihilation upconversion (TTA-UC) and fluorescent materials into polymeric nanocapsules and to protect the system from the influence of molecular oxygen. Different controlled strategies were used to achieve the goal of reducing the formation of singlet oxygen that quenches the properties.

In Section 4.2, the shell material of the nanocapsules was varied by using different polymers with different crystallinity nature to investigate the change in upconversion properties. Poly(methyl methacrylate) (PMMA) and poly(L-lactic acid) (PLLA) nanocapsules were successfully synthesized using the solvent evaporation method to encapsulate the hydrophobic organic dye molecules (sensitizer: PdOEP and emitter: perylene). The intensive UC fluorescence of perylene with  $\lambda_{\max} = 470$  nm was only observed in PMMA nanocapsules but not in PLLA ones, which may be explained by the formation of polymer coagulum during preparation of the capsules. Furthermore, to observe the change in upconversion, different polymeric nanocapsules were successfully synthesized via free-radical polymerization. The TTA-UC dye molecules were successfully encapsulated in polystyrene (PS), PMMA, poly(acrylonitrile) (PAN), and poly(acrylonitrile/styrene) P(AN-co-S). The UC fluorescence of perylene with  $\lambda_{\max} = 470$  nm was only observed in PS and PMMA nanocapsules. The absence of UC emission in PAN and P(AN-co-S) nanocapsule was correlated with a high intensity emission at 570 nm, which could be due to the formation of molecular dimers from the emitter molecule (perylene). Overall, we conclude that using different polymeric materials in the nanocapsule shell does not influence significantly the upconversion properties.

In Section 4.3, the nanocapsules containing TTA-UC dyes were successfully synthesized under protective conditions (i.e., complete darkness and argon atmosphere) by free-radical miniemulsion polymerization. Both UC fluorescence and residual sensitizer phosphorescence were strongly enhanced in the polystyrene nanocapsules synthesized under argon atmosphere and darkness when compared to the ones synthesized under ambient and daylight conditions. We demonstrate that argon and darkness play a very important role in the improvement of the UC process as a result of an increased rate of triplet-triplet transfer from the PdOEP to perylene. By using this strategy, UC emission was successfully observed upon very low excitation intensity of  $\lambda = 532$  nm laser (intensity is tens of  $\text{mW cm}^{-2}$ ).

In Section 4.4, the enhancement of the fluorescent process was achieved by armoring with CeO<sub>2</sub> polystyrene nanocapsules containing a model fluorophore molecule (i.e., terylene diimide). The photo-oxidation process of the fluorescent molecule was successfully reduced by the in-situ crystallization of the metal oxide on the surface of the nanocontainers. The presence of oxygen vacancies in the structure of cerium(IV) oxide nanoparticles on the surface of polystyrene nanocapsules are useful to enhance the fluorescence. Thus, molecular oxygen from the external environment can be trapped into vacancy sites, prohibiting its entrance into the nanocapsules, which results in the reduction of the formation of singlet oxygen within the system. The fluorescence intensity was higher in hybrid CeO<sub>2</sub>/polymer nanocapsules prepared at ambient conditions under air than in pure polymer nanocapsules carefully synthesized under oxygen-free, inert atmosphere.

In Section 4.5, we compare the effectivity of using different inorganic materials (Laponite RD, hydroxyapatite and CeO<sub>2</sub>) in the armoring of polystyrene nanocapsules. Laponite RD was successfully deposited by using layer-by-layer deposition method. Controlled in-situ crystallization was used to deposit hydroxyapatite and CeO<sub>2</sub> on the nanocapsule surface. The triplet-triplet energy transfer from the sensitizer to the emitter molecule was increased by the presence of inorganic materials on the surface and further the photodegradation process of perylene molecule was reduced in the nanocapsules.

Finally in Section 4.6, we investigated the use of Pickering miniemulsions to create hybrid clay-polystyrene nanocapsules. The particles were successfully placed on the surface and results in the enhancement of UC properties. The UC enhancement can be explained by two effects: (i) the presence of clay particles on the surface of capsules, which hinders the molecular oxygen to enter into nanocapsules; and (ii) the increase in the size of capsules, which helps the free movement of sensitizer and emitter molecules within the system, resulting in an increase of the triplet-triplet energy transfer.

The different strategies described in this work provide a pool of different routes to control the structure of polymer and polymer/inorganic hybrid nanocontainers to enhance their luminescent properties. A combination of various inorganic components and polymers can be used to obtain hybrid nanocontainers with a wide variety of applications.

## 6. Zusammenfassung der Ergebnisse

Die vorgelegte Arbeit befasst sich mit der Verwendung polymerer Nanokapseln zur Verkapselung hydrophober Materialien, die triplet-triplet Annihilation Upconversion (TTA-UC) ermöglichen oder fluoreszierende Eigenschaften haben. Durch die Verkapselung werden diese Systeme vor molekularem Sauerstoff geschützt, wobei verschiedene Strategien entwickelt wurden, um die Bildung von Singulett Sauerstoff zu vermeiden.

In Abschnitt 4.2 werden unterschiedliche polymere Materialien für die Hülle der Nanokapseln vorgestellt, wobei der Zusammenhang zwischen Kristallinität der Polymere und der Upconversion Eigenschaften diskutiert wird. Nanokapseln aus Polymethylmethacrylat (PMMA) und Poly-L-lactid (PLLA) wurden erfolgreich hergestellt unter Verwendung der Lösungsmittels-Verdampfungs Methode (solvent evaporation method) um hydrophobe organische Farbstoffe (Sensibilisator: PdOEP und Emitter: Perylen) in die Kapsel einzuschließen. Die intensive UC Fluoreszenz von Perylen mit  $\lambda_{\max} = 470$  nm konnte nur im Falle der PMMA jedoch nicht im Falle der PLLA Nanokapseln beobachtet werden, was auf eventuelle Formation von Polymerkoagulaten Während der Kapselherstellung zurückzuführen ist. Der Anteil des Triplettenergie transfers vom Sensibilisator zum Emitter ist vermindert aufgrund des verringerten Gehaltes der Perylenmoleküle innerhalb der PLLA Kapsel. Im Gegensatz dazu erwiesen sich die PMMA Nanokapseln als sehr effizient im Hinblick auf die Upconversion Emission.

Darüber hinaus wurden verschiedene polymere Nanokapseln über freie radikalische Polymerisation hergestellt. Die TTA-UC Farbstoffmoleküle wurden erfolgreich in Polystyrol (PS), PMMA, Polyacrylnitril (PAN) und Poly(acrylnitril-co-styrol) P(AN-co-S). Die UC Fluoreszenz von Perylen ( $\lambda_{\max} = 470$  nm) wurde nur für PS und PMMA Nanokapseln beobachtet. Im Falle der PAN und P(AN-co-S) Kapseln wurde an Stelle der UC Emission eine hohe Emission bei 570 nm beobachtet, was auf die Ausbildung von Dimeren des Emitters zurückgeführt wird.

Abschnitt 4.3 befasst sich mit der Herstellung von TTA-UC Farbstoff enthaltenden Nanokapseln unter inerten Bedingungen (d.h. in Dunkelheit und unter Argon Atmosphäre) durch frei-radikalische Miniemulsions Polymerisation. Polystyrol Nanokapseln, die unter inerten Bedingungen hergestellt wurden, zeigten sowohl eine verstärkte UC Fluoreszenz als auch eine verstärkte Phosphoreszenz des Sensibilisators im Vergleich zu Polystyrol

Nanokapseln, die unter den regulären Bedingungen (Tageslicht und unter Luftatmosphäre) hergestellt wurden. Damit konnten wir zeigen, dass Inertgas und Dunkelheit eine sehr wichtige Rolle für die Verbesserung von UC Prozessen spielen. Sogar bei sehr geringen Anregungsintensitäten (schon ab Intensitäten ab  $0.06 \text{ W cm}^{-2}$ ) bei  $\lambda = 532 \text{ nm}$  konnte UC Emission erfolgreich beobachtet werden.

Die erfolgreiche Verstärkung des Fluoreszenzprozesses durch das Hinzufügen von  $\text{CeO}_2$  in Polystyrol Nanokapseln, die einen Modellfarbstoff (Terrylendiimid) enthalten, wird in Abschnitt 4.4 beschrieben. Der Photooxidationsprozess des Fluoreszenzmoleküls wurde erfolgreich reduziert durch die in-situ Kristallisation des Metalloxids an der Oberfläche der Nanokapsel. Das Auftreten freier Sauerstoffkoordinationsstellen in der Struktur der  $\text{CeO}_2$  Nanopartikel an der Oberfläche der Polystyrol Nanokapseln ermöglichen das Verstärken der Fluoreszenz, da molekularer Sauerstoff der Umgebung in diese freien Gitterplätze eingefangen werden kann. Dies verhindert den Eintritt des Sauerstoffs in die Nanokapseln, was wiederum die Ausbildung von Singulett Sauerstoff innerhalb des Systems reduziert. Im Vergleich zu Nanokapseln ohne  $\text{CeO}_2$ , die unter Argon Atmosphäre hergestellt wurden, konnte die Intensität der Fluoreszenz durch Verwendung von  $\text{CeO}_2$ /Polymer Nanokapseln, die in Gegenwart von Luft hergestellt wurden, verstärkt werden.

In Abschnitt 4.5 wird die Effektivität unterschiedlicher anorganischer Materialien (Laponit RD, Hydroxyapatit und  $\text{CeO}_2$ ) in Kombination mit PS Nanokapseln diskutiert. Laponit RD wurde erfolgreich durch layer-by-layer Technik aufgetragen. Kontrollierte in-situ Kristallisation wurde angewandt, um Hydroxyapatit und  $\text{CeO}_2$  auf den Nanokapseln anzubringen. Der Triplet-Triplet Energietransfer vom Sensibilisator zum Emittermolekül konnte durch die Gegenwart von anorganischen Materialien auf der Oberfläche der Nanokapseln verstärkt werden und weitere Photodegradation des Perylenmoleküls konnte in der Nanokapsel reduziert werden.

Schließlich haben wir die Verwendung von Pickering Miniemulsionen untersucht um Hybrid Laponit-Silicapartikel-Polystyrol Nanokapseln herzustellen, beschrieben in Abschnitt 4.6. Die Partikel wurden erfolgreich an der Oberfläche angebracht und konnten die UC Eigenschaften verbessern. Die Erhöhung der UP kann durch das Auftreten von zwei Effekten erklärt werden: i) Die Gegenwart von Laponit-Silicapartikel an der Oberfläche der Kapseln, die das Eintreten von Sauerstoffmolekülen verhindern und ii) die Vergrößerung der Kapselgröße, was die freie Beweglichkeit des Sensibilisators und des Emitters innerhalb des Systems ermöglicht und damit den Triplet-Triplet Energietransfer erhöht.



Die in dieser Arbeit vorgestellten Strategien stellen eine Vielfalt von Möglichkeiten dar, um die lumineszenten Eigenschaften in polymeren Nanokapseln mit UC Systemen zu verbessern.

Kombinationen aus verschiedenen anorganischen Komponenten und Polymeren kann zur Herstellung von Hybrid Nanokapseln genutzt werden, die Anwendung in verschiedenen Gebieten finden könnten.

## 7. Experimental section

### 7.1. Materials

**Table 5.1.** Details of the materials used in this work.

Chemical	Abbreviation	Supplier	Purity	CAS.No
Styrene	S	Sigma- Aldrich	>99%	100-42-5
Methyl methacrylate	MMA	Merck	>99%	80-62-6
Poly(methyl methacrylate)	PMMA	Sigma- Aldrich	$M_w = 120\ 000\ \text{g mol}^{-1}$	9011-14-7
Acrylonitrile	AN	Sigma- Aldrich	$\geq 99\%$	107-13-1
Poly(L-lactide)	PLLA	Sigma- Aldrich	$M_w = 80\ 000 - 160\ 000\ \text{g mol}^{-1}$	26161-42-2
Acrylic acid	AA	Sigma- Aldrich	99%	79-10-7
Hexadecane	HD	Sigma- Aldrich	99%	544-76-3
Sodium dodecyl sulfate	SDS	Alfa Aesar	99%	151-21-3
2,2'-Azobis(2-methylbutyronitrile)	V59	Wako		13472-08-7
Cetyltrimethylammonium bromide	CTAB	Sigma- Aldrich	$\geq 99\%$	57-09-0

Continue in next page

Table 5.1. Continuation

2-Aminoethyl methacrylatehydrochloride	AEMH	Sigma-Aldrich	90%	2420-94-2
Tetrahydrofuran	THF	Sigma-Aldrich	≥99%	109-99-9
Sodium hydroxide	NaOH	Sigma-Aldrich	≥97.0%	1310-73-2
Hydrochloric acid	HCl	Sigma-Aldrich	37%	7647-01-0
Calcium nitrate tetrahydrate	Ca(NO <sub>3</sub> ) <sub>2</sub> ·4H <sub>2</sub> O	Sigma-Aldrich	99%	13477-34-4
Diammonium hydrogen phosphate	(NH <sub>4</sub> ) <sub>2</sub> HPO <sub>4</sub>	Merck		7783-28-0
Clay (synthetic layered silicate)	Laponite RD	Rockwood clay based additives		
Ammonia solution	NH <sub>3</sub>	VWR	25 - 35%	1336-21-6
Chloroform	CHCl <sub>3</sub>	Fluka	>99%	67-66-3
Palladium (II) 2,3,7,8,12,13,17,18-octaethyl-21H,23H-porphyrin	PdOEP	Sigma-Aldrich	85% dye content	24804-00-0
Perylene		Sigma-Aldrich	≥99%	198-55-0

## 7.2. Experiment details for Section 4.2

### 7.2.1. Synthesis of poly(methyl methacrylate) nanocapsules

Poly(methyl methacrylate) nanocapsules (sample **KK-SE-01**) were synthesized by the solvent-evaporation method.<sup>187</sup> The continuous phase contains SDS (10 mg) and demineralized water (10 g). The disperse phase containing commercially available pre-synthesized polymer PMMA (150 mg) and hexadecane (300 mg) with the upconversion dyes (i.e., PdOEP and perylene) were dissolved/dispersed in chloroform (2.5 g). The two phases were mixed and pre-emulsified by stirring at 1000 rpm for 1 h. The emulsion was prepared by ultrasonication (Branson Digital Sonifier 450-D; ½” tip, 90% intensity, 2 min) while cooling in an ice-water bath to avoid the breakage of polymer chains due to heating. The evaporation of chloroform was performed by stirring in an open vial at room temperature and ambient pressure for 12 h.

### 7.2.2. Synthesis of poly(L -lactide) nanocapsules

Poly(L-lactide) nanocapsules (sample **KK-SE-02**) were synthesized by the solvent-evaporation method.<sup>109</sup> The continuous phase contains SDS (7.7 mg) and demineralized water (10 g). The disperse phase containing commercially available pre-synthesized polymer PLLA (250 mg) and hexadecane (250 mg) with the upconversion dyes (i.e., PdOEP and perylene) were dissolved/dispersed in chloroform (2.5 g). The two phases were mixed and pre-emulsified by stirring at 1000 rpm for 1 h. The emulsion was prepared by ultrasonication (Branson Digital Sonifier 450-D; ½” tip, 90% intensity, 2 min) while cooling in an ice-water bath to avoid the breakage of polymer chains due to heating. The evaporation of chloroform was performed by stirring in an open vial at room temperature and ambient pressure for 12 h.

### 7.2.3. Preparation of stock solutions

The UC dyes, PdOEP (the final concentration in hexadecane is  $1 \times 10^{-4}$  M) and perylene ( $1 \times 10^{-3}$  M), were dissolved in sufficient amounts of THF and transferred in the specific amounts of hexadecane as mentioned in the type of nanocapsules (PMMA & PLLA). Afterwards, the THF was completely removed by rotary evaporation (12 h at 200 mbar and 45 °C).<sup>187</sup>

#### 7.2.4. Synthesis of nanocapsules via miniemulsion polymerization

Polystyrene nanocapsules (sample **KK-MP-01**) were synthesized under ambient conditions by radical miniemulsion polymerization. The continuous phase contains SDS (30 mg) and demineralized water (30 g). The disperse phase contains styrene (1.8 g) and acrylic acid (0.2 g) as monomers, hexadecane (4 g) with the upconversion dyes (i.e., PdOEP and perylene), and the initiator V59 (100 mg). The two phases were mixed and pre-emulsified by stirring at 1000 rpm for 1 h. The emulsion was prepared by ultrasonication (Branson Digital Sonifier 450-D; ½” tip, 90% intensity, 2 min) while cooling in an ice-water bath to avoid polymerization due to heating. The polymerization reaction was carried out in a closed flask at 72 °C for 18 h under constant stirring.<sup>52, 120</sup>

The poly (methyl methacrylate) nanocapsules (sample **KK-MP-02**) were prepared in the same way, by using methyl methacrylate as a monomer (2 g) instead of styrene. The poly (acrylonitrile) nanocapsules (sample **KK-MP-02**) were also prepared in the same way, by using acrylonitrile as a monomer (2 g) instead of styrene. The poly(acrylonitrile/styrene) nanocapsules (sample **KK-MP-03**) were also prepared in the same way, by using acrylonitrile (1.32 g) and styrene (0.68 g) as monomers.

#### 7.2.5. Preparation of stock solutions

The stock solutions were prepared in the same way as described in the Section 5.2.3. The UC dyes, PdOEP (the final concentration in hexadecane is  $1 \times 10^{-4}$  M) and perylene ( $1 \times 10^{-3}$  M), were dissolved in sufficient amounts of THF and transferred in 4 g of hexadecane.

### 7.3. Experiment details for Section 4.3

#### 7.3.1. Synthesis of carboxyl-functionalized polystyrene nanocapsules

The polystyrene nanocapsules (the resulting sample is labeled as **NC1**) were prepared in the same way as described in the Section 5.2.4. The nanocapsules synthesized under argon atmosphere (the resulting sample is labeled as **NC2-A**) are carried out by transferring the emulsion into a closed flask after the ultrasonication process. The overnight polymerization reaction is carried out under argon atmosphere in a closed flask which is sealed tightly. The sample **NC3-D** and **NC4-D** nanocapsules were synthesized under darkness conditions. Every

step which is involved in the miniemulsion polymerization is carried out in a dark room and by also by sealing the samples with aluminum foil.

### 7.3.2. Preparation of stock solutions

The stock solutions were prepared in the same way as described in the Section 5.2.3. One batch of stock solution was prepared in daylight and another one in darkness.

## 7.4. Experiment details for Section 4.4

### 7.4.1 Synthesis of carboxylated polystyrene nanocapsules

The carboxylated functionalized polystyrene nanocapsules (sample **NC**) were prepared in the same way as described in the Section 5.2.4, by using *N,N'*-(2,6-diisopropylphenyl)-1,6,9,13-tetra[4-(1,1,3,3-tetramethylbutyl)-phenoxy]terrylene-3,4,11,12-bis(dicarboximide) (TDI) was dissolved in hexadecane instead of PdOEP and perylene as hydrophobic dyes. Synthesized nanocapsules were further used for the cerium oxide crystallization experiments with specific concentration. The surface charge density was determined at pH 10 to ensure the complete deprotonation of the carboxylic groups.

### 7.4.2. Synthesis of the TDI dye and preparation of its stock Solution

*N,N'*-(2,6-Diisopropylphenyl)-1,6,9,13-tetra[4-(1,1,3,3-tetramethylbutyl)-phenoxy]terrylene-3,4,11,12-bis(dicarboximide) (TDI) was synthesized according to the literature.<sup>141</sup> The prepared TDI was dissolved in sufficient amounts of THF and transferred in hexadecane (4 g) to obtain a final concentration of  $1 \times 10^{-4}$  M. Afterwards, THF was completely removed by rotary evaporation (1 h at 70 mbar and 50 °C).

### 7.4.3. Synthesis of the CeO<sub>2</sub>/polymer hybrid nanocapsules

The synthesized polymeric nanocapsules **NC** were used for the crystallization experiments and the resulting hybrid sample is denoted as **NC-CeO<sub>2</sub>**. The experiment was carried out at 35 °C in a closed flask under constant stirring and keeping the pH constant during the whole procedure. First, the pH of the dispersion was adjusted to pH 10 with a 28% ammonia solution. Then 5 mmol of metal salt per gram of dispersion nanocapsules was added and the dispersion was stirred for 2 h to allow the binding of cerium ions to the capsules surface. Cerium (III) nitrate hexahydrate was dissolved in 2 mL of demineralized water and 200 μL of

the latex dispersion was added to the solution. Afterwards, the precipitation of the oxide was carried out by adding dropwise 2 mL of a NaOH aqueous solution (0.1 M) using a syringe pump (dropping speed of 1 mL h<sup>-1</sup>). The mixture was further stirred for 24 h to complete oxide formation. The loaded samples were freeze dried for subsequent characterizations.

## 7.5. Experiment details for Section 4.5

### 7.5.1. Synthesis of polystyrene nanocapsules via miniemulsion polymerization method

The carboxylated functionalized polystyrene nanocapsules (sample **PS1**) were prepared in the same way as described in the Section 5.2.4. Synthesized nanocapsules were further used for the hydroxyapatite and cerium oxide crystallization experiments with specific concentration.

The amino functionalized polystyrene nanocapsules (sample **PS2**) were prepared in the same way, by using CTAB as a surfactant (50 mg) instead of SDS and 2-aminoethyl methacrylate hydrochloride as a comonomer instead of acrylic acid. The synthesized nanocapsules were further used for the deposition of Laponite RD on the surface of nanocapsules using layer-by-layer method.

### 7.5.2. Deposition of clay on the surface of amino-functionalized nanocapsules via layer-by-layer deposition method

Sample **PS3** was prepared by adapting a previously reported method.<sup>169</sup> Armoring the polystyrene nanocapsules with clay particles was done by adding Laponite clay (50 mg) to 30 mL of distilled water and sonicated for 4.5 min (Branson Digital Sonifier 450-D; ½” tip, 70% amplitude, 30 s pause every 1min of pulse). This dispersion was added to 1 g of latex dispersion (sample **PS1**, ~15 wt.-% of capsule content) and the pH was then adjusted to 3 by addition of 0.1 M HCl. Finally, the emulsion was stirred for 12 h to ensure the complete deposition of clay on to the surface of nanocapsules.

### 7.5.3. In situ crystallization of hydroxyapatite and ceria on the surface of carboxylate-functionalized nanocapsules

The in situ crystallization of hydroxyapatite and ceria on the surface of carboxylate-functionalized polystyrene nanocapsules (sample **PS2**) were prepared in the same way as

described in the Section 5.4.3. In the case of hydroxyapatite, 2.5 mL of a 0.1 M aqueous solution of  $(\text{NH}_4)_2\text{HPO}_4$  was used as a precipitating agent.<sup>173</sup>

### **7.5.4. Preparation of stock solutions**

The stock solutions were prepared in the same way as described in the Section 5.2.5.

## **7.6. Experiment details for Section 4.6**

### **7.6.1. Synthesis of polystyrene nanocapsules via polymerization method**

The amino functionalized polystyrene nanocapsules (sample **RP**) were prepared in the same way as described in the Section 5.5.1.

### **7.6.2. Synthesis of polystyrene nanocapsules via Pickering miniemulsion method**

Polystyrene nanocapsules with Laponite RD on the surface were synthesized by Pickering miniemulsion polymerization (sample **PM**) in accordance to a method previously reported for solid nanoparticles.<sup>185</sup> The continuous phase was prepared by dispersing 0.8 wt% of clay (40 mg) in 50 mL of distilled water. The suspension was then sonicated for 4.5 min at 70% amplitude with 30 s pause every 1 min of pulse using Branson Digital Sonifier 450-D; ½” tip. 0.1 mol/L of sodium chloride is added after first minute interval of ultrasonication. The disperse phase contains styrene (3.3 g), stock solution of the upconversion dyes in hexadecane (6.6 g), and the initiator V59 (150 mg). The two phases were mixed and pre-emulsified by stirring for 30 minutes at 1000 rpm. The emulsion was prepared by ultrasonication for 6.5 min (Branson Digital Sonifier 450-D; ½” tip, 70% amplitude, 30 s pause every 1 min of pulse) while cooling in an ice-water bath to avoid polymerization process due to heating. The polymerization reaction was carried in closed flask at 72 °C for 16 h under constant stirring. The size of the obtained nanocapsules was 340 nm ( $\pm$  53%) as measured by dynamic light scattering (DLS), with a capsule (polymer + hexadecane) content of ca. 18 wt.-%.

### **7.6.3. Preparation of stock solutions**

The stock solutions were prepared in the same way as described in the Section 5.2.5.



## 7.7. Analytical Tools

### 7.7.1. Scanning electron microscopy (SEM)

The images were taken using a LEO Gemini 1530 field-emission microscope operated at different extractor voltages in accordance to the polymers. Samples for SEM observation were prepared by dropping the diluted dispersions on silicon wafers and dried.

### 7.7.2. Transmission electron microscopy (TEM)

Transmission electron microscopy (TEM) was carried out with a Jeol 1400 electron microscope (JEOL Ltd., Japan), using a LaB<sub>6</sub> cathode at an acceleration voltage of 200 kV. The images were recorded using GATAN Ultrascan 1000 CCD camera (Gatan Inc., USA).

Samples for TEM observation were prepared by dropping the diluted dispersions on a carbon coated 300-mesh copper grids and dried. The further degradation during the measurement of PMMA and PLLA samples was avoided by coating a thin carbon layer on the grid with diluted dispersion, using a Leica EM Med020 Vacuum Coating System (Leica Micro Systems, Germany).

### 7.7.3. Dynamic light scattering (DLS)

Particle sizes of the prepared nanocapsules were determined by dynamic light scattering (DLS) using a Nicomp 380 PSS particle sizer (Santa Barbara, CA) at a fixed angle of 90°.

### 7.7.4. Particle charge detector (PCD)

The PCD measurements were carried out using a detector (Mütek GmbH, Germany) in combination with a Titrino Automatic Titrator (Metrohm AG, Switzerland). Samples were diluted to a solid content of 0.1 wt.-% for titration. The surface charge density of the negatively charged latex nanocapsules was determined by direct polyelectrolyte titration with a ~ 0.001 N solution of poly(diallyldimethyl ammonium chloride) (PDADMAC) and the positively charged latex nanocapsules was determined by direct polyelectrolyte titration with a ~ 0.001 N solution of sodium polystyrene sulfonate, detecting the end point with an automatic streaming current detector (SCD).<sup>126</sup>

### **7.7.5. Energy dispersive X-ray spectroscopy (EDX)**

Samples for EDX observation were prepared by dropping the diluted dispersions on silicon wafers and dried. EDX analysis combined with elemental mapping was carried out in a Hitachi SU8000 SEM microscope equipped with a Bruker AXS spectrometer with an operation voltage of 5 kV.

### **7.7.6. Thermogravimetric analysis (TGA)**

Thermogravimetric analysis of the freeze dried sample was conducted using Mettler Toledo ThermoSTAR TGA/SDTA 851 thermobalance (Mettler Toledo, Switzerland). The measurements cover a temperature range between 40-1000 °C at a heating rate of 10 °C/min.

### **7.7.7. X-Ray powder diffraction**

X-ray diffraction of the freeze dried sample was conducted on a Philips PW 1820 diffractometer with monochromatic  $\text{Cu}_{K\alpha}$  radiation ( $\lambda = 1.5418 \text{ \AA}$ , 40 kV, 30 mA, 5 s,  $\Delta\Theta = 0.02$ ).

### **7.7.8. Field desorption mass spectra measurements**

FD (field desorption) mass spectra were obtained on a VG Instruments ZAB 2-SE-FPD. The accuracy of measurement was in the range of 1-2 Da. The wire with a deposited from THF solution sample was maintained at a positive potential of 8 kV.

### **7.7.9. Photoluminescence measurements**

Fluorescence spectra were recorded using a home-made setup containing a diode laser with wavelength 635 nm laser (Roithner Lasertechnik GmbH, ADL-63201TL) with an excitation intensity of  $0.2 \text{ W cm}^{-2}$ . Upconversion spectra were recorded using a home-made setup containing a continuous-wave DPSS laser (532 nm, 40 mW, DJ532-40, Thorlabs Inc).

The measurements of photoluminescent properties of the synthesized nanocontainers and organic dyes were performed in a custom-build optical setup. A continuous-wave DPSS laser (532 nm, 40 mW, DJ532-40, Thorlabs Inc) or diode laser (635 nm, 20 mW, ADL-63201TL, Roithner Lasertechnik) was used for the investigation of the upconversion and fluorescence properties of organic dyes in bulk and nanoconfined matter. The rotatable reflective neutral filter was used for the attenuation of the laser power to desired level of excitation. The laser

beam was focused at the sample by the lens with a focal distance of 10 cm. The excited photoluminescence from the sample was collected by same lens and guided to a highly sensitive CCD-spectrometer (C10083CA, Hamamatsu Inc.) by additional set of lenses and mirrors. The rejection of the scattered excitation radiation was done by using of a notch filter (NF03-633E-25, or NF01-532E-25, Semrock Inc.).

In order to investigate temporal properties of emission, the laser diode current was modulated by a pulse generator (TTi TGA1244, 40 MHz arbitrary waveform generator). The sample emission was then guided to a time-resolving part of the setup where it was separated on two parts by a short-pass filter (FF01-694/SP-25, Semrock Inc.) for the separate detection of upconversion and residual phosphorescence. Each part of emission was additionally cleaned by the long and short pass filters and was detected by using of photo-multiplier tubes (type R374, Hamamatsu Inc.). The signal from PMTs was observed and saved by a digital oscilloscope (Agilent 54622A Oscilloscope 100 MHz).

## 8. Abbreviations and symbols

$h$	Planck's constant
$\nu_{em}$	Frequency of the emission light
$\Phi$	Quantum yield
$\nu_{exc}$	Frequency of excitation light
$h\nu_{UC}$	Frequency of the emitted delayed fluorescence
$V_T$	Total potential energy of the colloidal particles interaction
$V_A$	Attractive potential energy
$V_R$	Repulsive interaction
$R$	Particle radius
$A$	Hamaker constant
$D$	Distance
$\psi_0$	Stern potential
$k$	Constant
$C$	Concentration
$k_B$	Boltzmann constant
$\epsilon$	Dielectric constant
$\epsilon_0$	Vacuum
$\gamma_D$	Debye length
$V_m$	Energy barrier
$\chi$	Flory-Huggins parameter
$z$	Coordination number

$\gamma$	Interfacial tension
$p$	Pressure
$T$	Temperature
$E_{Adh}$	Adhesion energy
$\theta$	Contact angle
$S_i$	Spreading coefficient
$\Delta G$	Total free energy
$A$	Area
$\eta$	Viscosity
NIR	Near-infrared
UC	Upconversion
TTA-UC	Triplet–triplet annihilation upconversion
ISC	Intersystem crossing
TET	Triplet energy transfer
SDS	Sodium dodecyl sulfate
CTAB	Cetyl trimethylammonium bromide
CTAC	Cetyl trimethylammonium chloride
BAC	Benzalkonium chloride
CMC	Critical micellar concentration
S	Styrene
MMA	Methyl methacrylate
AN	Acrylonitrile

## 8. Abbreviations and symbols

---

PS	Polystyrene
PMMA	Poly (methyl methacrylate)
PAN	Poly(acrylonitrile)
PLLA	Poly(L-lactide)
AA	Acrylic acid
PdOEP	Pd (II) 2,7,8,12,13,17,18-octaethyl-porphyrinato
TDI	Terrylene diimide
TEM	Transmission electron microscopy
SEM	Scanning electron microscopy
DLS	Dynamic light scattering

## 9. References

1. J.-H. Park; L. Gu; G. Von Maltzahn; E. Ruoslahti; S. N. Bhatia; M. J. Sailor, *Nat. Mater.*, 2009, **8**, 331-336.
2. A. B. Chinen; C. M. Guan; J. R. Ferrer; S. N. Barnaby; T. J. Merkel; C. A. Mirkin, *Chem. Rev.*, 2015, **115**, 10530-10574.
3. X. Wu; W. Zhu, *Chem. Soc. Rev.*, 2015, **44**, 4179-4184.
4. G. Chen; I. Roy; C. Yang; P. N. Prasad, *Chem. Rev.*, 2016.
5. X. Gao; Y. Cui; R. M. Levenson; L. W. Chung; S. Nie, *Nat. Biotechnol.*, 2004, **22**, 969-976.
6. V. Holzapfel; A. Musyanovych; K. Landfester; M. R. Lorenz; V. Mailänder, *Macromol. Chem. Phys.*, 2005, **206**, 2440-2449.
7. S. Sengupta; D. Eavarone; I. Capila; G. Zhao; N. Watson; T. Kiziltepe; R. Sasisekharan, *Nature*, 2005, **436**, 568-572.
8. O. C. Farokhzad; J. Cheng; B. A. Teply; I. Sherifi; S. Jon; P. W. Kantoff; J. P. Richie; R. Langer, *Proc. Natl. Acad. Sci.*, 2006, **103**, 6315-6320.
9. M. R. Lorenz; V. Holzapfel; A. Musyanovych; K. Nothelfer; P. Walther; H. Frank; K. Landfester; H. Schrezenmeier; V. Mailänder, *Biomaterials*, 2006, **27**, 2820-2828.
10. C. S. Peyratout; L. Daehne, *Angew. Chem. Int. Ed. Engl.*, 2004, **43**, 3762-3783.
11. C. Burda; X. Chen; R. Narayanan; M. A. El-Sayed, *Chem. Rev.*, 2005, **105**, 1025-1102.
12. A. P. Johnston; C. Cortez; A. S. Angelatos; F. Caruso, *Curr. Opin. Colloid Interface Sci.*, 2006, **11**, 203-209.
13. S. W. Bae; W. Tan; J.-I. Hong, *Chem. Commun.*, 2012, **48**, 2270-2282.
14. J. Nam; N. Won; J. Bang; H. Jin; J. Park; S. Jung; S. Jung; Y. Park; S. Kim, *Adv. Drug Deliv. Rev.*, 2013, **65**, 622-648.
15. R. Bar-Shalom; N. Yefremov; L. Guralnik; D. Gaitini; A. Frenkel; A. Kuten; H. Altman; Z. Keidar; O. Israel, *J. Nucl. Med.*, 2003, **44**, 1200-1209.
16. J. Yao; M. Yang; Y. Duan, *Chem. Rev.*, 2014, **114**, 6130-6178.
17. B. Valeur; M. N. Berberan-Santos, *Molecular fluorescence: principles and applications*. John Wiley & Sons: 2012.
18. J. R. Lakowicz; G. Weber, *Biochemistry*, 1973, **12**, 4161-4170.

19. E. F. F. da Silva; F. M. Pimenta; B. W. Pedersen; F. H. Blaikie; G. N. Bosio; T. Breitenbach; M. Westberg; M. Bregnhøj; M. Etzerodt; L. G. Arnaut, *Integr. Biol.*, 2016, **8**, 177-193.
20. A. Segura-Carretero; C. Cruces-Blanco; B. Cañabate-Díaz; J. Fernández-Sánchez; A. Fernández-Gutiérrez, *Anal. Chim. Acta*, 2000, **417**, 19-30.
21. J. Kuijt; F. Ariese; A. T. Udo; C. Gooijer, *Anal. Chim. Acta*, 2003, **488**, 135-171.
22. L. Feng; C. Zhu; H. Yuan; L. Liu; F. Lv; S. Wang, *Chem. Soc. Rev.*, 2013, **42**, 6620-6633.
23. C. Wu; D. T. Chiu, *Angew. Chem. Int. Ed.*, 2013, **52**, 3086-3109.
24. K. Li; B. Liu, *Chem. Soc. Rev.*, 2014, **43**, 6570-6597.
25. D. O. Shah, *Macro-and Microemulsions: Theory and Applications*. ACS Publications: 1985, **272**.
26. S. Benita, *Microencapsulation: methods and industrial applications*. CRC Press: 2005.
27. S. K. Ghosh, *Functional coatings: by polymer microencapsulation*. John Wiley & Sons: 2006.
28. D. Crespy; K. Landfester, *Soft Matter*, 2011, **7**, 11054-11064.
29. M. G. Schwab; D. Crespy; X. Feng; K. Landfester; K. Müllen, *Macromol. Rapid Commun.*, 2011, **32**, 1798-1803.
30. D. Crespy; K. Landfester, *Beilstein J. Org. Chem.*, 2010, **6**, 1132-1148.
31. C. K. Weiss; K. Landfester, Miniemulsion polymerization as a means to encapsulate organic and inorganic materials. In *Hybrid Latex Particles*, Springer: 2010; pp 185-236.
32. C. R. Ronda, *Luminescence: from theory to applications*. John Wiley & Sons: 2007.
33. R. Scheps, *Prog. Quant. Electr.*, 1996, **20**, 271-358.
34. Z. Li; Y. Zhang; S. Jiang, *Adv. Mater.*, 2008, **20**, 4765-4769.
35. D. K. Chatterjee; M. K. Gnanasammandhan; Y. Zhang, *Small*, 2010, **6**, 2781-2795.
36. Y. Q. Sun; J. Liu; X. Lv; Y. Liu; Y. Zhao; W. Guo, *Angew. Chem. Int. Ed.*, 2012, **51**, 7634-7636.
37. F. Auzel, *Chem. Rev.*, 2004, **104**, 139-174.
38. M. Haase; H. Schäfer, *Angew. Chem. Int. Ed. Engl.*, 2011, **50**, 5808-5829.
39. W. Denk; J. H. Strickler; W. W. Webb, *Science*, 1990, **248**, 73-76.
40. P. E. Keivanidis; S. Balushev; T. Miteva; G. Nelles; U. Scherf; A. Yasuda; G. Wegner, *Adv. Mater.*, 2003, **15**, 2095-2098.
41. C. Parker; C. Hatchard, *Trans. Faraday Soc.*, 1963, **59**, 284-295.



42. S. Balushev; P. Keivanidis; G. Wegner; J. Jacob; A. C. Grimsdale; K. Müllen; T. Miteva; A. Yasuda; G. Nelles, *Appl. Phys. Lett.*, 2005, **86**, 061904.
43. S. Balushev; V. Yakutkin; T. Miteva; Y. Avlasevich; S. Chernov; S. Aleshchenkov; G. Nelles; A. Cheprakov; A. Yasuda; K. Müllen, *Angew. Chem. Int. Ed.*, 2007, **46**, 7693-7696.
44. T. Miteva; V. Yakutkin; G. Nelles; S. Balushev, *New J. Phys.*, 2008, **10**, 103002.
45. S. Balushev; T. Miteva; V. Yakutkin; G. Nelles; A. Yasuda; G. Wegner, *Phys. Rev. Lett.*, 2006, **97**, 143903.
46. S. Balushev; V. Yakutkin; T. Miteva; G. Wegner; T. Roberts; G. Nelles; A. Yasuda; S. Chernov; S. Aleshchenkov; A. Cheprakov, *New J. Phys.*, 2008, **10**, 013007.
47. Q. Liu; T. Yang; W. Feng; F. Li, *J. Am. Chem. Soc.*, 2012, **134**, 5390-5397.
48. K. Tanaka; K. Inafuku; Y. Chujo, *Chem. Commun.*, 2010, **46**, 4378-4380.
49. A. Turshatov; D. Busko; S. Balushev; T. Miteva; K. Landfester, *New J. Phys.*, 2011, **13**, 083035.
50. M. Penconi; P. L. Gentili; G. Massaro; F. Elisei; F. Ortica, *Photochem. Photobiol. Sci.*, 2014, **13**, 48-61.
51. A. J. Svagan; D. Busko; Y. Avlasevich; G. Glasser; S. Balushev; K. Landfester, *ACS Nano*, 2014, **8**, 8198-8207.
52. C. Wohnhaas; A. Turshatov; V. Mailänder; S. Lorenz; S. Balushev; T. Miteva; K. Landfester, *Macromol. Biosci.*, 2011, **11**, 772-778.
53. J. Fickert; C. Wohnhaas; A. Turshatov; K. Landfester; D. Crespy, *Macromolecules*, 2013, **46**, 573-579.
54. P. R. Ogilby, *Chem. Soc. Rev.*, 2010, **39**, 3181-3209.
55. X.-d. Wang; O. S. Wolfbeis; R. J. Meier, *Chem. Soc. Rev.*, 2013, **42**, 7834-7869.
56. X.-d. Wang; O. S. Wolfbeis, *Chem. Soc. Rev.*, 2014, **43**, 3666-3761.
57. W. M. Yen; H. Yamamoto, *Phosphor handbook*. CRC press: 2006.
58. J. Birks In *Fluorescence quantum yield measurements*, Standardization in Spectrophotometry and Luminescence Measurements: Proceedings of a Workshop Seminar Held at the National Bureau of Standards, Gaithersburg, Maryland, November, November 19-20, 1975, US Department of Commerce, National Bureau of Standards: 1976, 1.
59. S. Balushev; T. Miteva, Non-Coherent Up-Conversion in Multi-Component Organic Systems. In *Next Generation of Photovoltaics*, Springer: 2012, 157-190.
60. C. S. Foote; J. Valentine; A. Greenberg; J. F. Liebman, *Active oxygen in chemistry*. Springer Science & Business Media: 2012, **2**.

61. W. Zhao; F. N. Castellano, *J. Phys. Chem. A*, 2006, **110**, 11440-11445.
62. C.-P. Hsu, *Acc. Chem. Res.*, 2009, **42**, 509-518.
63. G. D. Scholes, *Annu. Rev. Phys. Chem.*, 2003, **54**, 57-87.
64. T. Cosgrove, *Colloid science: principles, methods and applications*. John Wiley & Sons: 2010.
65. E. Werway; J. T. G. Overbeek, *Amsterdam-New York*, 1948, 34.
66. D. Everett, *Chem.: London*, 1988, 156.
67. B. V. L. Derjaguin, L. D. , *Acta Physicochim. URSS* 14, 1944, **14**, 633-662.
68. H. Hamaker, *Physica*, 1937, **4**, 1058-1072.
69. D. H. Napper, *Ind. Eng. Chem. Res.*, 1970, **9**, 467-477.
70. D. H. Napper, *J. Colloid Interface Sci.*, 1977, **58**, 390-407.
71. P. A. Lovell; M. S. El-Aasser, *Emulsion polymerization and emulsion polymers*. Wiley: 1997.
72. K. Landfester, *Macromol. Rapid Commun.*, 2001, **22**, 896-936.
73. F. J. Schork; Y. Luo; W. Smulders; J. P. Russum; A. Butté; K. Fontenot, *Adv. Polym. Sci.*, 2005, **175**, 129-256.
74. H. J. G. Butt, K.; Kappl, M., 2013, **3**.
75. J. H. S. Schulman, W.; Prince, C., *J. Phys. Chem*, 1959, **63**, 1672.
76. J. Ugelstad; H. Lervik; B. Gardinovacki; E. Sund, *Pure Appl. Chem.*, 1971, **26**, 121-152.
77. J. Ugelstad; M. El-Aasser; J. Vanderhoff, *J. Polym. Sci. Polym. Lett. Ed.*, 1973, **11**, 503-513.
78. K. Landfester In *Recent developments in miniemulsions—formation and stability mechanisms*, Macromolecular Symposia, Wiley Online Library: 2000, 171-178.
79. C. Tanford, *The Hydrophobic Effect: Formation of Micelles and Biological Membranes 2d Ed*. J. Wiley.: 1980.
80. D. Crespy. Tuning polymeric latex functionality via the miniemulsion technique. Citeseer, 2006.
81. R. Muñoz-Espí. Surface-functionalized latex particles as additives in the mineralization of zinc oxide. Johannes Gutenberg-Universität Mainz, 2006.
82. M. Antonietti; K. Landfester, *Prog. Polym. Sci.*, 2002, **27**, 689-757.
83. N. Bechthold; K. Landfester, *Macromolecules*, 2000, **33**, 4682-4689.
84. J. M. Asua, *Prog. Polym. Sci.*, 2002, **27**, 1283-1346.

85. K. Landfester; N. Bechthold; S. Förster; M. Antonietti, *Macromol. Rapid Commun.*, 1999, **20**, 81-84.
86. M. J. Rosen, *Surfactants and Interfacial Phenomena, Third Edition*, 2004, 105-177.
87. H. Schubert, *Emulgiertechnik, Behrs Verlag, Hamburg*, 2012, **3**.
88. C. Miller; P. Blythe; E. Sudol; C. Silebi; M. El-Aasser, *J. Polym. Sci. A Polym. Chem.*, 1994, **32**, 2365-2376.
89. J. Reimers; F. Schork, *Polymer. React. Eng.*, 1996, **4**, 135-152.
90. S. U. Pickering, *J. Chem. Soc. Transactions*, 1907, **91**, 2001-2021.
91. R. Aveyard; B. P. Binks; J. H. Clint, *Adv. Colloid Interface Sci.*, 2003, **100**, 503-546.
92. B. P. Binks, *Curr. Opin. Colloid Interface Sci.*, 2002, **7**, 21-41.
93. B. P. Binks; T. S. Horozov, *Colloidal particles at liquid interfaces*. Cambridge University Press: 2006.
94. B. P. Binks; J. H. Clint, *Langmuir*, 2002, **18**, 1270-1273.
95. Y. Chevalier; M.-A. Bolzinger, *Colloids Surf., A. Physicochem Eng.*, 2013, **439**, 23-34.
96. S. Levine; B. D. Bowen; S. J. Partridge, *Colloids Surf.*, 1989, **38**, 325-343.
97. F. Jansen; J. Harting, *Phys. Rev. B*, 2011, **83**, 046707.
98. L. Dong; D. Johnson, *Langmuir*, 2003, **19**, 10205-10209.
99. E. Vignati; R. Piazza; T. P. Lockhart, *Langmuir*, 2003, **19**, 6650-6656.
100. S. Torza; S. Mason, *J. Colloid Interface Sci.*, 1970, **33**, 67-83.
101. Y. C. Chen; V. Dimonie; M. S. El-Aasser, *Macromolecules*, 1991, **24**, 3779-3787.
102. M. Okubo; Y. Katsuta; T. Matsumoto, *J. Polym. Sci. Polym. Lett. Ed.*, 1982, **20**, 45-51.
103. S. Lee; A. Rudin, *J. Polym. Sci. A Polym. Chem.*, 1992, **30**, 2211-2216.
104. Y. Hong; C. Gao; Y. Shi; J. Shen, *Polymer. Adv. Tech.*, 2005, **16**, 622-627.
105. R. J. Williams; B. A. Rozenberg; J.-P. Pascault, Reaction-induced phase separation in modified thermosetting polymers. In *Polymer Analysis Polymer Physics*, Springer: 1997, 95-156.
106. D. C. Sundberg; A. P. Casassa; J. Pantazopoulos; M. R. Muscato; B. Kronberg; J. Berg, *J. Appl. Polym. Sci.*, 1990, **41**, 1425-1442.
107. T. J. de Faria; A. Machado de Campos; E. Lemos Senna In *Preparation and Characterization of Poly (D, L-Lactide)(PLA) and Poly (D, L-Lactide)-Poly (Ethylene Glycol)(PLA-PEG) Nanocapsules Containing Antitumoral Agent Methotrexate*, Macromolecular symposia, Wiley Online Library: 2005, 228-233.

108. R. H. Staff; M. Gallei; M. Mazurowski; M. Rehahn; R. d. Berger; K. Landfester; D. Crespy, *ACS Nano*, 2012, **6**, 9042-9049.
109. Y. Zhao; J. Fickert; K. Landfester; D. Crespy, *Small*, 2012, **8**, 2954-2958.
110. S. L. Flegler; J. W. Heckman; K. L. Klomparens, *Spektrum Akademischer, Heidelberg*, 1995.
111. W. Brown, *Dynamic light scattering: the method and some applications*. Oxford University Press, USA: 1993, **49**.
112. B. J. P. Berne, R., *Courier Dover Publications, ISBN 0-486-41155-9*, 2000.
113. *Nicomp 380 User Manual, Santa Barbara*, 2003.
114. A. J. Fatiadi, *J. Res. Natl. Bureau Stds.-A. Physics and Chemistry*, 1968, **72**, 39-47.
115. N. A. Burke; M. Templin; J. E. Guillet, *J. Photochem. Photobiol. A* 1996, **100**, 93-100.
116. P. Sotero; R. Arce, *J. Photochem. Photobiol. A* 2008, **199**, 14-22.
117. M. Nowakowska; B. White; J. Guillet, *Macromolecules*, 1989, **22**, 2317-2324.
118. Y. Fujimaki; Y. Nakamura; A. Uchida; I. Oonishi; S. Fujisawa; S. Ohshima, *Polycycl. Aromat. Comp.*, 2002, **22**, 395-400.
119. J. Brandrup; E. H. Immergut; E. A. Grulke; A. Abe; D. R. Bloch, *Polymer Handbook*. Wiley New York: 1999, **89**.
120. K. Landfester, *J. Dispersion Sci. Technol.*, 2002, **23**, 167-173.
121. K. Katta; D. Busko; Y. Avlasevich; R. Muñoz-Espí; S. Balushev; K. Landfester, *Macromol. Rapid Commun.*, 2015, **36**, 1084-1088.
122. K. Landfester, *Angew. Chem. Int. Ed. Engl.*, 2009, **48**, 4488-4507.
123. K. Katta; D. Busko; Y. Avlasevich; R. Muñoz-Espí; S. Balushev; K. Landfester, *Manuscript submitted*, 2015.
124. Y. Lu; M. Hoffmann; R. S. Yelamanchili; A. Terrenoire; M. Schrunner; M. Drechsler; M. W. Möller; J. Breu; M. Ballauff, *Macromol. Chem. Phys.*, 2009, **210**, 377-386.
125. S. Wu; J. Dzubiella; J. Kaiser; M. Drechsler; X. Guo; M. Ballauff; Y. Lu, *Angew. Chem. Int. Ed.*, 2012, **51**, 2229-2233.
126. V. Fischer; I. Lieberwirth; G. Jakob; K. Landfester; R. Muñoz-Espí, *Adv. Funct. Mater.*, 2013, **23**, 451-466.
127. R. Muñoz-Espí; Y. Mastai; S. Gross; K. Landfester, *Cryst. Eng. Comm.*, 2013, **15**, 2175-2191.
128. M. A. Hood; M. Mari; R. Muñoz-Espí, *Materials*, 2014, **7**, 4057-4087.
129. M. Mari; B. Müller; K. Landfester; R. Muñoz-Espí, *ACS Appl. Mater. Interfaces.*, 2015, **7**, 10727-10733.

130. S. Hess; M. M. Demir; V. Yakutkin; S. Balushev; G. Wegner, *Macromol. Rapid Commun.*, 2009, **30**, 394-401.
131. C. Wu; B. Bull; K. Christensen; J. McNeill, *Angew. Chem. Int. Ed.*, 2009, **48**, 2741-2745.
132. D. B. Papkovsky; R. I. Dmitriev, *Chem. Soc. Rev.*, 2013, **42**, 8700-8732.
133. K. Fischer; M. Wilken, *J. Chem. Thermodyn.*, 2001, **33**, 1285-1308.
134. T. Sato; Y. Hamada; M. Sumikawa; S. Araki; H. Yamamoto, *Ind. Eng. Chem. Res.*, 2014, **53**, 19331-19337.
135. U. Paiphansiri; J. Dausend; A. Musyanovych; V. Mailänder; K. Landfester, *Macromol. Biosci.*, 2009, **9**, 575-584.
136. X. Zhang; S. Rehm; M. M. Safont-Sempere; F. Würthner, *Nat. Chem.*, 2009, **1**, 623-629.
137. Z. Gu; L. Yan; G. Tian; S. Li; Z. Chai; Y. Zhao, *Adv. Mater.*, 2013, **25**, 3758-3779.
138. C.-C. Hung; W.-C. Huang; Y.-W. Lin; T.-W. Yu; H.-H. Chen; S.-C. Lin; W.-H. Chiang; H.-C. Chiu, 2015.
139. C. Jung; B. K. Müller; D. C. Lamb; F. Nolde; K. Müllen; C. Bräuchle, *J. Am. Chem. Soc.*, 2006, **128**, 5283-5291.
140. T. T. Lee; J. R. García; J. I. Paez; A. Singh; E. A. Phelps; S. Weis; Z. Shafiq; A. Shekaran; A. Del Campo; A. J. García, *Nat. Mater.*, 2015, **14**, 352-360.
141. F. Nolde; J. Qu; C. Kohl; N. G. Pschirer; E. Reuther; K. Müllen, *Chem. Eur. J.*, 2005, **11**, 3959-3967.
142. S. Daehne; U. Resch-Genger; O. S. Wolfbeis, *Near-infrared dyes for high technology applications*. Springer Science & Business Media: 2012, **52**.
143. F. O. Holtrup; G. R. Müller; H. Quante; S. De Feyter; F. C. De Schryver; K. Müllen, *Chem. Eur. J.*, 1997, **3**, 219-225.
144. H. N. Kim; L. Puhl; F. Nolde; C. Li; L. Chen; T. Basché; K. Müllen, *Chem. Eur. J.*, 2013, **19**, 9160-9166.
145. H. Piwoński; A. Sokołowski; J. Waluk, *J. Phys. Chem. Lett.*, 2015, **6**, 2477-2482.
146. Q. Liu; B. Yin; T. Yang; Y. Yang; Z. Shen; P. Yao; F. Li, *J. Am. Chem. Soc.*, 2013, **135**, 5029-5037.
147. J.-H. Kim; F. Deng; F. N. Castellano; J.-H. Kim, *ACS Photonics*, 2014, **1**, 382-388.
148. J.-H. Kim; J.-H. Kim, *J. Am. Chem. Soc.*, 2012, **134**, 17478-17481.
149. R. Li; Z. Ji; J. Dong; C. H. Chang; X. Wang; B. Sun; M. Wang; Y.-P. Liao; J. I. Zink; A. E. Nel, *ACS Nano*, 2015, **9**, 3293-3306.

150. F. Marsico; A. Turshatov; R. Peköz; Y. Avlasevich; M. Wagner; K. Weber; D. Donadio; K. Landfester; S. Balushev; F. R. Wurm, *J. Am. Chem. Soc.*, 2014, **136**, 11057-11064.
151. M. A. Filatov; E. Heinrich; D. Busko; I. Z. Ilieva; K. Landfester; S. Balushev, *Phys. Chem. Chem. Phys.*, 2015, **17**, 6501-6510.
152. A. Trovarelli, *Catalysis by ceria and related materials*. World Scientific: 2002; Vol. 2.
153. Q. Fu; H. Saltsburg; M. Flytzani-Stephanopoulos, *Science*, 2003, **301**, 935-938.
154. A. Trovarelli; C. de Leitenburg; M. Boaro; G. Dolcetti, *Catal. Today* 1999, **50**, 353-367.
155. S. Park; J. M. Vohs; R. J. Gorte, *Nature*, 2000, **404**, 265-267.
156. I. Celardo; J. Z. Pedersen; E. Traversa; L. Ghibelli, *Nanoscale*, 2011, **3**, 1411-1420.
157. Y. Li; X. He; J. J. Yin; Y. Ma; P. Zhang; J. Li; Y. Ding; J. Zhang; Y. Zhao; Z. Chai, *Angew. Chem. Int. Ed.*, 2015, **54**, 1832-1835.
158. C. Walkey; S. Das; S. Seal; J. Erlichman; K. Heckman; L. Ghibelli; E. Traversa; J. F. McGinnis; W. T. Self, *Environ. Sci. Nano.*, 2015, **2**, 33-53.
159. F. Tiarks; K. Landfester; M. Antonietti, *Langmuir*, 2001, **17**, 908-918.
160. P. Gomez-Romero, *Adv. Mater.*, 2001, **13**, 163-174.
161. C. Sanchez; B. Julián; P. Belleville; M. Popall, *J. Mater. Chem.*, 2005, **15**, 3559-3592.
162. S. Kango; S. Kalia; A. Celli; J. Njuguna; Y. Habibi; R. Kumar, *Prog. Polym. Sci.*, 2013, **38**, 1232-1261.
163. S. Kalia; Y. Haldorai, *Organic-inorganic Hybrid Nanomaterials*. Springer: 2015.
164. F. Caruso, *Adv. Mater.*, 2001, **13**, 11-22.
165. X. Shi; M. Shen; H. Möhwald, *Prog. Polym. Sci.*, 2004, **29**, 987-1019.
166. J.-P. Chapel; J.-F. Berret, *Curr. Opin. Colloid Interface Sci.*, 2012, **17**, 97-105.
167. W. Tong; X. Song; C. Gao, *Chem. Soc. Rev.*, 2012, **41**, 6103-6124.
168. M. Nakamura; K. Katagiri; K. Koumoto, *J. Colloid Interface Sci.*, 2010, **341**, 64-68.
169. B. zu Putlitz; K. Landfester; H. Fischer; M. Antonietti, *Adv. Mater.*, 2001, **13**, 500-503.
170. A. Schrade; K. Landfester; U. Ziener, *Chem. Soc. Rev.*, 2013, **42**, 6823-6839.
171. A. Dinsmore; M. F. Hsu; M. Nikolaidis; M. Marquez; A. Bausch; D. Weitz, *Science*, 2002, **298**, 1006-1009.
172. S. Cauvin; P. J. Colver; S. A. Bon, *Macromolecules*, 2005, **38**, 7887-7889.
173. A. Ethirajan; U. Ziener; K. Landfester, *Chem. Mater.*, 2009, **21**, 2218-2225.

- 
174. S. D. Cook; K. A. Thomas; J. F. Kay; M. Jarcho, *Clin. Orthop. Relat. Res.*, 1988, **232**, 225-243.
175. P. Duheyne; J. Beight; J. Cuckler; B. Evans; S. Radin, *Biomaterials*, 1990, **11**, 531-540.
176. A. A. Campbell; G. E. Fryxell; J. C. Linehan; G. L. Graff, *J. Biomed. Mater. Res.*, 1996, **32**, 111-118.
177. J. Zhou; Q. Liu; W. Feng; Y. Sun; F. Li, *Chem. Rev.*, 2014, **115**, 395-465.
178. O. S. Kwon; H. S. Song; J. Conde; H.-i. Kim; N. Artzi; J.-H. Kim, *ACS Nano*, 2016.
179. F. Zhang, *Photon Upconversion Nanomaterials*. Springer: 2015, **416**.
180. E. Balnois; S. Durand-Vidal; P. Levitz, *Langmuir*, 2003, **19**, 6633-6637.
181. P. Mongondry; J. F. Tassin; T. Nicolai, *J. Colloid Interface Sci.*, 2005, **283**, 397-405.
182. B. Ruzicka; E. Zaccarelli, *Soft Matter*, 2011, **7**, 1268-1286.
183. O. D. Velev; K. Furusawa; K. Nagayama, *Langmuir*, 1996, **12**, 2374-2384.
184. D. Voorn; W. Ming; A. Van Herk, *Macromolecules*, 2006, **39**, 2137-2143.
185. S. A. Bon; P. J. Colver, *Langmuir*, 2007, **23**, 8316-8322.
186. L. L. Hecht; C. Wagner; K. Landfester; H. P. Schuchmann, *Langmuir*, 2011, **27**, 2279-2285.
187. C. Wohnhaas; V. Mailänder; M. Dröge; M. A. Filatov; D. Busko; Y. Avlasevich; S. Balushev; T. Miteva; K. Landfester; A. Turshatov, *Macromol. Biosci.*, 2013, **13**, 1422-1430.

## 10. Acknowledgements

Firstly, I would like to thank Prof. Dr. Katharina Landfester for giving me the opportunity to work on an interesting topic. I heart fully thank you for accepting me in your group and driving my interest towards polymer and colloidal chemistry. With your continuous encouragement and scientific help, I completed my PhD thesis.

I would like to give a special thanks to Dr. Rafael Muñoz-Espí, for the scientific discussions with innovative ideas and for helping me during my whole PhD thesis. It's good to work with a supportive project leader like you in our research group. I heart fully thank you also for your patience and kindness to me. The way you helped me by giving valuable suggestions in colloidal and polymer chemistry, and in personal life had helped me to complete my PhD. I am very proud and happy to work under a nice person like you.

Thanks to Dr. Stanislav Balushev for valuable scientific discussions with innovative ideas and suggestions that you had given me from the day I started working in the group. I have gained scientific knowledge in the topic of luminescence spectroscopy and physics behind it whenever I discussed with a knowledgeable person like you. Your suggestions in the scientific field and in other topics had helped me to learn and to complete my PhD.

Furthermore, I am very grateful for the help of many people who assisted me in several aspects and without whom this thesis would probably not exist. These are in particular:

- Prof. Dr. Peter Wich for being assessor of my PhD thesis.
- Prof. Dr. Rudolf Zentel for accepting to be the chairman of my PhD defense.
- I am personally thankful to Dr. Dmitry Busko for being part of numerous luminescence measurements during my PhD and discussion to interpret the obtained results. It helped me to gain knowledge in the topic which I worked on my thesis.
- I would like to thank my good friends Dr. Daniel Hofmann, Dr. Bernd Oschmann, Dr. Shahed Behzadi, Victor Bergmann, for their valuable support with suggestions and constant fun in Mainz.
- The International Research Training Group 1404 for financial support and for collaboration with Seoul National University.
- Prof. Dr. Byeong-Hyeok Sohn for accepting me in his group and work in his laboratories for 6 months during my PhD exchange program.



- Gunnar Glaßer for SEM measurements, Katrin Kirchhoff for TEM measurements, Elke Muth for PCD measurements, Petra Räder for TGA measurements.
- Finally everyone present in the group for their valuable suggestions, discussions, measurements and fun time.

Finally but not least, I would like to convey a special thanks to my parents and my brother for accepting me to study in abroad and complete my PhD. My parents had encouraged and supported me for every step in my life. To my parents and my brother: I Love You!

# Curriculum Vitae

## Kartheek Katta

---

◆ Hechtscheimer Straße 37a ◆ 55131 Mainz, Germany

◆ E-mail: [katta.kartheek88@gmail.com](mailto:katta.kartheek88@gmail.com)

## Personal Details

---

**Date of Birth**                      19<sup>th</sup> April 1988

**Nationality**                        Indian

## Education Credentials

---

**05/2013 - 07/2016**                      Max Planck Institute for Polymer Research, Mainz, Germany  
PhD student in Prof. Dr. Katharina Landfester group  
Seoul National University, Seoul, South Korea  
Exchange PhD student of a dual PhD program

**09/2010 – 12/2012**                      University of Siegen, Germany  
Master of Science in Chemistry  
Master thesis in Prof. Dr. Claudia Wickleder group  
Title: “Photoluminescence of Eu<sup>2+</sup> and Yb<sup>2+</sup> in the Chloride-based Spinel Li<sub>2</sub>MCl<sub>4</sub> (M = Mg, Cd and Zn)”.

**08/2005 - 08/2009**                      The TamilNadu Dr. M.G.R. Medical University, Chennai, India  
Bachelors in Pharmacy  
Bachelor thesis in Prof. Dr. R. Vasuki group  
Title: “A Retrospective Exposition on Alzheimer’s Disease”.

# Scientific Contributions

## Publications

- **Katta, K.**; Busko, D.; Avlasevich, Y.; Muñoz-Espí, R.; Balushev, S.; Landfester, K., Synthesis of Triplet–Triplet Annihilation Upconversion Nanocapsules under Protective Conditions. *Macromol. Rapid Commun.* **2015**, *36*, 1084-1088.
- **Katta, K.**; Busko, D.; Avlasevich, Y.; Landfester, K.; Balushev, S.; Muñoz-Espí, R., Improving the Efficiency of Encapsulated Fluorophores with Ceria/Polymer Hierarchical Nanocapsules. Manuscript in preparation.
- **Katta, K.**; Busko, D.; Landfester, K.; Balushev, S.; Muñoz-Espí, R., Inorganic protection of polymer nanocapsules: A strategy to improve the efficiency of optically active molecules. Manuscript in preparation.
- Balushev, S.; **Katta, K.**; Landfester, K., Teaching optics to nanocapsules: step by step to annihilation upconversion in nanoconfinement. Manuscript submitted.

## Presentations in Conferences

- 26/08/2013 - 29/08/2013: 8<sup>th</sup> German-Korean Polymer Symposium, University of Hamburg, Germany. Poster: Broadening of the Excitation Spectrum for Photocatalytic Hydrogen Generation by Triplet-Triplet Annihilation Photon Energy Upconversion.
- 17/02/2014 - 22/02/2014: Korea-Germany IRTG Symposium on self-organized materials for Optoelectronics, Korea. Poster: Encapsulation of Upconversion Materials by Heterophase Methods.

- 
- 14/07/2014 - 18/07/2014: IRTG1404 Summer Symposium 2014, Mainz & Freiburg im Breisgau. Oral presentation: Encapsulation of Upconversion Materials by Heterophase Methods (Passive Oxygen Protection).
  - 04/01/2015 - 07/01/2015: Korea-Germany IRTG Symposium on self-organized materials for Optoelectronics, Korea. Poster: Synthesis of Annihilation Upconversion Nanocapsules under Protective Conditions.
  - 16/08/2015 - 20/08/2015: 250<sup>th</sup> ACS National Meeting & Exposition, Boston, USA. Oral presentation: Encapsulation of Upconversion Materials by Heterophase Methods and Improvement in Luminescence Properties (Passive Oxygen Protection)





